CHALMERS
UNIVERSITY OF TECHNOLOGY

Energy Savings Using a Direct Current Distribution Network in a PV and Battery Equipped Residential Building

Thesis for Licentiate of Engineering in Electrical Power Engineering

PATRIK OLLAS

Division Electric Power Engineering
CHALMERS UNIVERSITY OF TECHNOLOGY
Gothenburg, Sweden 2020

Thesis for Licentiate of Engineering 2020

Energy Savings Using a Direct Current Distribution Network in a PV and Battery Equipped Residential Building

PATRIK OLLAS

CHALMERS
UNIVERSITY OF TECHNOLOGY

Department of Electrical Engineering
Chalmers University of Technology
Gothenburg, Sweden 2020

Energy Savings Using a Direct Current Distribution Network in a PV and Battery Equipped Residential Building

Supervisors: Caroline Markusson & Mattias Persson, RISE Research Institutes of Sweden
Examiner: Torbjörn Thiringer, Electrical Engineering

Thesis for Licentiate of Engineering 2020

ISSN No.: 1403-266X
Department of Electrical Engineering
Division of Electrical Power Engineering
Chalmers University of Technology
SE-412 96 Gothenburg
Telephone +46 31 772 1000

Cover: Research Villa at RISE in Borås, Sweden used for the demonstration of the direct current distribution network with solar photovoltaic, battery storage and DC operated loads. Photo credit: RISE.

Printed by Chalmers Reproservice
Gothenburg, Sweden 2020

Energy Savings Using a Direct Current Distribution Network in a PV and Battery Equipped Residential Building

PATRIK OLLAS
Department of Electrical Engineering
Chalmers University of Technology

Abstract

Energy from solar photovoltaic (PV) are generated as direct current (DC) and almost all of today's electrical loads in residential buildings, household appliances and HVAC system (Heating Ventilation and Air-conditioning) are operated on DC. For a conventional alternating current (AC) distribution system this requires the need for multiple conversion steps before the final user-stage. By switching the distribution system to DC, conversion steps between AC to DC can be avoided and, in that way, losses are reduced. Including a battery storage–the system's losses can be reduced further and the generated PV energy is even better utilised.

This thesis investigates and quantifies the energy savings when using a direct current distribution topology in a residential building together with distributed energy generation from solar photovoltaic and a battery storage. Measured load and PV generation data for a single-family house situated in Borås, Sweden is used as a case study for the analysis. Detailed and dynamic models–based on laboratory measurements of the power electronic converters and the battery–are also used to more accurately reflect the system's dynamic performance.

In this study a dynamic representation of the battery's losses is presented which is based on laboratory measurements of the resistance and current dependency for a single lithium-ion cell based on Lithium iron phosphate (LFP). A comparative study is made with two others, commonly used, loss representations and evaluated with regards to the complete system's performance, using the PV and load data from the single-family house. Results show that a detailed battery representation is important for a correct loss prediction when modelling the interaction between loads, PV and the battery.

Four DC system topologies are also modelled and compared to an equivalent AC topology using the experimental findings from the power electronic converters and the battery measurements. Results from the quasi-dynamic modelling show that the annual energy savings potential from the suggested DC topologies ranges between 1.9–5.6%. The DC topologies also increase the PV utilisation by up to 10 percentage points, by reducing the associated losses from the inverter and the battery conversion. Results also show that the grid-tied converter is the main loss contributor and when a constant grid-tied efficiency is used, the energy savings are overestimated.

Keywords: Direct-Current Distribution, Residential Buildings, Battery Energy Storage System, Battery Modeling, Solar Photovoltaic System, System Performance, Energy Efficiency, Energy Savings, PV Utilisation

Acknowledgements

I would like to acknowledge my examiner, Professor Torbjörn Thiringer at the department of Electrical Power Engineering for being outermost supportive and helpful, and for always being available for discussions, idea creation and problem solving.

My supervisors at RISE–Caroline Markusson and Mattias Persson–for their helpfulness and guidance within the field of research. A special thanks to Caroline for giving me this opportunity! I would also like to thank my colleagues at RISE for their support and for creating a superb working environment–with good laughs and coffee breaks! A special thanks to my mentor and go-to-guy, Peter Kovacs for all the help, teaching and guidance throughout the years.

This study could not have been done without the financial support, I would therefore like to thank the financier Swedish Energy Agency who has financed this through grant numbers 43276–1 and 47273–1.

Finally, I would like to thank my friends and family! Especially my wife–Eva–for being loving, supportive and encouraging, both privately and professionally.

Patrik Ollas, Gothenburg, February 2020

Nomenclature

Symbols, Subscripts, Abbreviations and Definitions

Symbols

		Unit
A	Area	m^2
η	Efficiency	%
ϑ	Temperature	°C
C	Capacitance	$m^{-2}kg^{-1}s^4A^2$ (Farad)
I, i	Current	A
λ	Thermal conductivity	$Wm^{-1}K^{-1}$
l	Length (cable)	m
L	Inductance	$kgm^2s^{-2}A^{-2}$ (Henry)
ρ	Cable resistivity	Ωm
Q	Battery charge level	kWh
ρ	Density	kg/m^3
R, r	Resistance	Ω
t_k	Discrete time step	–
V, v	Voltage	V
Z	Impedance	Ω
ω	Angular velocity (2πf)	Rad^{-1}

Subscripts

avg	Average
batt	Battery
BL	Battery to Load
box	Styrofoam box
C	Capacitance or C-rate
charge	Charge (of battery)
cond	Conduction (cables)
conv	Converter/Conversion
corr	Correction
discharge	Discharge (of battery)
hx	Heat-exchanger

k_1–k_3, q_1–q_2	Curve fit parameters for converter efficiency characteristics
L	Inductance
d	Input
max	Maximum
min	Minimum
o	Output
PV	Photovoltaic
ϕ	Phase or phase difference between current and voltage

Abbreviations

AC	Alternating Current
BIPV	Building Integrated Photovoltaic
BMS	Battery Management System
C-rate	Current level at which the battery is completely discharged during 1 hour
DA	Day-Ahead (battery dispatch algorithm)
DB	Day-Behind (battery dispatch algorithm)
DC	Direct Current
DG	Distributed Generation (of energy)
DHW	Domestic Hot Water
DSM	Demand Side Management
LCC	Life-Cycle Cost
MPP	Maximum power point (PV module)
NZEB	Net-Zero Energy Building
OCV	Open-Circuit Voltage
PFC	Power Factor Correction (converter)
PV	Photovoltaic
RE	Renewable Energy
RMS	Roout-Mean-Square
RMSE	Root-Mean-Square Error
SC	Self-Consumption
SOC	State of Charge (battery)
SS	Self-Sufficiency
STC	Standardised Test Conditions (PV modules)
TZ	Target Zero (battery dispatch algorithm)

Definitions

c_p	Heat capacity
D	Duty cycle
e_{batt}	Instantaneous battery energy
E_{BATT-L}	Energy from battery to load, i.e. discharge
$E_{batt,\ rated}$	Rated battery energy
e_{BL}	Energy from battery to load
$e_{grid,\ battery}$	Energy from grid to battery

E_{load}	Total load demand from system
E_{losses}	Total system losses (annual)
$\mathsf{E}_{PV,\ DC}$	Total DC produced energy from PV
E_{demand}	Total annual energy demand, i.e. E_{load} + E_{losses}
$\mathsf{E}_{PV-GRID}$	Energy exported from PV to grid
E_{PV-L}	Energy from PV to load (directly), i.e. self-consumption
e_{PV}	Total generated PV energy
e_{PVSC}	Energy from PV directly to load
e_{TOT}	Total electrical load
f_{sw}	Switching frequency
η_{batt}	Instantaneous battery charge/discharge efficiency
$\eta_{PV,\ system}$	PV utilsation factor defined by Fregosi et al. (2015)
η_{system}	System efficiency defined by Gerber et al. (2018)
MPP(T)	Maximum power point (tracking), PV modules
p_{charge}	Battery charge power
$\mathsf{p}_{discharge}$	Battery discharge power
p_{batt}	Battery power
p_{load}	Load power
p_{pv}	Solar photovoltaic power
P_{rated}	Rated power
Self-Sufficiency (SC)	Ratio of locally consumed PV energy normalised to the load (amount of PV energy covering the load, and which is not bought from the grid)
Self-Consumption (SC)	Ratio of PV energy consumed locally normalised to overall generated PV energy, i.e. share of PV generated energy used directly to supply the load
T_s	Switching time period

Contents

1
Introduction

1.1 Background

Despite last year's strive towards more energy efficient usage, the total electricity consumption has grown steadily the last 20+ years [1]. This trend will most likely continue due to an increased electrification of the building, industry and transportation sectors. Since the majority of electricity generation globally is fossil fuels based (oil, gas and coal) the global pollution and CO2 emissions will continue increasing, and actions are needed to not overshoot the target set by the Paris Agreement of a maximum two-degree temperature increase [2].

Energy generation from solar photovoltaic (PV) is seen as one possibility to create a more sustainable energy mix by offering renewable and non-polluting energy generation. Continues price reductions and an increased environmental awareness have generated an exponential penetration of PV modules which has grown by more than 270% globally during the period 2013–2018 with a total installation capacity in 2018 of 512 GW [3]. In Sweden, the installed PV capacity has almost 10-folded during the same period with a total installed capacity in 2018 of 425 MW which accounted for 0.3% of the national energy generation [4].

System combinations with PV and stationary batteries can help increase the self-consumed energy generated by the PV panels through intraday (short term) storage and limits the potential power curtailment problematic where surplus PV energy could be lost due to grid regulations. Since PV generated energy is intermittent by nature, meaning that output is only generated during sufficient conditions—with respect to solar irradiance, temperature, etc.–a large share of renewable energy sources also puts more stress on the grid through its characteristics and unpredictability. For this, a battery storage can be used to smooth out the net load profile and create better conditions for the grid. The number of stationary batteries in residential buildings are growing fast where decreasing retail prices, self-sufficiency awareness and resilience are some of the main drivers [5]. In Bloomberg, 2019, it is reported that battery prices have fallen by more than 84% since 2010 and are estimated to continue the same pattern, reaching around 62$/kWh in 2030 [6].

Power from the PV panels are generated as direct current (DC) and batteries operates with DC, and almost all electronic loads in buildings are natively DC operated. In today's conventional alternating current (AC) systems with PV and battery storage, there are conversions required before the final user-stage, and all these conversions are associated with losses. By adopting a DC distribution network in the building, many of these conversion losses can be avoided and thus increase

the system's performance and utilization of the PV energy. Lately, there have been numerous attempts to sort out whether DC is superior to AC in terms of energy efficiency on a system level and what circumstances affects these results. Dastgeer et al. (2019) published a literature comparison of past and present work in the area and concluded that gains from in-house DC distribution differ greatly, varying from 1.3–20%, including studies that show no efficiency gain with DC supply [7]. Furthermore, it is also concluded in the same reference that comprehensive research efforts are needed with detailed modelling–stressing the importance of accurate assumptions of power electronic components–and demonstrations, to give a fair comparison between the two scenarios.

A contributing factor to an efficient DC system is the coupling with distributed generation (DG) and battery storage. Already with these two additions, assuming DC coupling, some of the conversion losses are avoided and the PV generated energy is better utilised. Furthermore, local market regulations are today designed to promote self-consumption of the generated energy, increasing the incentive for local energy storages.

Last year's technological development in power electronics [8] together with the exponential growth in PV and battery deployment makes this all-out DC solution interesting, both from an energy efficiency and grid-relief aspect. The projected growth in electrical vehicles with DC charging is an additional factor pointing towards an increased use of DC in buildings [9]. An expert assessment with market players identified the potential energy savings from DC distribution networks as the top characteristic, followed by reliability and efficient storage [10].

1.2 Identified Research Gap

A gap identified from the literature review on PV and battery system's is the lack of consideration of the battery's current dependent efficiency, which in this study, have proven to be crucial for accurately determining the system performance. In literature, multiple studies can be found on PV and battery system modelling and how the battery impacts the overall system performance, and to some extent also the economy, often with regards to the increase in the systems self-consumption (SC) and self-sufficiency (SS) [11–16]. A comprehensive literature review of some of the published articles from PV and battery systems can be found in [17] that summarises the results of gains in SC and SS when using battery storage and demand side management (DSM). Most of the previous studies dealing with PV and battery systems in buildings ignore the battery efficiency's dynamic dependency and assumes a constant round-trip efficiency between 85–96% [11, 18–30]. Battke et al. highlights the importance of careful selection of the battery's round-trip efficiency as it is one of the main factors to consider when studying the life-cycle cost (LCC) of a battery investment [31]. In that study, Monte Carlo simulations are made using a battery efficiency distribution found in literature (85–95%) without presenting any recommendations regarding what value to choose. Another drawback with the constant efficiency approach is that it depends on the selected battery as well as the relative power utilisation of the battery. In applications with very dynamic conditions–such as in vehicles–the modelling approach of using a resistance representation [32] or resis-

tance network representation [33,34] is sometimes utilised to determine the losses in the battery. However, the impact of current level dependence [35] is scarcely treated in literature. Thus, a more detailed model-based battery loss representation–even in such applications–would be highly valuable. Nonetheless, what is an appropriate efficiency and loss representation of a battery? It will of course depend on the battery chosen, but how is a procedure to determine this formulated and how will the final output vary with the selected representation? In this work, a model is presented that considers a dynamic battery internal resistance to capture its characteristics. Results show that for a four-hour charge cycle, the losses differ by 2.9 percentage points compared to the, in literature, commonly used constant round-trip efficiency approach. Furthermore, annual losses are more than 4 times lower with the dynamic model compared to the conventional approach used.

There have been many attempts in literature to estimate the energy savings when switching from AC to DC distribution in residential buildings. The findings differ substantially, varying from 1.5–25.0% depending on the chosen reference case, types of appliances (loads included) and system's studied, e.g. with or without the inclusion of PV and battery, etc. [36–40]. Findings in literature on DC savings for individual household appliances/HVAC-components also vary significantly, [41–44] presents results between 1.5–9%, which is strongly reflected in the final result. From literature a significant divergence is also observed in the used converter efficiencies, and constant efficiencies are typically used, ignoring the load dependent efficiency characteristics [36, 43–47].

An important deficit, as identified in [48], when comparing AC and DC topologies is the need for a more detailed modelling of the battery performance, using a load dependant efficiency, to have more accurate results.

As pointed out by Dastgeer et al. [7], more comprehensive research efforts are needed with a deeper detail level on the modelling, as well as demonstrations, to enable a fair comparison between the two topologies. Also, other studies have pointed out the need for a comprehensive analysis to show whether, and under what circumstances, an internal DC network is superior to an equivalent AC network [7, 10, 49].

Based on the identified research gaps, this thesis has been formulated to: (i) model the energy savings and increased PV utilization potential for a DC topology compared to an AC equivalent (ii) quantifying the impact of using a load dependent and constant grid-tied efficiency characteristic for the system's performance, (iii) establish the characteristics and performance of power electronic component and (iv) characterize the battery's dynamic behavior and loss representation with a current depending resistance. For the analysis of the system performance a single-family residential house in Borås, Sweden is used as a case study with PV and load data for one year's operation.

1.3 Purpose & Contribution

The aim of this thesis is to investigate the energy savings potential and increase in solar photovoltaic (PV) utilization when using a direct current (DC) topology in a residential building, compared to the conventional alternating current (AC) topology. From this study, the following contributions are added:

I. Determination of the impact on system performance from different battery sizes and dispatch algorithms.
II. Characterisation of a battery cell through laboratory measurements, and quantifying the impact of using this battery model in comparison to other, commonly used, approaches when modelling a PV and battery system in buildings.
III. Quantify the efficiency gains of representative power electronic converters, when omitting the rectification stage, and establishing their complete efficiency characteristics through laboratory measurements.
IV. Determine the energy savings potential and main loss contributors for a DC distribution topology using the results from the measurements on the battery (II) and power electronic converters (III).
V. Quantify the increase of PV utilisation when using a DC distribution topology for a single-family residential building.
VI. Quantifying the impact on energy savings and PV utilization when using a constant and dynamic efficiency characteristic for the grid-tied converter.
VII. Demonstration of a direct current distribution topology with solar photovoltaic, battery storage and DC operated loads in a single-family residential building.

All results except for bullets III and VII are found, from a system perspective, for a single-family residential building located in Sweden, using measured load and PV data.

1.4 Thesis Outline

The thesis is outlined as follows: Chapter 2 sets the theoretical framework for this study introducing the theory together with a description of the electrical load profiles and system topologies. Chapter 3 describes the studied cases, the method used for the quasi-static modelling and measurement set-up for the component analysis. The intermittent results from the component analysis is presented in Chapter 4. This analysis is followed by Chapter 5 where results are evaluated and presented from a system perspective. Chapter 6 presents identified market barriers related to DC distribution networks. In Chapter 7 conclusions are presented based on the findings and the Thesis finishes with Chapter 8 where suggested future works are identified and presented.

1.5 List of Publications

Published

A. **P. Ollas**, J. Persson, C. Markusson & U. Alfadel *"Impact of Battery Sizing on Self-Consumption, Self-Sufficiency and Peak Power Demand for a Low Energy Single-Family House With PV Production in Sweden"*, World Conference on Photovoltaic Energy Conversion (WCPEC-7) Conference Proceedings, Hawaii USA (**2018**). doi:10.1109/pvsc.2018.8548275

Submitted – Under Review

(i) **P. Ollas**, T. Thiringer, M. Persson & C. Markusson *"Static vs. Dynamic Battery Efficiency: Impact on PV/Battery System Performance in a Net-Zero Energy Residential Building"*[1]

(ii) **P. Ollas**, T. Thiringer & C. Markusson *"Energy Efficiency Savings Through the Usage of Direct Current Distribution in a Residential with Solar Photovoltaic and Battery Storage"*[2]

[1] Submitted on February 13th, 2020 to Elsevier, Applied Energy
[2] Submitted on February 16th, 2020 to Elsevier, Applied Energy

2

Theoretical Framework

2.1 Electricity Usage in Buildings

An important aspect for good utilisation of distributed energy generation, e.g. from PV generation, is the conformity with its internal loads, i.e. match between supply and demand. Current economical legislations for single-family residential buildings in Sweden promote direct usage in buildings with the highest economical pay-off from the avoided energy purchased from the grid through self-consumption. Therefore, one of the top priorities when designing a PV system is to consider the electrical demand load profile, throughout the year but most importantly, the instantaneous match between generation and load with high temporal resolution. Figure 2.1 shows the monthly radiation on the horizontal surface for Gothenburg, Sweden[1] for the period January 2007–December 2018. Noticeable is the large seasonal variations with 90% of the radiation occurring during March–September and that January and December together amounts to only 2% of the annual total. Annual total measured radiation in the horizontal plane varies between 1000 kWh/m^2±5% for the studied period.

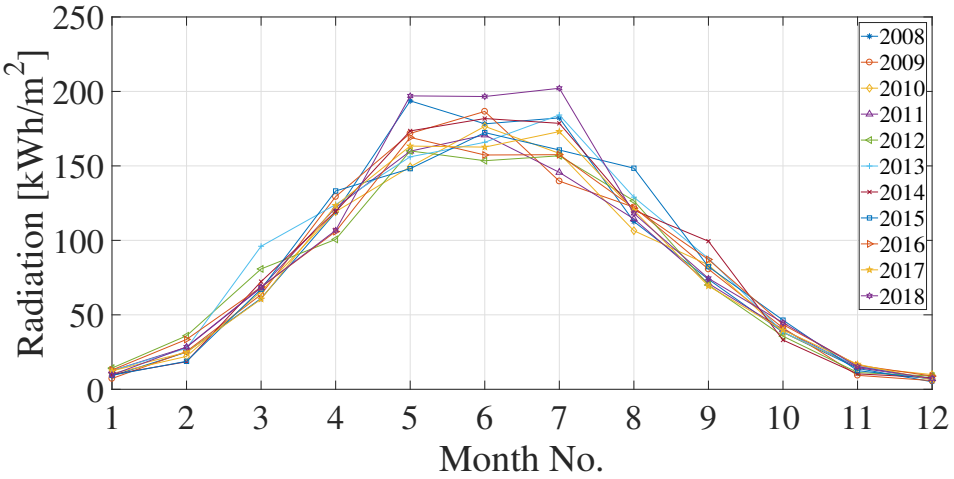

Figure 2.1: Monthly measured horizontal radiation in Gothenburg for the period January 2007–December 2018.

In 2008, a study was published that analysed how an increased PV penetration would impact the electric grid and presented what is now known as the ”duck curve”

[1] Data taken from the Swedish Meteorological and Hydrological Institute, SMHI

[50]. The "duck curve" shape of the net grid[2] load profile occurs when there are demand peaks in the morning and evening and excess PV generation during mid-day, forcing the conventional power plants to more frequent ON/OFF operation. In [51] it was presented that the excess generation of PV could potentially lead to curtailment of PV surplus, increasing its cost and reduce the environmental benefits.

In the following chapters, typical load profiles for three different building types are presented for single-family houses, multi-family houses and offices/commercial buildings and their characteristics in terms of daily and seasonal variations, and how they align with available PV generation are explained.

2.1.1 Single-Family Residential Buildings

Typically, the energy demand in a single-family house has its peaks during morning and evening, coinciding with activities related to cooking[3] and other household activities. Figure 2.2 shows PV generation and load demand for a single-family residential building in Sweden during a typical summer day in Sweden, with peak demands in the morning and evening, and peak PV generation around noon.

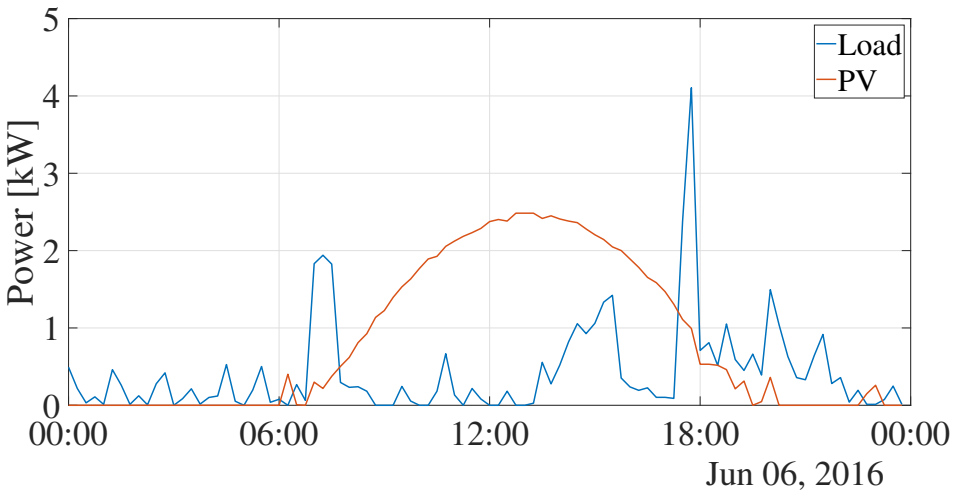

Figure 2.2: Typical load and PV generation profiles for a single-family residential building on a summer day in Sweden.

In general, there is a poor match between supply and demand during the summer season when studying available solar PV generation, with its bell-shaped supply curve. This mismatch for single-family houses is especially true for Sweden with low demand during summer days when people are at work and with peak energy demands during heating seasons[4] when PV energy generation is limited due to low irradiance. This supply and demand mismatch, in the absence of any storages, makes the self-consumption of the generated energy low and thus the investment less economically feasible, as the main revenue is made from displacement of grid

[2] Net grid equals the different between sold and bought energy to/from the grid.
[3] In Sweden, almost all cooking is done via electrically operated ovens and stoves
[4] In 2016 48% of the single-family houses used electricity for heating, 33% bio fuels, 17% district heating and 2% other [52].

energy through self-consumption. It shall be noted that most single-family houses in Sweden today uses electricity (via heat pumps) for space heating and domestic hot water (DHW) production. Where the latter demand profile is fairly constant throughout the year and can be partially covered by the available PV generation, while the former shows less conformity with the available PV generation.

A measure to compensate for this mismatch between supply and demand is to use stationary batteries that can store energy from excess PV generation, occurring during the day, and supply the demands later during the day. This increases the self-consumption and self-sufficiency of the system and reduces the need for grid energy import.

2.1.2 Multi-Family Residential Buildings

In 2016, 90% of the heat supplied to multi-family houses in Sweden came from district heating [52]. Electrical loads in multi-family houses are commonly divided into two main parts, (i) household electricity used in the apartments and, (ii) electricity used by building services (ventilation, pumps, elevators etc.). In general, for multi-family-buildings heated by district heating, the building services electrical and household loads remain fairly constant throughout the year with a slight decrease during summertime [53].

In addition to direct self-consumption from PV coverage of electrical loads, a way to increase the self-consumption in multi-family houses is to transform the excess PV generation into heat and store it for later usage, as identified in [53]. This can be done in a few different ways, including hot water storage tanks or bore holes. The latter also has the benefit of enabling a seasonal storage. Another possible measure is to include battery storage that–as for single-family houses–can be used to store excess PV generation during peak hours and store it intraday to cover demands during the evening/night.

2.1.3 Offices & Commercial Buildings

With its load profile characteristics of having its peak demands around noon, office buildings have a better match between PV supply and load demand compared to residential buildings. Figure 2.3 shows monthly variations for the simulated office's electrical loads from [54] for June (Figure 2.3a) and November (Figure 2.3b), where a lower demand is seen when office occupants are expected to be absence due to vacation during June and with an overall higher demand during November. Noticeable is also the lower demands during weekends, e.g. off-working hours (Saturday and Sunday). The seasonal difference does not align with the availability of solar supply, which has its peak during April–August and with very limited supply during the darker periods, e.g. November. Nevertheless, load profile with peaks around noon are still in good consistency with available PV generation.

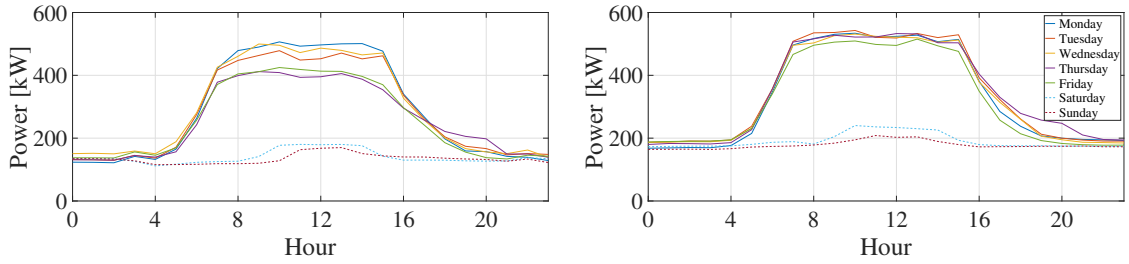

(a) **(b)**

Figure 2.3: Typical office building annual average electrical load profiles per day for **(a)** June and **(b)** November from [54].

2.2 Household Electrical Storage

There are several storage technologies available for buildings including storage for electrical and thermal energy (e.g. in hot water storage tanks). Today, heat storage is the dominating solution, but the market for electrical storage's are growing, but from a low level. Hydrogen storage solutions are another electrical storage possibility with the main advantage of offering seasonal (long term) storage and if coupled with local energy generation, allows for off-grid possibilities. However, this technology is currently a niche application and the price is too high for mainstream commercial interest. This thesis focuses only on electrical storage in batteries.

A residential battery offers multiple services; both for the household itself and the external grid, including,

- increasing self-consumption of locally generated energy and thus lowering the electricity bill, and increasing the usage of renewable energy on-site,
- back-up power–offering system resilience and power during grid outages,
- reduction of peak demands–avoiding power tariffs and lowering the stress on the grid (and possible power curtailment),
- flexibility by offering services for supply and demand to actively participate in grid stabilisation.

These are just a few examples of the services a stationary battery can provide[5], and more business models are being developed to enable batteries to provide grid services and thus increase its profitability.

Lindahl has compiled statistics of installed battery capacity in combination with solar PV and presented it for Sweden and the period 2016–2018, see Table 2.1 [4]. It shall be noted that these figures represent battery capacity installed by PV installation companies in connection to distributed PV systems and that these numbers were first collected in 2016. Thus, the actual number of cumulative installed battery capacity is probably higher since installations prior to 2016 are not included.

Looking forward, the number of local electrical storages are expected to increase following the expansion of the solar PV market and nationally with the help of

[5] Currently, there is also a theoretical possibility for residential storage's to participate in other grid services, e.g. frequency regulations. However, the legal framework is today not adapted for this, but there are on-going discussions to revise these to also include residential batteries.

Table 2.1: Annual installed grid connected battery capacity in different systems (private/commercial) in Sweden in combination with PV systems

Year	Private [kWh]	Commercial [kWh]	Total [kWh]
2016	177	1365	1542
2017	1128	1288	2416
2018	2384	1520	3904

the introduction of a direct capital subsidy for batteries, where private actors get a subsidy of 60% of the investment cost for the battery (but no more than SEK 50000) [55][6]. This subsidy is given for storage's that fulfils the following requirements,

- connected to an electricity production system for self-consumption of renewable electricity,
- connected to the grid,
- helps to store electricity for use at a time other than the time of production, which increases the annual share of self-produced electricity used within the property to better meet the electricity consumption

Studies have been made for battery storage cost trajectories and summarised in [56]. Here, the mutual gains of battery storage coupled with renewable on-site electricity generation is demonstrated with trajectories into the future on product prices, volumes and curtailed energy from renewable sources. It is concluded in the low-cost battery storage scenario that this will lead to a significant deployment of storage units and this in turn will lead to an increased use of renewable energy sources and the phasing out of other less favourable alternative sources.

2.3 System Self-Consumption & Self-Sufficiency

As mentioned, the supply-demand mismatch between available PV generation and load demand can partly be compensated for intraday with a battery storage that enables a reduction of the grid interaction by discharging the battery when the load demand exceeds the available PV generation and charges it during times with PV surplus.

One of the most common factors used in literature to evaluate the systems performance and impact from a battery storage is the system's self-consumption (SC) and self-sufficiency (SS). Self-consumption for a PV system is the share of PV generated energy (e_{PV}) used either to supply the loads directly (e_{PVSC}) or via the battery storage (e_{BL}). A battery's operation is determined by its dispatch (control) algorithm, determining how–and when–charge and discharge shall be done. For the simplest battery dispatch algorithm, where no charging of the battery is made from the grid, SC for the PV/battery system is defined as

$$SC = \int_{t_1}^{t_2} \frac{e_{PVSC}(t) + e_{BL}(t)}{e_{PV}(t)} dt \tag{2.1}$$

[6] The subsidy program was introduced in Sweden in November 2016 with an annual budget for 2017 to 2019 at SEK 50 million per year. In 2019, this period was extended to December 2020.

Another key performance factor for a PV/Battery system is the system's self-sufficiency (SS). This is the ratio of used PV generated energy, either directly (e_{PVSC}) or via the battery storage (e_{BL}), and the total electrical energy use (e_{TOT}), and is defined as

$$SS = \int_{t_1}^{t_2} \frac{e_{PVSC}(t) + e_{BL}(t)}{e_{TOT}(t)} dt \tag{2.2}$$

When the battery is allowed to discharge, and/or, charge to/from the grid the self-consumption and self-sufficiency are defined as

$$SC' = \int_{t_1}^{t_2} \frac{e_{PVSC} + e_{BL} \pm e_{grid,\ battery}}{e_{PV}} \tag{2.3}$$

$$SS' = \int_{t_1}^{t_2} \frac{e_{PVSC} + e_{BL} \pm e_{grid,\ battery}}{e_{TOT}} \tag{2.4}$$

where the energy interaction between the battery and the grid, $e_{grid,\ battery}$, is taken into consideration.

An arbitrary time frame (t_1 to t_2) can be used when evaluating the system's self-consumption and self-sufficiency, most commonly it is done for an entire year to reflect the annual performance of the system.

2.3.1 Household Battery Utilisation – Dispatch Algorithms

The dispatching (i.e. charging and discharging) of a household battery can be done in different ways depending on its objective function. Most commonly the battery is operated to maximise the self-consumption of locally generated energy by only allowing to charge from surplus PV energy and discharge (to the loads) during PV deficits, and not interact (charge/discharge) with the grid. Other strategies might have additional objectives such as peak power shaving, i.e. reducing peak power imports from the grid, (night-time) charging when prices are low, etc. The battery management system (BMS) can also have an underlying forecasting of the up-coming load demand and PV supply and based on this choose to operate the battery in a certain manner that includes battery charging from the grid to cover morning peak while maximising self-consumption during days with high generation. Below, some of these dispatch algorithms are explained more in detail.

2.3.1.1 Maximising Self-Consumption

The "Target Zero" (TZ) method is the most commonly used method with the aim of maximising the self-consumption (SC) of the generated solar PV energy by prioritising load coverage and battery charging before feeding any excess PV to the grid. The Target Zero method, defined in [57], does only allow for battery charging via PV surplus and not from the grid. The objective function for TZ can be described using the following equation and conditions

$$p_{target}(t) = p_{load}(t) - p_{PV}(t) \tag{2.5}$$

$$p_{batt}(t) = \begin{cases} \min\left(P_{rated}\ ,\ \frac{p_{load}(t)}{\sqrt{\eta_{batt}}}\right), & p_{target}(t) > 0\ \&\ e_{batt}(t) \geq 0 \\ \max(-P_{rated}\ ,\ -p_{load}(t)\sqrt{\eta_{batt}}), & p_{target}(t) < 0\ \&\ e_{batt}(t) \leq E_{rated} \\ 0, & \text{Otherwise} \end{cases} \tag{2.6}$$

where $\sqrt{\eta_{batt}}$ is the one-way efficiency, e.g. charging or discharging. Thus, battery discharging to the loads are done using the minimum value of rated battery power P_{rated} and $p_{load}/\sqrt{\eta_{batt}}$ and charging with maximum value of $-P_{rated}$ and $p_{load}\ \sqrt{\eta_{batt}}$. If generated solar PV energy, p_{PV}, is equal to the load, p_{load}, the battery status is not changed ($p_{batt} = 0$).

Another factor that determines the battery's charging and discharging is its state-of-charge, SOC, which quantifies how much charging content that is available in the battery at a given time, "t_k" , and is defined as

$$SOC(t_k) = \frac{Q_{batt}(t_k)}{Q_{batt,\ rated}} = \frac{\int i_{batt}(t_k)dt}{Q_{batt,\ rated}} \tag{2.7}$$

where $Q_{batt}(t_k)$ and $Q_{batt,\ rated}$ are the battery's instantaneous charge level and rated capacity respectively. If the battery is at its maximum or minimum SOC and is asked to charge or discharge respectively, p_{batt} is set to "0" in (2.6) to not violate the SOC constraints.

A drawback of using the TZ dispatch algorithm for Nordic climates is that the battery will be idle during longer time periods in the winter[7] when PV generation is very low, leading to a poor utilisation of the battery. Also, in cases where there are regulations with feed-in limitations–in terms of peak power curtailment (fed to the grid)–this dispatch will have a negative effect on the utilisation of the generated PV energy. An example of this is when the battery is charged using its maximum power and becomes fully charged at an early stage, then excess PV later is fed to the grid and possibly curtailed due to the power limitations. This will impact the system's revenue due to losses of grid power feed-in revenue.

2.3.1.2 Grid Power Peak Shaving

In addition to increasing the utilisation of in-house PV usage, a battery can be used both as a grid-relief by limiting the peak power transfers to/from the grid and for revenue purposes by avoiding peak tariffs and potential power curtailments, resulting in revenue losses.

In practice, peak power shaving can be done by allowing for the battery to interact with the grid to either cover peak import demands during high loading demands or limit the power export to avoid revenue losses in the presence of curtailment limits. The latter might occur for south-facing PV systems around mid-day where high peak powers are fed to the grid from excess generation.

Using batteries for peak power shaving often requires some type of forecast to predict the net energy balance for the up-coming period and then uses this prediction to either discharge or charge the battery to/from the grid. Typically, charging

[7] This statement is also valid if the load power is significantly higher than the peak PV generation.

from the grid or PV is done for a residential house during the night/early morning and afternoon to cover morning and evening peaks during times with low PV generation. During seasons with high PV generation, battery discharge might occur in the morning to give space for the peak PV generation around noon to limit the power export and economic losses due to curtailment. Allowing the battery to interact with the grid might impact the self-consumption of the system as excess PV, that could have been stored in the battery, might be replaced by grid energy. The economic benefit with such a dispatch algorithm is dependent on a numerous of factors, such as price differentiation between bought and sold energy, the presence and size of peak power tariffs and curtailment limits.

2.3.1.3 Alternative Battery Dispatch Algorithm

Taking the electricity price and power tariffs into consideration when setting the operating strategy for the battery dispatch can have an impact on the systems economic performance as concluded by [58] where a capacity dependent tariff is introduced and the annual cost savings with this type of operation is compared to a reference cases without storage and the conventional ”TZ” strategy.

Ideal battery dispatch could be achieved if it would be possible to have a perfect knowledge of the coming PV generation, electrical load demand and electricity price fluctuations. In [59], a 24 h day-ahead rolling horizon approach was used to forecast PV generation and load demand with an hourly time resolution with the aim of minimising the electricity bill with regards to price tariffs and system self-consumption. The outcome is also compared to a relay-based operation with the objective to maximise the self-consumption and a reference case without any battery storage. The study concludes that the forecast-based operation can generate economical savings by feeding the grid during times with high prices and storing excess PV energy during hours with high production and lower electricity prices. On the other hand, forecasting errors leads to higher grid imports to the battery and thus a reduction in the system's self-consumption.

2.4 Electrical System Topologies in Single-Family Houses

In this study, two different system topologies for electrical distribution in buildings are studied–AC and DC distribution. Below, the two topologies are presented when PV and battery storage are included and explain more in detail.

2.4.1 AC Topology

Apart from very rural areas without a common electrical grid, AC-supply is today totally dominating the electric power supply in all types of buildings. Figure 2.4 shows such a typical AC topology for a residential building, in this case also equipped with solar PV and battery storage. Here, loads a separate into ”big” and ”small” depending on their maximum power demand. In Figure 2.4 it is assumed that all

loads are operated on DC at their final stage. The AC/DC conversion for the loads is made in two steps–firstly rectification (AC/DC) and then DC/DC conversion to the desired DC voltage level [60,61]. The DC/DC conversion (see dashed perimeter) is typically done using a PFC (Power Factor Correction) converter.

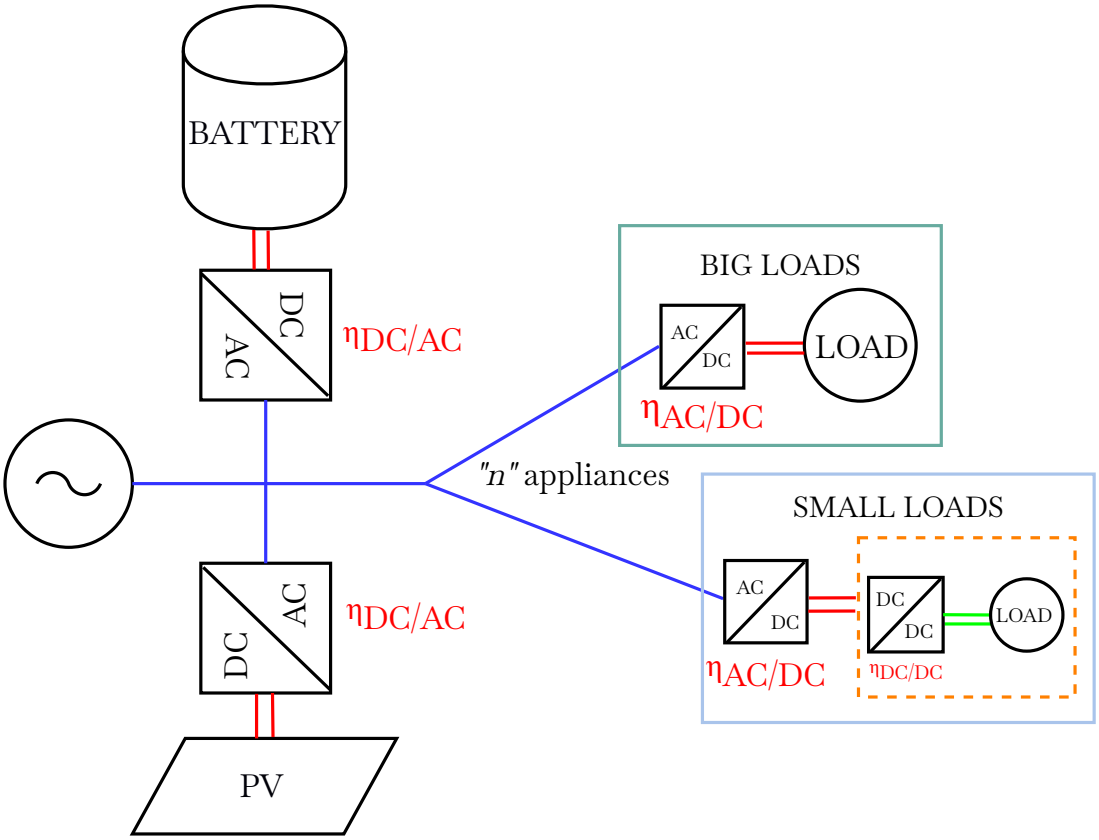

Figure 2.4: Typical AC topology with a PV and battery system with AC and DC where the rectification (AC/DC) and DC/DC conversion is done within the appliances.

A worst-case scenario from Figure 2.4, of maximum conversion steps, is when excess PV (converted as DC/AC) is stored in the battery through two conversions; AC/DC and DC/AC, and then supplied to the smaller loads with an additional two conversions steps–AC/DC and DC/DC–which would give the following five conversion steps[8]

$$p_{load} = p_{pv} \cdot \eta_{DC/AC} \cdot \eta_{AC/DC} \cdot \eta_{DC/AC} \cdot \eta_{AC/DC} \cdot \eta_{DC/DC} \tag{2.8}$$

Furthermore, PV is generated as DC and battery storage is also done as DC, and they are both AC-coupled in this topology, i.e. connected to the main AC link. An alternative approach, that is starting to become popular, is that the DC sources, i.e. battery and PV array could be connected to a separate DC link as presented in [16]. Still, converters are needed, however, the losses of a DC/DC converter are lower compared to the one of an AC/DC converter.

[8] Please refer to the online version or a color-printed version for a better visualisation of the step-wise conversions.

2.4.2 DC Topology

Compared to the AC topology in Figure 2.4, an equivalent DC topology is seen in Figure 2.5 with a DC-coupled PV and battery system and with a grid-tied bi-directional converter. Unlike the AC system, the rectification from the AC grid is done centrally for all import/export and the distribution is made throughout the system using DC. Larger loads (heating, stove, dish washer, etc.) are proposed to operate directly from the main DC bus and the smaller loads (lighting, multimedia, fridge/freezer, etc.) are fed from the main DC bus voltage or, alternatively using a lower sub-voltage level, via an additional DC/DC converter. The dashed perimeter in the two topologies are considered equal, where the DC/DC step is used for low-power appliances. As PV generation and battery storage is done as DC, the rectification stages are removed in the DC topology, reducing the losses.

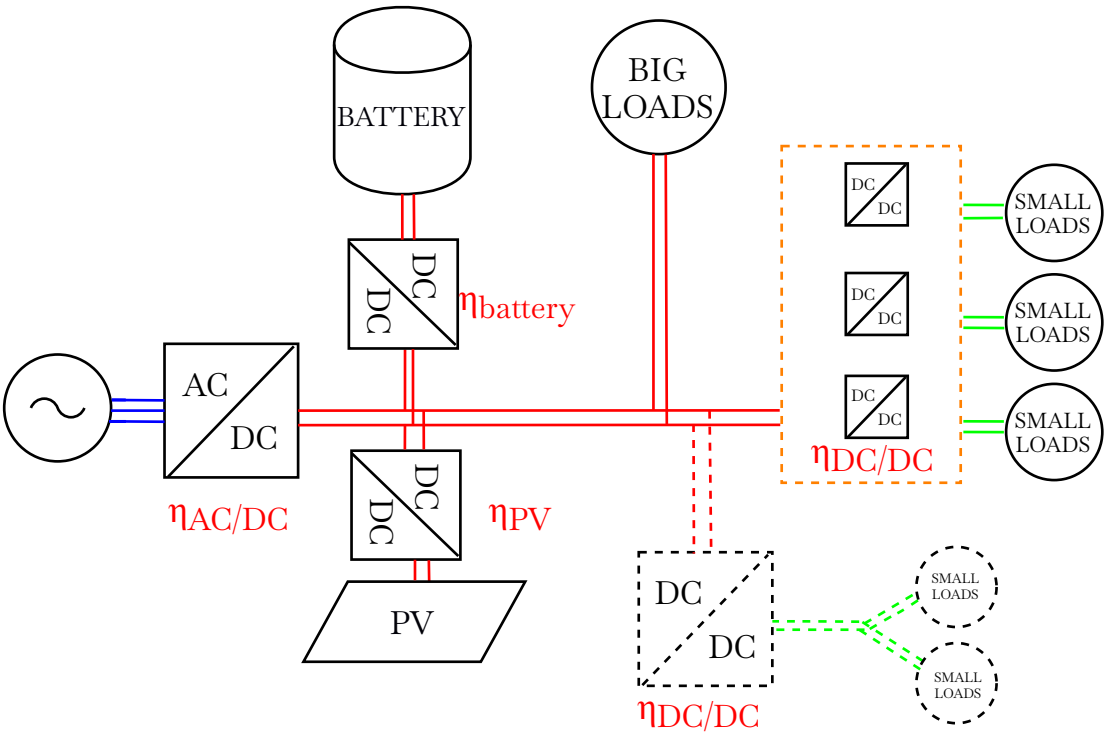

Figure 2.5: Example of DC system topology with two DC voltage levels including PV array, battery storage and bi-directional AC/DC converter, with the following colour coding for distribution: AC, 380 VDC and 24/48 VDC. Dashed perimeter for the DC/DC conversion at the smaller loads is done using a PFC and is treated equally for both the AC and DC topologies in this study, see also Figure 2.4. Dashed DC/DC conversion is the case where voltage distribution is done at a sub-voltage DC level for the "n" number of low-power appliances via a central converter.

In the DC topology, more of the generated PV is stored in the battery and better utilised due to the lower losses, compared to the AC typology seen in Figure 2.4. Using the same example as for the AC-topology above, see (2.8), where PV energy is first stored in the battery before being supplied to the smaller loads, the

equivalent conversion steps are reduced from five to four steps as follows[9]

$$p_{load} = p_{pv} \cdot \eta_{DC/DC} \cdot \eta_{DC/DC} \cdot \eta_{DC/DC} \cdot \eta_{DC/DC} \tag{2.9}$$

where the last low-power DC/DC conversion is the same for both the AC and DC topology as seen by the dashed perimeters in Figures 2.4 and 2.5.

2.5 Battery Modelling

Below is the theory for three different battery loss representations presented–ohmic, constant round-trip efficiency and an equivalent battery circuit.

2.5.1 Ohmic Losses

A commonly used battery loss representation is to consider the internal resistance and current throughput. The battery current, i_{batt}, varies with the power charged or discharged, p_{batt}, and the instantaneous battery voltage, u_{batt}, where the latter is mainly governed by the battery's SOC level. The battery current for each time step, "t_k", is related to the power and battery voltage as

$$i_{batt}(t_k) = \frac{p_{batt}(t_k)}{u_{batt}(t_k)} \tag{2.10}$$

To capture the losses as a function of the battery current throughput, $i_{batt}(t_k)$, for any time step, t_k, the following relations are used, which gives a loss dependency as a function of the battery current throughput

$$p_{loss,\ ohmic}(t_k) = R_0 i_{batt}^2(t_k) \tag{2.11}$$

and

$$E_{loss,\ ohmic} = \sum_{t=t_{k1}}^{t_{k2}} p_{loss,\ ohmic}(t_k) \tag{2.12}$$

where R_0 is the battery's internal resistance value and the total losses, $E_{loss,ohmic}$ are summarised for the time period t_{k1}–t_{k2}. With this approach the battery's ohmic losses, $p_{loss,\ ohmic}$ is dependent on the current throughput, which in turn is related via the ratio of power and battery voltage from (2.10).

2.5.1.1 Dynamic Resistance

Batteries have an internal resistance dependency as a function of its current throughput due to, amongst other reasons, the hysteresis caused by the chemical reaction during charge and discharge. In [35], a measured example is given, providing the battery's internal resistance variation with the current throughput, meaning that a constant internal resistance representation as presented in Section 2.5.1 might only be valid for a certain operating range. Accordingly, a methodology taking this effect

[9] Please refer to the online version or a color-printed version for a better visualisation of the step-wise conversions.

into account would be favourable to use. In this article, the current-dependent resistance value is found by measuring the voltage-current ratios for different charging rates, i.e. C–rates, and in this way it is possible to establish the internal resistance variation as a function of current throughput, $r(i_{batt})$, using the following relation

$$r(i_{batt}) = \frac{u_{charge}(i_{batt}) - u_{discharge}(i_{batt})}{2i_{batt}} \tag{2.13}$$

where $u_{charge}(i_{batt})$ and $u_{discharge}(i_{batt})$ are the charge and discharge voltages at a certain battery SOC level for the current i_{batt}. The losses can then be calculated according to (2.11) considering the variation of the internal resistance as a function of current throughput as

$$p_{loss,\ dynamic}(t_k) = r(i_{batt})i^2_{batt}(t_k) \tag{2.14}$$

and

$$E_{loss,\ dynamic} = \sum_{t=t_{k1}}^{t_{k2}} p_{loss,\ dynamic}(t_k) \tag{2.15}$$

2.5.2 Constant Round-Trip Efficiency

Common in literature, that is not within the electro-technical genre, is to use a constant battery efficiency when studying the performance of a PV and battery system. Here follows a brief definition of the used relations. Constant charge and discharge efficiency's, η_{charge} and $\eta_{discharge}$ respectively are defined in [62, 63] as

$$\eta_{charge}(t_k) = \frac{\Delta Q(t_k)}{Q_{charge}(t_k)} \tag{2.16}$$

$$\eta_{discharge}(t_k) = \frac{Q_{discharge}(t_k)}{\Delta Q(t_k)} \tag{2.17}$$

where, $\Delta Q(t_k)$ is the change in battery capacity (Wh), and $Q_{charge}(t_k)$ and $Q_{discharge}(t_k)$ the charged and discharged energies respectively at time "t_k".

The fixed battery round-trip efficiency, $\eta_{batt}(t)$, without considering any throughput dependency (current profile), is defined for instance in [62, 63] using (2.16) and (2.17) as

$$\eta_{batt} = \eta_{charge} \cdot \eta_{discharge} = \frac{Q_{discharge}}{Q_{charge}} \tag{2.18}$$

Total battery losses, assuming a fixed round-trip efficiency and identical start and end battery SOC levels, are given as the difference in charged and discharged powers as

$$E_{loss,\ fixed} = \int_0^T u(t)i_{charge}(t)dt - \int_0^T u(t)i_{discharge}(t)dt \tag{2.19}$$

defined for time period "T". As mentioned above, the same constant charge and discharge currents are assumed.

2.5.3 Equivalent Battery Circuit Model

In case quicker phenomena are to be studied, on a second or fraction of a second time scale, an equivalent circuit approach can be used [64,65]. The equivalent circuit model (ECM) of a battery can be represented with an ideal inductor, L, a series resistance, R_0, and parallel connected resistance and capacitor (RC) elements. The equivalent impedance, Z_{RC}, of the circuit can be expressed as

$$Z_{RC}(\omega) = j\omega L + R_0 + \sum_{i=1}^{n} \frac{1}{1/R_i + j\omega C_i} \tag{2.20}$$

where ω equals 2πf, and the number of adequate RC elements "n" is determined when studying the characteristics and through a curve fit of (2.20) to the measured data. The equivalent circuit model can also be seen in Figure 2.6 for 'n' number of parallel RC links.

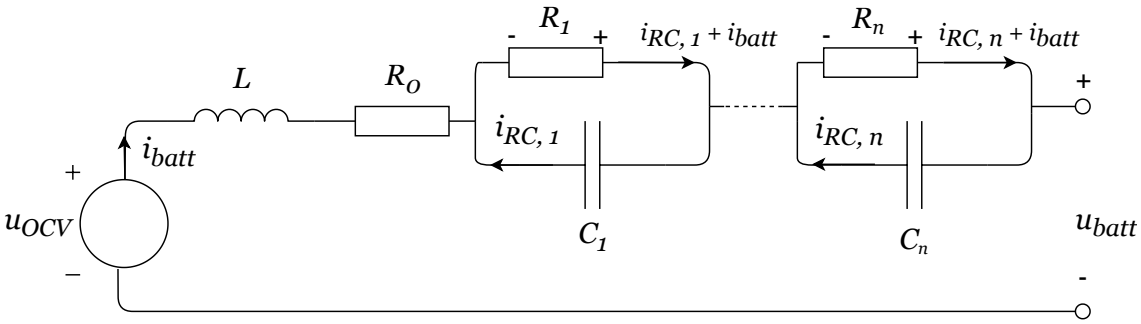

Figure 2.6: Principle design of equivalent battery circuit with inductance, L, series resistance, R_0, and n parallel circuits with resistance, R, and capacitance, C.

The battery losses for the ECM battery representation are calculated by summarising the losses through the series resistance and all modelled RC links in Figure 2.6 as

$$p_{loss,\ RC}(t_k) = \sum_{t_k=t_{k1}}^{t_{k2}} \left(R_0 i_{batt}^2(t_k) \ + \ \sum_{n=1}^{n} R_n [i_{R,\ n}(t_k) + i_{batt}(t_k)]^2 \right) \tag{2.21}$$

with i_{batt} as the total battery current throughput and $i_{R,n}$ the current through each parallel resistance, R_n.

2.6 Electrical Losses in Buildings

There are two types of electrical losses in buildings–conduction and conversion–and their theory are explained in the following two sub-chapters. Conduction losses occur from the power transferring in the cables and conversion when voltage levels, or form (AC, DC), are altered. In this study, three converters are used and presented below: buck (DC/DC) converter, PFC (Power Factor Correction) converter and an H-bridge rectifier/inverter.

2.6.1 Cable Conduction Losses

For binary loads, with ON/OFF operation, and the power demand, p_{load}, the conduction losses, p_{cond}, in the cables at the discrete time step "t_k" can be expressed as

$$i_{load}(t_k) = \frac{p_{load}(t_k)}{u_{load}(t_k)} \tag{2.22}$$

$$p_{cond}(t_k) = i_{load}(t_k)^2 R = \left(\frac{p_{load}(t_k)}{u_{load}(t_k)}\right)^2 R \tag{2.23}$$

where u_{load} and i_{load} as the system voltage and current respectively. The cable resistance, R, is given as

$$R = \rho \frac{l}{A} \tag{2.24}$$

where ρ is the resistivity of the cable material, l the "one-way" feeder length of the cable and A the cable's cross-section area. The selection of conducting area is done according to thermal considerations. For a building, the required cross-section area can be found using the IEC 60228 standard [66] according to Table 2.2.

Table 2.2: Standardised cable cross-section area as a function of current throughput according to IEC 60228

Current [A]	**Cross section [mm^2]**
6	0.75
10	1.5
16	2.5
20	4
25	6
34	10
45	16

The power losses for the electrical cable are found as

$$p_{cond}(t_k) = 2Ri(t_k)^2 \tag{2.25}$$

where the resistance, R, is determined from (2.24). The factor "2" is due to the return conductor. 3-phase internal distribution withing buildings is limited, unless it is a multi-family house, commercial building, industry, etc., then the conduction loss is given as

$$p_{cond,\ 3-\phi}(t_k) = 3Ri(t_k)^2 \tag{2.26}$$

2.6.2 Conversion Losses

Conversion losses occur when voltage level, or form (AC, DC), are altered and, in this thesis are due to power electronics. These losses can be divided into two separate parts; conduction and switching losses, where the former occurs in during conduction and the latter during the switching (as a function of the switching frequency, f_{sw}).

In this Section, the underlying theory and brief explanations of the power electronic components used in this study are introduced to the reader but will not be studied more in detail in this work.

2.6.2.1 Components – Diode & Transistor (MOSFET & IGBT)

Figure 2.7 shows the symbols and functionality of a diode (Figure 2.7a) and transistor (Figure 2.7b). The ideal diode conducts whenever a positive voltage, v, is applied over it. Similarly, the transistor–here a MOSFET (Metal Oxide Semiconductor Field Effect Transistor)–conducts when there is an ON-signal to the gate. These ideal components have no voltage drop over themselves when they are conducting and no leakage currents when they are off.

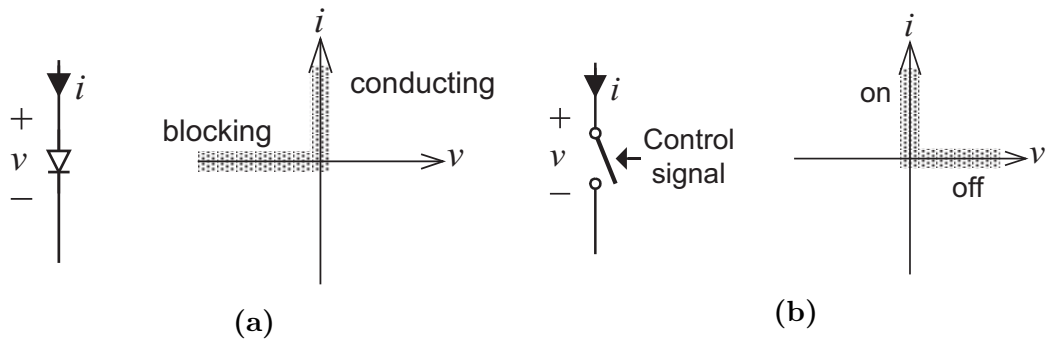

Figure 2.7: Symbol and functionality of an ideal diode **(a)** and transistor **(b)**.

In the non-ideal state, the diode has a forward voltage drop during conduction. Figure 2.8 shows an example of its realistic i-v characteristics that also shows the reverse blocking region that prevents reverse voltage breakdowns, i.e. backwards conduction.

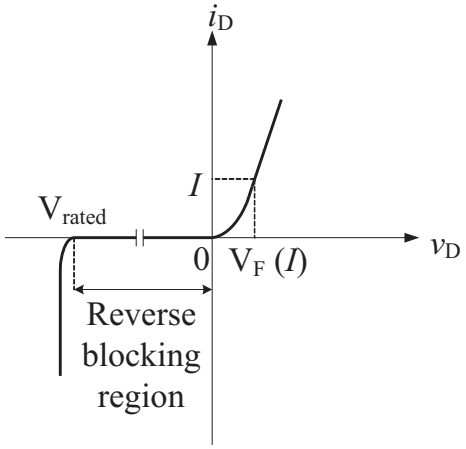

Figure 2.8: Current-voltage characteristics of non-ideal diode.

Figure 2.9 shows the symbols (Figure 2.9a) and non-ideal i-v characteristics (Figure 2.9b) of a MOSFET. For higher power applications an IGBT (Insulated

Gate Bipolar Transistor) is used. Similar to the MOSFET transistor, its conduction is controlled via the gate, "*G*". Its symbol, ideal and non-ideal characteristics are shown in Figures 2.10a–2.10c respectively.

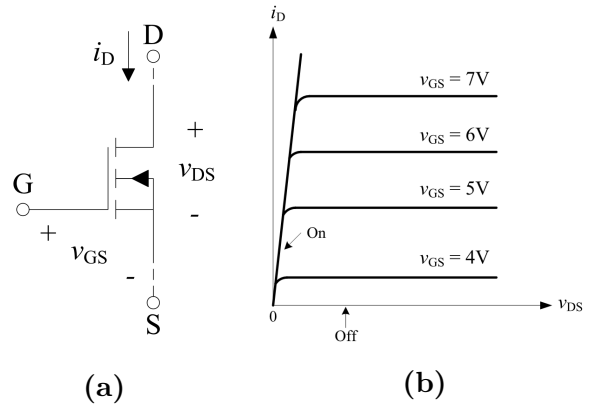

Figure 2.9: Symbol **(a)** and *i-v* characteristics **(b)** of a MOSFET.

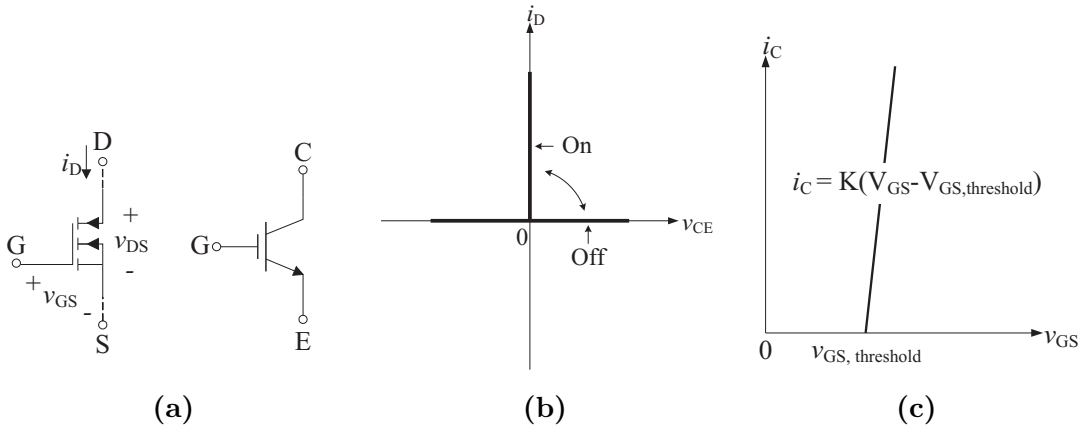

Figure 2.10: Symbol **(a)**, ideal characteristics **(b)** and non-ideal characteristics **(c)** of an Insulated Gate Bipolar Transistor (IGBT). With: "G" = Gate, "D" = drain, "S" = source.

This means that there are losses from the components every time the current passes through them, i.e. conduction losses. In addition, there are also losses when the components turn ON and OFF, i.e. switching losses. In a converter, which is made up from semiconductors like diodes and transistors, the semiconductors are the dominating ones.

2.6.2.2 DC/DC Converter

There are in principle two basic converter types used for DC/DC conversion–Step-down (**buck**) and Step-up (**boost**) converters. Other variants of DC/DC converters, e.g. Step-down/step-up (buck-boost) and Cúk and Full-bridge converters are all derived from the buck and boost topologies. The working principle for a switch-mode DC/DC converter is to transform the input DC voltage to a desired output

voltage level by controlling the switching cycles, i.e. their ON and OFF periods. Figure 2.11 shows the circuit diagram of a buck converter that steps-down the input voltage, V_d, to the desired output voltage, V_o. Either the green or red current flows, however only one component has current through it at the same time.

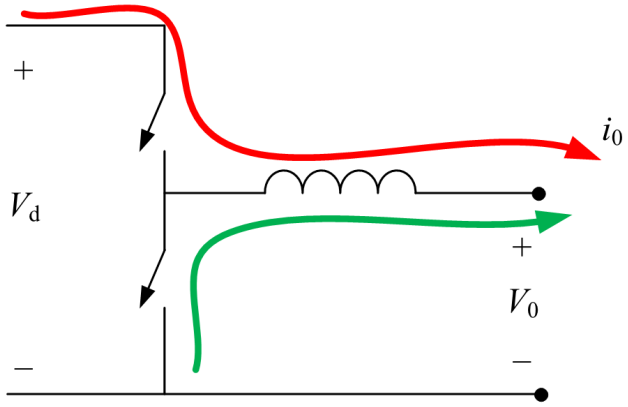

Figure 2.11: Buck (step-down) converter for voltage conversion.

In this study, a DC/DC converter is used between the PV array and battery, and the main DC link.

2.6.2.3 Rectifiers and Inverters

Conversion of voltage levels and between AC and DC can be done in a multitude of ways. In this study, a non-galvanically-isolated approach is used for the bi-directional units, i.e. AC/DC and DC/AC conversion. One way of doing this is using a so-called H-bridge if galvanic isolation is not needed, which is derived from the step-down converter. Figure 2.12 shows the operating principle for such a rectifier using four switching elements. Here, the upper-left (S_1) and lower-right (S_4) switches are working in pair, and similarly the top-right (S_2) and lower-left switches (S_3). For the first cycle ($0 < t \leq \pi$)–see red current path–switches S_1 and S_4 are conducting and S_2 and S_3 are reversed biased. Similarly, during the second cycle ($\pi < t \leq 2\pi$), S_2 and S_3 are conducting–green current path–and the other two switches are reversed bias.

Compared to the buck converter in Figure 2.11, where current only passes through one semiconductor, the current in the H-bridge must pass through two semiconductors and thus generate more losses. Here, only two current paths are displayed. However, there are two more states, also having the current passing through two semiconductors.

The single-phase H-bridge can also be used as an inverter where the input DC signal is converter to AC output using any of these three modulation types[10] [67],

1. Pulse-with-modulation (PWM),
2. Square-wave modulation,
3. Single-phase inverters with voltage cancellation

[10]For voltage source inverters (VSI).

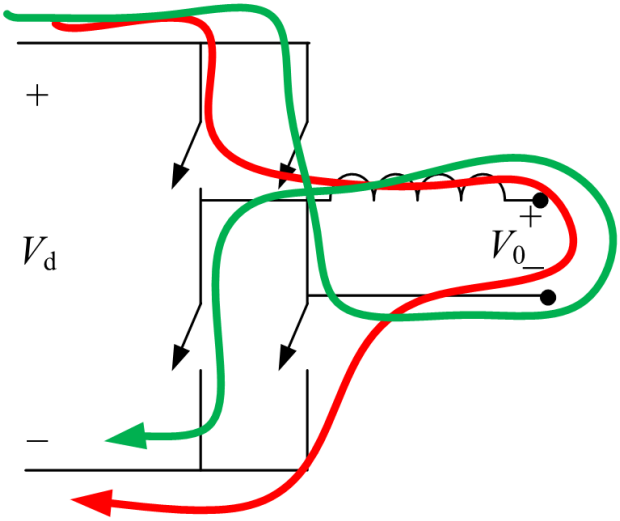

Figure 2.12: Single-phase H-bridge rectifier, where red and green lines are current paths, V_d is input voltage and V_o the output voltage.

An example of its usage–related to this study–is the conversion from the solar photovoltaic output to usable AC for the residential household distribution system. This conversion is associated with losses, and the efficiency can be expressed as

$$\eta_{DC/AC}(t_k) = \frac{p_{AC}(t_k)}{p_{DC}(t_k)} \tag{2.27}$$

with $p_{DC}(t_k)$ as the DC input and $p_{AC}(t_k)$ the AC output. In this study, the H-bridge is used for conversions between single-phase AC, the battery and the PV array.

The PFC (Power Factor Correction) circuit is widely used for rectification of single-phase AC. Figure 2.13 shows the circuit diagram of a PFC converter where rectification (AC/DC) of the input AC is firstly done using the four diodes (two switch pairs), before the step-up converter stage where the output signal is filtered. If the output capacitance, C_d, is large enough, the output voltage, v_d, can be assumed to be DC, i.e. $v_d(t) = V_d(t)$.

The output voltage of the PFC converter is around 380–400 VDC, and this is one of the reasons why the proposed DC topology typically have this voltage level. Typically, the PFC is used for the smaller loads. For higher powers, a three-phase converter is used, see [67]. In this work, the grid-tied converter seen in Figure 2.5 has this design.

2.6.3 Converter Loss Determination

Loss determination can be done using two, in principle, different methods; electrical and calorimetrical, and their theory is explained in the two following sub-sections.

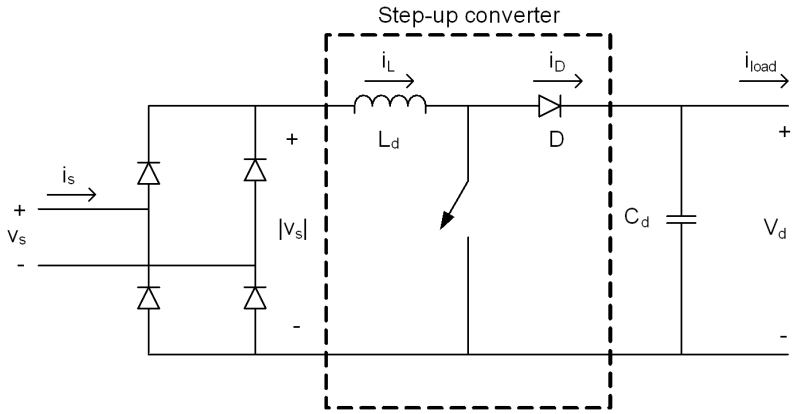

Figure 2.13: Circuit diagram of a PFC (Power Factor Correction) converter with a full-bridge rectification and step-up converter for output filtering.

2.6.3.1 Electrical Loss Determination

To determine the losses from a voltage conversion, the input and output quantities can be measured, and the difference is the losses. Single-phase AC and DC powers are calculated in each time step "t_k" as

$$p_{AC}(t_k) = u_{AC}(t_k) i_{AC}(t_k) \tag{2.28}$$

$$p_{DC}(t_k) = u_{DC}(t_k) i_{DC}(t_k) \tag{2.29}$$

where $u_{AC}(t_k)$ and $i_{AC}(t_k)$ are the AC voltage and current, and $u_{DC}(t_k)$ and $i_{DC}(t_k)$ the DC equivalents.

The conversion efficiency, assuming AC/DC conversion is calculated using (2.28) and (2.29) as

$$\eta_{conv,\ AC/DC}(t_k) = \frac{p_{DC}(t_k)}{p_{AC}(t_k)} \tag{2.30}$$

The corresponding conversion losses are then calculated as

$$p_{conv}(t_k) = \Big(1 - \eta_{conv,\ AC/DC}(t_k)\Big) p_{load}(t_k) \tag{2.31}$$

where $p_{load}(t_k)$ is the converter power throughput for each time instance.

In [68] the DC/AC inverter efficiency is expressed as a function of inverter loading as

$$\eta_{inv}(t_k) = \frac{p(t_k)}{m \cdot p(t_k)^2 + p(t_k) + p_0} \tag{2.32}$$

with p_0 and m calculated from the efficiencies at 10 and 100% loadings, see [68] for numerical values, and $p(t_k)$ the loading ratio at each time step, "t_k", as

$$p(t_k) = \frac{p_{out}(t_k)}{P_{rated}} \tag{2.33}$$

where $p_{out}(t_k)$ is the inverter output and P_{rated} the rated power of the inverter.

2.6.3.2 Calorimetric Loss Determination

Calorimetric tests can be used to accurately determine the losses from a component/system, where the heat dissipation from a device in a controlled environment is measured [69, 70]. The controlled environment usually consists of a thermally insulated containment that is cooled via a liquid cooling system. The heat dissipated from the DUT (device under test) can be determined as

$$p_{loss} = c_p v \rho \Delta\vartheta \tag{2.34}$$

where c_p is the specific heat capacity of the transfer medium, v the flow rate, ρ the density of the transfer medium and $\Delta\vartheta$ the temperature difference between inlet and outlet of the closed loop.

2.7 Photovoltaic Systems

Today's conventional photovoltaic (PV) systems are made up of two essential components: modules and inverter(s). Where the power generation is done in modules, as DC, and then transformed to AC in the inverters before being distributed further.

2.7.1 Photovoltaic Module Technology

Today's market of photovoltaic (PV) modules consists of two major types: thin film and crystalline silicon, where the latter can be divided into mono and multi (poly) crystalline cells. The crystalline silicon technology made up almost the entire market in 2018, with 50% made from multi crystalline, 47% of mono crystalline cells and the remaining 3% from thin film solar cells [3]. In addition to these types, there are also other technologies, such as perovskites, organic and inorganic cells, Grätzel (dye sensitized), advanced multi-junction types, etc.

Figure 2.14 shows the voltage and current characteristics for a typical crystalline PV module, and the resulting power outputs, at different cell temperatures. Notable is the temperature dependency observed, where an increase in temperature leads to a lower power output.

The PV power output, P_{DC} is calculated as

$$P_{DC,\ max} = I_{DC} U_{DC} \tag{2.35}$$

where I_{DC} and U_{DC} are the output current and voltage respectively.

2.7.1.1 Crystalline Silicon Solar Cells

These types of modules are made from two different types of solar cells: mono- or multi-crystalline (poly) cells. They are both made from the same material (silicon) and the only difference is the manufacturing process, where the mono type is cooled down in a controlled process, forming a single crystal, unlike the poly type where the cooling period is more rapid and thus results in a multi crystal formation. The mono-crystalline modules are more expensive than the multi ones but also has a higher

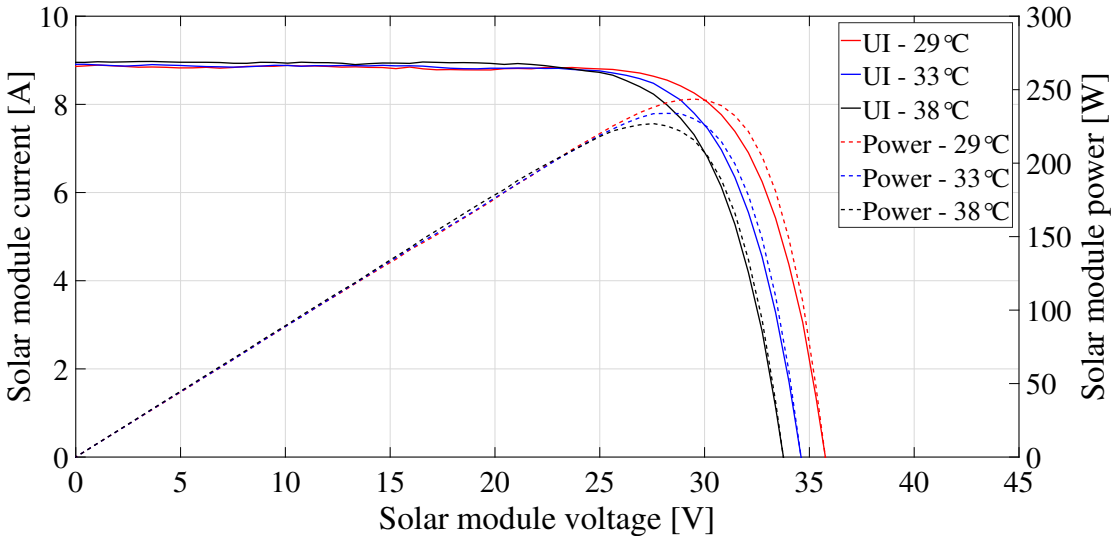

Figure 2.14: Typicall voltage and current (UI) characteristics from measurements and corresponding power outputs for a PV module at different temperatures at an irradiance of 1000 W/m^2. Results are presented from three cell temperatures to show the temperature dependency.

efficiency[11]. Visually, they are easily distinguished by looking at the shape of the individual cell, where the mono-crystalline cells have the rounded edges, assembling and octagon, while the poly-crystalline cell is shaped as a rectangle with four sharp edges. Typically, the power output of today's crystalline silicon modules ranges from 250–350 Wp output at STC conditions[12]. Crystalline cells can also be assembled in so-called bi-facial modules that generates energy for both sides [71]. By using the direct irradiance from the front and reflected irradiance on the back, it can produce up to 20% more energy than the conventional crystalline modules [72].

2.7.1.2 Thin Film Solar Cells

Thin film solar cells are made of semiconductors attached to glass, plastic or metals. The three most common types of thin film solar cells are: cadmium telluride (CdTe), amorphous silicon (a-Si) and copper indium gallium (di)selenide (CIGS). The cells themselves are often 20 times thinner than the crystalline cells making them lightweight and flexible. These properties of the thin film enable them to be integrated in building structures and elements in so-called building integrated photovoltaic (BIPV), which offers symmetric and aesthetically appealing installations. Other advantageous of thin film solar cells is the less prominent temperature dependency–as seen in Figure 2.14 for a crystalline cell–which means that an increase in temperature reduces the performance [73], and a better ability to convert diffuse irradiance–e.g. during cloudy days–than crystalline cells [74].

[11] Best research-cell efficiencies recorded - https://www.nrel.gov/pv/assets/pdfs/best-reserch-cell-efficiencies.pdf

[12] Standardised Test Conditions (STC) is at 1000 W/m^2 and 25°C cell temperature with an air mass 1.5 (AM 1.5).

2.7.2 PV Inverter Technology

There are two main operating functions of a solar inverter: (i) transform generated DC power to AC and (ii) at each moment load the module optimally to withdraw maximum power (e.g. Maximum Power Point Tracking, MPPT). These two functions are usually integrated into the same equipment in centralised inverters. Each inverter in the system is connected to one or more strings where each string consists of multiple solar PV modules connected in series. An inverter can also have multiple MPPT's, each with its own input. Multiple MPPT's are useful for systems with modules/strings working at different operating conditions, e.g. caused by shading. A solar PV system can consist of one (or many) central inverters with multiple MPPT's for several of modules, or each solar PV module can have its own micro inverter, allowing for totally independent operation of each module. Systems with micro inverters on each PV module are less prominent to module mismatches (e.g. caused by module shading). A third option is individual optimisers at each (or multiple) modules but with a centralised unit for DC/AC transformation.

Solar inverter efficiency can be expressed in three different ways

- Peak efficiency expressed at optimal power output
- European efficiency, η_{EU}, is a weighted number considering how often the inverter will operate at different power outputs. It is sometimes more useful than peak efficiency as it considers how the inverter performs at different output levels during varying conditions.
- California Energy Commission efficiency, η_{CEC}, is also a weighed efficiency, like the European efficiency, but it uses different values for the weighing factors.

A solar inverter's conversion efficiency, η_{conv}, is the ability to transform the produced DC energy to AC and is expressed as

$$\eta_{conv} = \frac{p_{out}}{p_{in}} = \frac{p_{AC}}{p_{DC}} \tag{2.36}$$

where p_{AC} is the AC output after the transformation and p_{DC} the produced solar PV output from the modules.

The inverters ability to control the load for maximum solar output at each instance, regardless of the insolation intensity, is called Maximum Power Point Tracking (MPPT) efficiency and is expressed as

$$\eta_{MPP} = \frac{p_{DC}}{p_{MPP}} \tag{2.37}$$

where p_{MPP} is the maximum theoretical power output and p_{DC} the actual power output.

The inverter's overall efficiency, η_{inv}, can be expressed using (2.36) and (2.37) as

$$\eta_{inv} = \eta_{conv}\eta_{MPP} \tag{2.38}$$

The overall efficiency for an inverter is dependent on the actual power output and thus the insolation. The annual overall efficiency can therefore be expressed for two different cases, EU or California weighted efficiency as explained above. The main difference between the European and CEC efficiency's is that the assumptions

about the occurrence of each power levels for an inverter and are based on the data for Central Europe in the former case, and California in the latter [75]. The respective efficiencies can be expressed as

$$\eta_{EU} = 0.03 \cdot \eta_{5\%} + 0.06 \cdot \eta_{10\%} + 0.13 \cdot \eta_{20\%} + \\ + 0.10 \cdot \eta_{30\%} + 0.48 \cdot \eta_{50\%} + 0.20 \cdot \eta_{100\%} \tag{2.39}$$

$$\eta_{CES} = 0.04 \cdot \eta_{10\%} + 0.05 \cdot \eta_{20\%} + 0.12 \cdot \eta_{30\%} + \\ + 0.21 \cdot \eta_{50\%} + 0.53 \cdot \eta_{75\%} + 0.05 \cdot \eta_{100\%} \tag{2.40}$$

where $\eta_{X\%}$ is the efficiency's at different inverter loadings.

2.8 National & International PV Markets

The PV market penetration is under-going rapid expansion; in both the Swedish and international market, driven by rapid price reductions, technological developments and a global energy awareness in the light of the present climate changes. Below are brief summaries of the domestic and international market developments, showing some figures quantifying the expansion, capacity and penetration.

2.8.1 Sweden

Data on sold and accumulative solar PV capacity in Sweden is summarised in [4] for the period 1992–2018. This data was collected via direct communication with the sales companies up until 2016 and thereafter through reporting from the grid operators.

The installation rate of solar PV is continuously increasing in Sweden and during 2018 the domestic market grew by 59% compared to the year before. In absolute numbers the newly installed capacity in 2018 was 158.3 MW, compared to 84.7 MW in 2017. The biggest increase is seen in the 'Grid connected distributed' sector which is displayed in Figure 2.15. The main drivers for the large domestic market penetration were the introduction of the direct capital subsidy system in 2006 and last year's rapid system price reduction. The public's acceptance and last year's attempts to ease the regulations for micro-producers are other key factors in the PV system boom.

Despite last year's rapid growth in the domestic solar PV market the share of solar PV generated compared to total electricity generated was merely 0.3% in 2018 [4]. Electricity generation in Sweden is dominated by hydro and nuclear power– amounting to a total of close to 80% of the domestically generated energy in 2017, with 40.1% and 39.5% respectively [76]. The availability of the cheap hydro power generated in the northern part of Sweden determines how much of the more expensive generation that is needed to meet the total demand. Having much of the electricity production done by relatively low CO2 emitters, such as hydro and nuclear, together with a relatively low electricity price are two of the reasons why the PV market in Sweden started fairly late and is still small compared to other global markets.

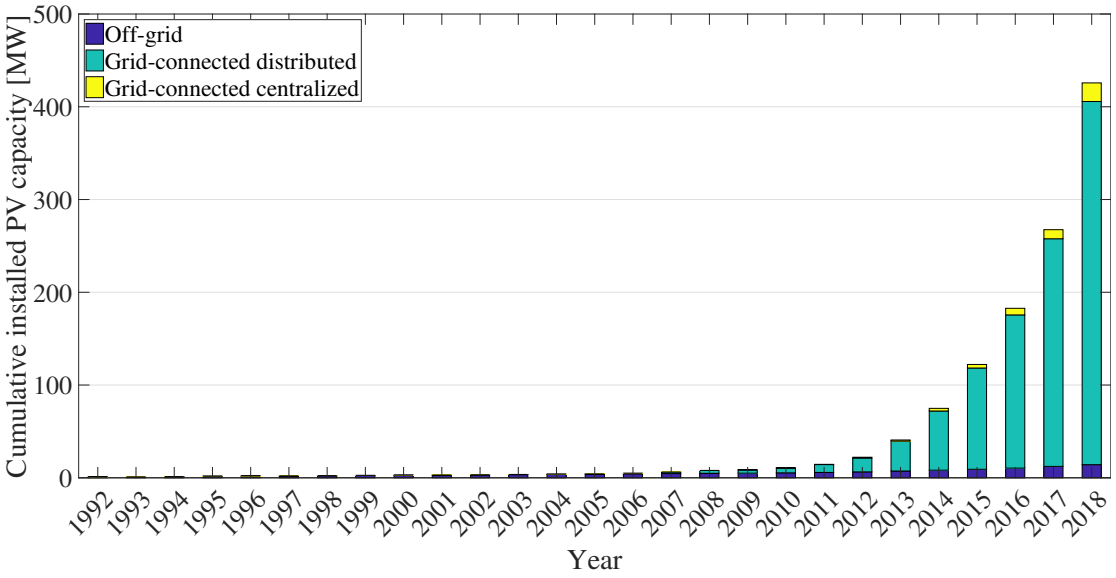

Figure 2.15: Swedish solar PV market development for the period 1992–2018

2.8.2 Internationally

Internationally, 2018 was a record-breaking year in terms of installed PV capacity, adding more than 100 GW, and with a cumulative installed capacity of over 512 GW [3]. The main contributors to this development were China (44.3 GW of installed capacity in 2018), India (10.8 GW), USA (10.7 GW) and Japan (6.7 GW). As acknowledged in the report from the International Energy Agency Photovoltaic Power Systems Programme (IEA-PVPS), an important growth is seen in the emerging PV markets in the Asia-Pacific region. With the accumulated capacity in 2018, PV energy is estimated to provide 2.9% of the global electricity supply. Top countries regarding PV penetration, in terms of total electricity generation in 2018, includes Honduras (11%), Italy (9.2%), Malta (9%), Germany (8.4%) [3]. Noteworthy is also our neighbours in Denmark with 3.2% and the massive market in China where 3.6% PV penetration.

3

Methodology

In order to evaluate DC-distribution in single-family houses a DC-distribution network is installed in a single-family building at RISE's premises in Borås. The building is called the RISE Research Villa. Further, topology model is developed for the villa, including PV-generation, battery storage and loads. Data from the Research Villa, Section 3.1, in combination with data from a replica building, Section 3.2–with a family living in it–is used as a base for the model. In Section 3.4 a description of the methodology and approaches used for the dynamic modelling of the performance gains is presented, when operating a DC distribution network for a single-family house. In Section 3.3 the methodology and methods used for the battery sizing for RISE's Research Villa is introduced.

Furthermore, Section 3.5 introduces the set-up made for the battery measurements and the methodology used for the evaluations together with the ditto for the power electronic components in Section 3.6.

3.1 RISE Research Villa – A Full-Scale Demonstration Site

RISE's Research Villa in Borås, Sweden, see Figure 3.1, was developed within an EU-FP7 collaborative project (NEED4B)[1] to demonstrate cost-effective and energy efficient technologies for design, construction and operation of very low energy buildings. As a part of the project a replica house was built in a neighbouring city for a family to live in, this to serve as a reference. These houses were equipped with measurement sensors to monitor and evaluate the energy performance. Sensors installed include (but are not limited to), temperatures, flow rates, energies and powers. The measurements are recorded with a 10 second sampling rate and are then average to 15-minute values.

RISE's Research Villa is equipped with 14 solar PV panels (at 260 Wp each) with an annual electricity generation (AC) of approx. 3100 kWh. Heating of the house is done via a ground-source heat pump (with an external storage tank of 100 litres) and an FTX ventilation unit (forced ventilation in all rooms with heat recovery).

[1] More information about the villa can be found here: http://need4b.eu/?lang=en

Figure 3.1: RISE Research Villa in Borås, Sweden used for demonstrating the DC system operation with Solar PV, battery storage and DC operated loads.

3.1.1 DC System Topology in RISE Research Villa

As a part of this study, a DC distribution network was installed in the Research Villa. The local direct current (DC) distribution system consists of both a uni- and bipolar voltage supply at 380 and 760 VDC respectively, see Figure 3.2. A comment here is that 760 VDC is used more than what is generally the case in the continuation of this work. External energy supply to the internal DC network is done via the bi-directional AC/DC converter that is connected to the external AC grid, where the 230 VAC is rectified to bipolar ±380 VDC. Energy is also generated and stored using the PV array and battery respectively. In the demonstration, two loads, a heat pump and a ventilation unit, are connected to the 380 VDC link.

3.2 NZEB Replica Building

Measured load demand and PV generation are also taken from a replica building in a neighbouring city–having the same energy performance and layout–but with a family living in it. Measured load data from household appliances are taken from this building as well as measured data for the AC topology for electrical load and PV generation with a temporal resolution of 15 minutes for an entire year, see Figure 3.3a, and used as a basis for this study and the model presented below. Total load demand for this case is 6208 kWh and PV generation equals 3113 kWh. Figure 3.3b shows the daily energy usage and PV generation per day throughout the studied year of 2016, where it can be noted that there is a higher energy demand during the

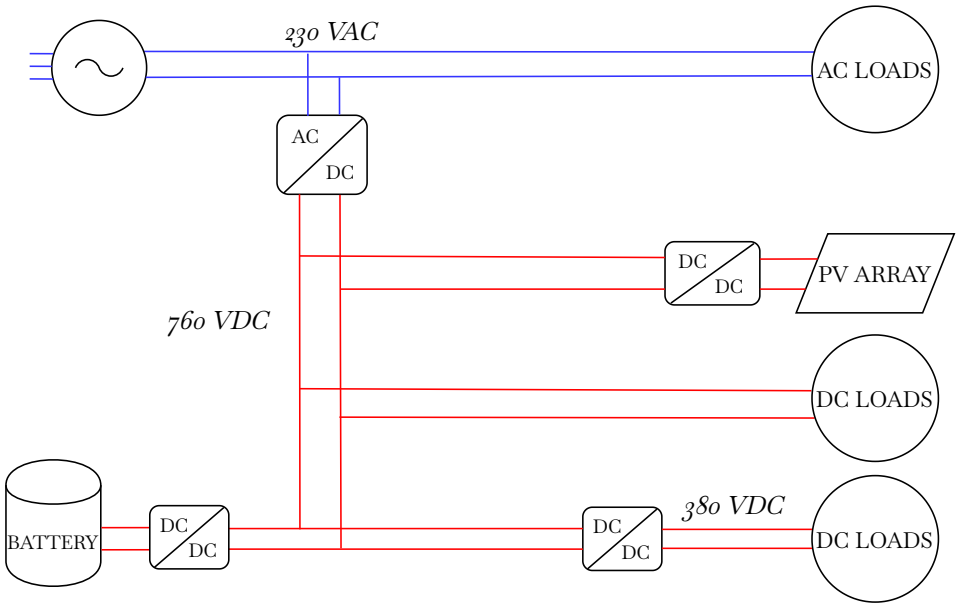

Figure 3.2: DC system topology for RISE Research Villa with a main DC voltage of 760 VDC and sub-voltage level of 380 VDC.

colder months, due to a larger heating demand, while the PV generation shows the opposite trend, with higher generation during the summer months. In Figures 3.3c and 3.3d the load and power from the PV panels are shown for a summer and winter day respectively to illustrate a discrepancy in load demand and PV generation.

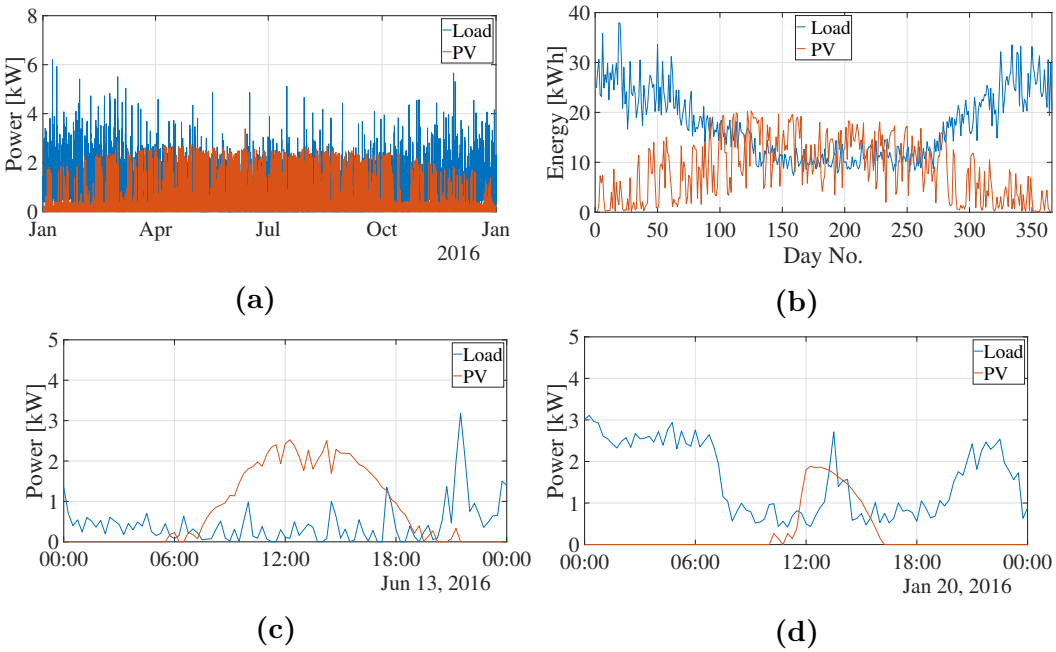

Figure 3.3: Measured load and PV generation data for the NZEB replica building; **(a)** 15-minute power, **(b)** daily energy sum of PV and load, and measured PV and load power for **(c)** June 13^{th} (summer) and **(d)** January 20^{th} (winter) day.

3.3 Applied Battery Modelling – Sizing & Dispatch Algorithm

Choosing the battery storage size for the demonstration project in the Research Villa, see Section 3.1, was done by modelling the effect on self-consumption (SC), self-sufficiency (SS) and peak power shaving of imported grid energy [77]. This was done via two separate methods, (i) using a built-in peak power shaving algorithm from SAM (System Advisory Model) and (ii) the "Target Zero" (TZ) algorithm adopted from [57]. The two dispatch algorithms from SAM–day-ahead (DA) and day-back (DB)–are both designed to decrease the peak power demand from the grid. In the day-ahead approach a clear foresight of the up-coming day's solar energy generated and load demand is assumed from the imported data. In the day-back approach the PV energy and load profile from the day before are taken as if it will be the actual data for the day in progress. Neither of these dispatch algorithms allows battery discharge to the grid. The "TZ" method is used to maximise the self-consumption (SC) and self-sufficiency (SS) of the generated solar PV energy by minimising imports from the grid. Load profiles were taken from one year's measurement with a 15-minute temporal resolution from the Research Villa in Borås and solar PV production was simulated using SAM's built-in function based on weather data input[2].

The selection of the battery size and dispatch algorithm, assuming a fixed PV array, was made by studying the impact on the system's self-consumption when different battery sizes were chosen. For all battery sizes, it was assumed that the battery's peak power was 80% of its energy capacity, i.e. for 7.5kWh the battery power equals 6kW.

3.4 Quasi-Dynamic Modelling of AC & DC Topologies

In this study, five cases are compared using the measured data of the load demand and PV generation together with the efficiency gains measured or found in the literature for the power electronic converters. The five modelled cases are:

- **230 VAC – Reference**
  Conventional system, with conduction losses from a 230 VAC voltage supply, see Figure 2.4 for system layout including PV and battery system.

- **DC_1 – 380 VDC**
  Conduction losses at 380 VDC. This voltage level is selected using the EMerge Alliance 380 VDC standard for data centre power distribution [78–80] and is also the result of an expert assessment of suitable DC distribution levels from [10]. This case is modelled for two system boundary scenarios:

[2] This was done since SAM cannot work with imported PV data

a) Bi-directional (grid-tied) conversion with a load dependent efficiency at the house's grid connection.
b) Bi-directional conversion done at a fixed efficiency of 97.8% [81–84] in the grid's sub-station.

- **DC_2 – 380 & 48 VDC**
  In addition to case DC_1, a sub-voltage level at 48 VDC is added to supply the smaller load via a central DC/DC converter[3]. The sub-voltage level is selected to be 'class A' voltage since these voltage levels are harmless, and thus, safety designs can be made cheaper[4].

- **DC_3 – 380 & 20 VDC**
  Same setup as case DC_2 but with a sub-voltage level at 20 VDC to supply the smaller loads and lighting directly. This sub-voltage level represents the supply voltage of the USB Type–C standard.

3.4.1 System Modelling

Based on the chosen cases from Section 3.4, the distribution cable's conduction losses for each application are calculated using (2.24) and (2.25) where the distribution in the AC case (case 1) is done at 230 VAC and for the DC cases (case 2–4) at 380, 48 and 20 VDC.

The bi-directional AC/DC converter in Figure 2.5 has a load dependent efficiency and modelled according to (2.32) for the DC case's[5] (cases DC_1–DC_3) whenever energy is exported/imported to/from the external AC grid. In the presence of PV generation, the bi-directional converter works both ways (assuming the same efficiency dependency) and supplies excess energy to the grid during times when the PV generation exceeds the load demand and when the battery is fully charged.

For all modelled cases where a battery is included, the voltage from the battery must be converted to the desired main link voltage, e.g. 230 VAC and 380 VDC for case $230VAC$ and DC_1–DC_3 respectively (AC and DC coupled battery).

The generated PV energy is subject to losses through the rectification stage. Thus, PV energy from the measured data–given in AC–is compensated to DC equivalent using the following relation

$$e_{PV,\ DC} = \frac{e_{PV,\ AC}}{\eta_{DC/AC}} \tag{3.1}$$

if the inverter efficiency, $\eta_{DC/AC}$, is constant over the entire working interval.

[3] See Figure 1 in [48] for an example of such a system topology

[4] ISO 6469-3 **Electrically propelled road vehicles – Safety specifications** Part 3: **Protection of persons against electric shocks**. [Def.:] "Voltage class A – classification of an electrical component or circuit with a maximum working voltage of less than 30 VAC (rms) or 60 VDC."

[5] Except for DC_{1b} where the conversion is done with a fixed efficiency at the grid's sub-station.

3.4.2 Modified Load Profile

For the purpose of modelling the efficiency gains from a DC distribution network, each load must be separated to calculate the individual losses from cable conduction, rectification and conversion (DC/DC). Therefore, a modification is made for those loads that where not measured individually in Figure 3.3a, i.e. user specific loads and lighting. For this, four typical seasonal week load profiles were generated, i.e. winter, spring, summer and fall, and scaled to an entire year's consumption.

Table 3.1 shows the load demand–per post–and PV generation for the three user-cases in this study–RISE's Research Villa, NZEB replica and modified NZEB replica building used in the DC topology modelling. The major difference between RISE's villa and the replica is the demand from user specific loads since the former does not have any 'real' occupants and thus a lower demand from user appliances, e.g. stove/oven, microwave, cleaning, washing, etc.

Table 3.1: Summary of load demand and PV generation for the three studied cases–RISE's Research Villa ("RISE, NZEB"), NZEB replica building ("NZEB, replica") and modified NZEB replica building used in the DC topology modelling ("NZEB, replica (mod.))".

	User-case		
Load Type	**RISE, NZEB**	**NZEB, replica**	**NZEB, replica (mod.)**
Heating	1905	2213	2213
Ventilation	775	801	801
Water pumps	0	272	272
Lighting	439	359	343
User specific	235	2710	2580
Total Demand	**3354**	**6355**	**6209**
PV	3026	3178	3178

3.4.3 Loss Modelling of Topology Comparison

The system's losses are modelled for one year's operation using the time-series load profiles from Section 3.4.2. In the two sections below, the methodology for the modelling of the conduction and conversion losses are explained more in detail.

3.4.3.1 Cable Conduction Losses

For modelling of the conduction losses, the feeder lengths from Table B.1 are used together with the distribution voltage, U_{dist}, and (2.24)–(2.26). Where the cable cross-section area from Table 2.2 is set by the maximum current during one year's operation. For the lighting, it is assumed that the current to each room–being the sum of the current to all active lamps in that room–is fed through one cable to the room and then distributed to individual branches, depending on the lighting layout. Lighting feeder lengths are set depending on which lamps are active. Each room

consists of 2–11 LED lights at 7 W each, see Figures A.1 and A.2. Individual room sockets are treated in a similar way, with a common current to each room and then distributed to the active socket(s) at each time step. Stationary appliances, some of them mapped out in Figures A.3 and A.4, are modelled with a fixed feeder length and the conduction losses for these are calculated using (2.24)–(2.26).

3.4.3.2 Converter Losses

Converter losses for the two topologies in Figures 2.4 and 2.5 are determined, for each time step, using (2.23) and the efficiencies for each converter. In the AC topology, an H-bridge is used between the PV and battery, and the AC link, see Figure 2.12, while in the DC topology, this is done using a buck converter, see Figure 2.11. The losses from the grid-tied inverter in the DC cases, as explain in Section 3.4, is determined using both a constant and a load dependent efficiency.

3.4.4 System Performance Evaluations

The system's performance has been evaluated for an entire year's operation using the modified load profiles for the NZEB replica building, see Section 3.4.2. Losses from the battery are calculated using the dynamic resistance representation presented in Section 2.5.1.1 and losses from electrical power components using the findings from the laboratory measurements presented in Section 3.6.

For a comparison of the system's performance, the overall system efficiency, adopted from [49] and is–for this specific study–calculated as

$$\eta_{system,i} = \left(1 - \frac{E_{losses,i}}{E_{load}}\right) \tag{3.2}$$

where $E_{losses,i}$ are the annual energy losses for system "i" and E_{load} the annual energy consumed by the loads[6]. The systems total energy demand, E_{demand}, is calculated as

$$E_{demand,i} = E_{load} + E_{losses,i} \tag{3.3}$$

Another system performance factor, adopted from [44], is the PV utilisation factor, $\eta_{PV,\ system}$, that defines the useful PV energy, with the internal losses from the PV inverter and battery storage taken into consideration. When battery charging is solely done via PV surplus, it is calculated as

$$\eta_{PV,\ system} = \frac{E_{PV-L} + E_{BATT-L} + E_{PV-GRID}}{E_{PV,\ DC}} \tag{3.4}$$

where E_{PV-L} is the PV energy fed directly to the load, E_{BATT-L} energy supplied from the PV through the battery storage, $E_{PV-GRID}$ exported PV energy (to the grid) and $E_{PV,\ DC}$ the generated PV energy (as DC).

[6] Annual energy demand, E_{load}, is equal for all modelled cases.

3.4.4.1 Energy System Management

The modelling and analysis with the inclusion of a PV/battery system is done using the "Target Zero" (TZ) battery dispatch algorithm, adopted from [57], together with a PV/Battery system configuration of 3.7 kWp and 7.5 kWh storage capacity respectively. The selection of the battery size is based on the related study in [85] which concluded that for this system, the additional performance gains for battery sizes exceeding 7.2 kWh were limited. Maximum and minimum SOC levels of the battery (SOC_{max} and SOC_{max}) used in the modelling were 15 and 90% respectively. The battery's efficiency characteristics is modelled using a dynamic series resistance as a function of current throughput according to Section 2.5.1.1.

3.5 Battery Measurements Set-up

To have an accurate representation of the battery's characteristics, a test was made for a single cell to have the battery's internal voltage as a function of its SOC level and from that establish the internal resistance variation as a function of current throughput according to (2.13). Table 3.2 shows the technical specifications given by the manufacturer for the $LiFePO_4$ battery cell used in the laboratory tests and system modelling.

Table 3.2: Technical specifications from manufacturer for the battery cell used for testing and modelling.

Parameter Name	Value	Comment
Chemistry	$LiFePO_4$	
Model No.	LAF12-1865150	
Nominal capacity	12 Ah	
Nominal voltage	3.2 V	
Charge/discharge cut-off voltage	3.65/2 V	
Internal resistance	3 mΩ	
Cycle life	>2000 cycles	@ 1 C and DoD = 100%

3.5.1 Open-Circuit Voltage Test and resistance determination test

To establish the relation between battery SOC and voltage, u_{batt}, charging and discharging of the battery is done for a very low current, 0.12 A (0.01 C[7]) over its entire SOC interval (0–100%) at room temperature. The test is conducted using a PEC ACT0550 and a Gamry REF3000 instrument.

Further measurements are also conducted in the current range of 0.36–18 A (0.03–1.5 C) in order to determine the resistance value valid for longer time periods,

[7] "C" is the current level at which the battery is completely discharged during 1 hour, in this case 1 C = 12 A

i.e. minutes and hours. The results from these tests are fed into (2.13) to determine the internal resistance dependency as a function of battery current, and, as mentioned above, done for a wide range of charge/discharge rates to cover the whole working interval. In this work, the same resistance, r, is assumed for charge and discharge.

3.5.2 Electrochemical Impedance Spectroscopy Test

To determine the battery impedance characteristics, an Electrochemical Impedance Spectroscopy (EIS) measurement is done over a range of frequencies and SOC levels by varying the voltage and current of the battery. This data of the impedance variation at different frequencies is used to translate the electrochemical characteristics to electrical equivalents using an RC model with parallel resistances and capacitance.

The EIS test is done by applying a single-frequency sinusoidal AC excitation signal, *u(t)*, and measuring the corresponding current response, *i(t)*, as

$$i(t) = Icos(\omega t) \tag{3.5}$$

$$u(t) = Vcos(\omega t + \phi) \tag{3.6}$$

with I and V as the current and voltage magnitude values respectively and ϕ the phase difference between the current and voltage.

3.6 Loss Determination Set-up – Electrical Components

Due to the discrepancy of converter efficiencies found in literature and to improve the quality of the modelling of the topologies, a selection of power electronic converters are measured using two different methods–electrical and calorimetrical–to determine their losses (and efficiency) at different loading conditions. The two methods are presented below.

3.6.1 Loss Determination – Electrical Measurements

Low-power AC/DC converters rated at 75, 120 and 150 W were measured in the laboratory to determine its performance and efficiency characteristics as a function of loading. The electrical measurement setup is seen in Figure 3.4, where AC is fed from the grid at 230 V and 50 Hz and converted to the final DC level at the final stage through two conversion steps–230 VAC/350 VDC and 350 VDC/X VDC[8]. Measurements were conducted for the loading interval 5–60% of rated power with a Yokogawa WT1800 with a power accuracy of 0.05% for both AC and DC, see Figure 3.5.

Measurements on a DC/DC converter (6 kW rated power) were also conducted in-situ–located between the battery and the main DC link–in RISE's Research Villa in the loading range 0–67% to establish its performance and efficiency variation at different loading conditions.

[8] The final DC voltage levels were 24 (x2) and 27 VDC for the three measured converters.

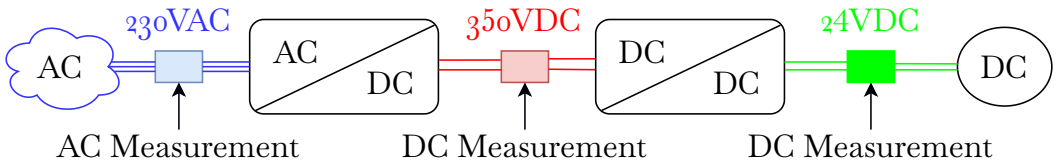

Figure 3.4: Measurement setup for determining AC/DC and DC/DC conversion efficiencies with the colour coding: AC and DC/DC.

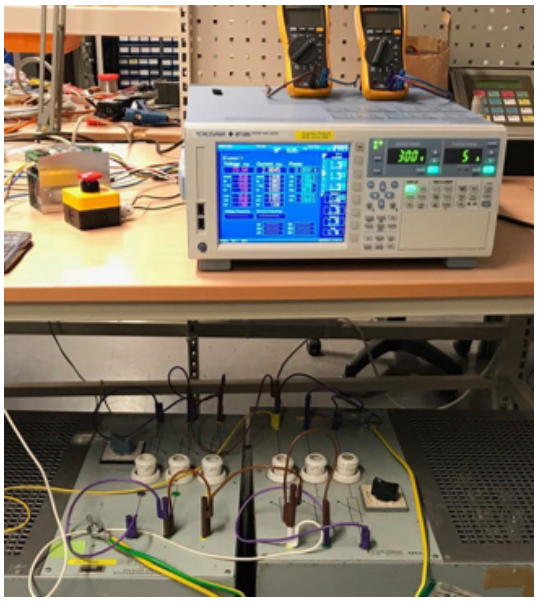

Figure 3.5: Set-up for the electrical measurements using the Yokogawa.

3.6.2 Loss Determination – Calorimetric Measurements

As a complement and verification, calorimetric measurements were also conducted and is an especially suitable method for the low-powered converters as it gives good accuracy when measuring low losses.

3.6.2.1 Calibration of Calorimetric Measurements

Prior to the calorimetric measurements, the calorimetric system was investigated using a resistor element with constant voltage and current, a flowrate of 0.0075 l/s and with the specific heat capacity, c_p, for water at room temperature. Figure 3.6 shows the set-up of the calorimetric measurements.

Supplying the resistor element with 32.1 VDC and 0.406 A gives an electrical input power, p_{el}, as

$$p_{el} = 32.1 \cdot 0.406 = 13.03W \tag{3.7}$$

Using (2.34) with the temperature difference of 0.4°C from inlet and outlet at steady-state operation–as seen in Figure 3.7–gives

$$p_{fluid} = 12.56W \tag{3.8}$$

which shows a satisfying accuracy.

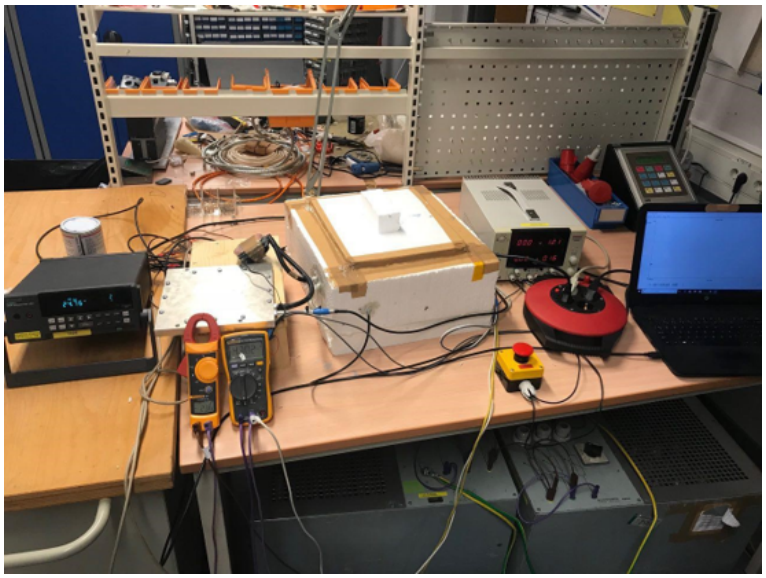

Figure 3.6: Laboratory set-up for the calorimetric measurements.

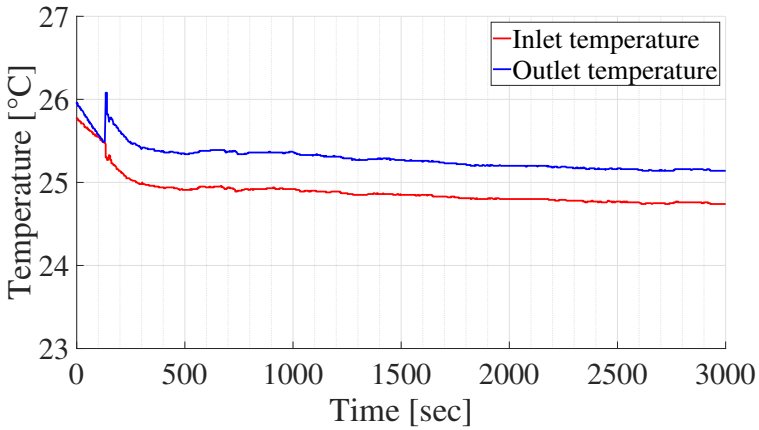

Figure 3.7: Measured inlet and outlet temperatures for loss calculations.

3.6.2.2 Calorimetric Measurements

To verify the electrical measurements from Section 3.6.1, the converter was placed inside the containment box on-top of a heat exchanger with water cooling. Two PT-100 temperature sensors were used to measure the temperature difference of the water inlet and outlet. When a temperature equilibrium was reached, the converter losses were calculated using (2.34). Two measurement points were registered from the calorimetric test at 35 and 59% loading. The resulting water temperatures can be seen in Figure 3.8.

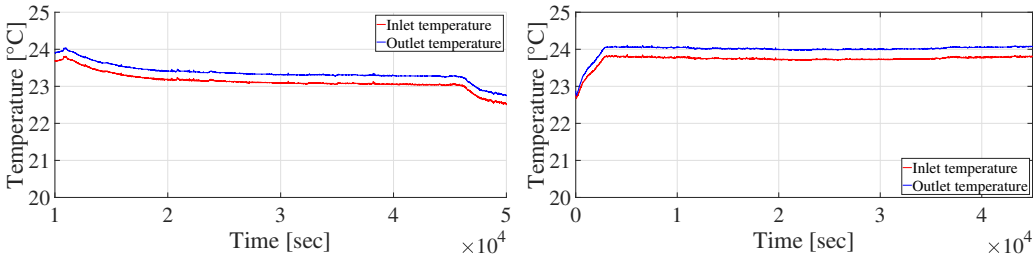

Figure 3.8: Temperature measurements from calorimetric loss determination with **(a)** water at 35% loading, and **(b)** water at 59% converter loading.

4

Results – Components

The battery and power electronic converters have been studied individually using laboratory measurements to have their respective performance and characteristics. These results are then used in the study of the system performance in Section 5.

4.1 Analysis of Battery Measurements & Resulting Characteristics

To get an accurate representation of the battery's characteristics, different measurements are made on a single cell, see Section 3.5. Below are the results from the different tests for the battery cell presented in Table 3.2.

4.1.1 Open-Circuit Voltage

A current sweep is made at 0.12 A to determine the SOC level's dependency on u_{batt}. Figure 4.1 shows the battery's voltage variation as a function of its charge content for the tested current level. Here, it can be noted that this cell has a large hysteresis effect. The resulting polynomial used in the system modelling is taken as the average voltage value of a charge and discharge current of 0.12 A (0.01 C) and is given as

$$u_{batt}(SOC) = 0.011 \cdot SOC + 3.24 \quad \forall\ 15 < SOC < 90 \tag{4.1}$$

which gives a linear relation in the SOC interval 15–90%.

4.1.2 Resistance Determination

4.1.2.1 Steady-State Resistance

Using (2.13) and the measurements at 50% SOC level for different C–rates gives the relation between the battery's internal resistance, r, and current throughput, i_{batt}, according to Table 4.1[1]. It can be noted that there is a very strong current dependency on the resistance value. The losses and efficiencies presented are also shown in Figure 4.2 together with the measured resistances as a function of C–rate, curve fitted internal resistance[2] and the internal resistance given from the data sheet,

[1] The calculated efficiency is for one-way, i.e. charge or discharge.
[2] The curve fit is done with an $R^2 = 1.000$ and RMSE = 0.0004458

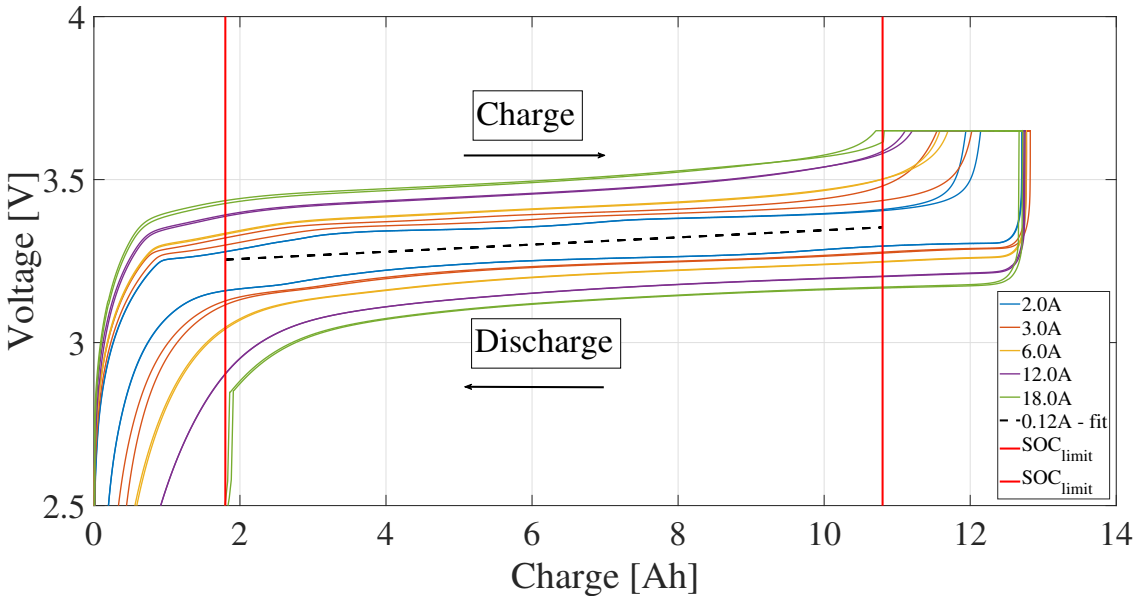

Figure 4.1: Measured battery open-circuit voltage (OCV) as a function of charge content together with the curve fit at 0.12 A (0.01 C) and SOC limits.

see Table 3.2. From here, it is evident that the value given in the data sheet does not give an accurate representation of the internal resistance for these slow charge and discharge values. Consequently, the losses would be underestimated if the data sheet value was used. A constant efficiency value can give a correct loss value, but it is only valid for one single current magnitude.

Table 4.1: Modelled relation between the battery's internal cell resistance and current throughput, and calculated battery losses for 192 cells in series and the calculated one–way dynamic efficiency, with U_{batt} at 50% SOC = 635 V.

Current [A]	**C–rate [h^{-1}]**	**Resistance [mΩ]**	**P$_{loss}$ [W]**	η_{dyn} [%]
0.12	0.01	170.8	0.5	99.4
0.36	0.03	70.8	1.8	99.2
1.2	0.1	32.1	8.9	98.8
2	0.17	26.0	20.0	98.4
3	0.25	21.3	36.9	98.1
6	0.5	17.4	120.4	96.8
12	1.0	12.8	353.7	95.4
18	1.5	10.4	649.7	94.3

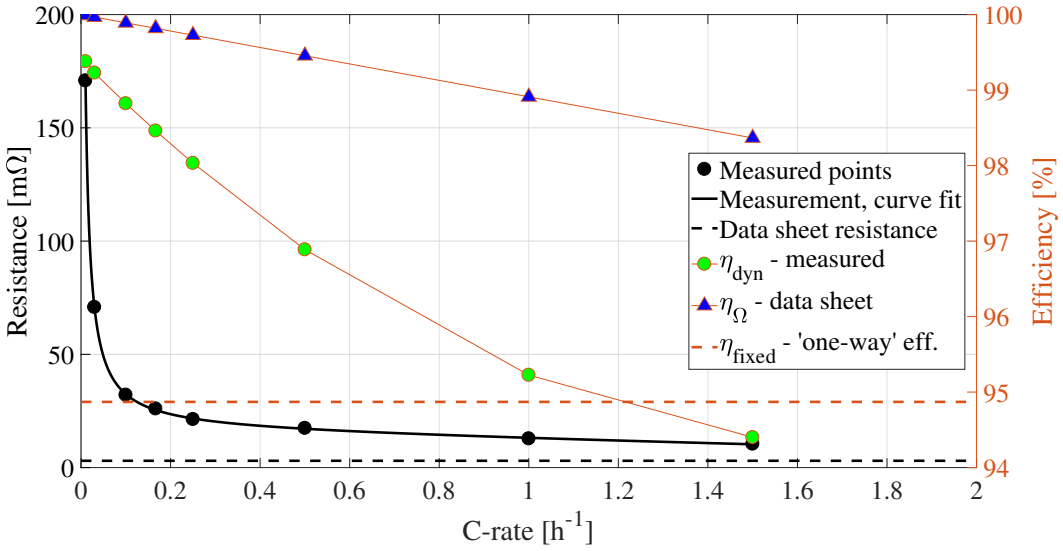

Figure 4.2: Measured and curve fitted internal resistance for the dynamic case together with the internal resistance value from the battery's data sheet in Table 3.2 and the corresponding efficiencies as a function of battery charge rate (C–rate). **NB!** Efficiencies refers to "one-way" values, i.e. either charge or discharge.

4.1.3 Electrochemical Impedance Spectroscopy (EIS)

The resistance in a battery is also time dependent, as presented in [35]. Figure 4.3 shows a Nyquist plot of the measured electrical characteristics for one battery cell for the SOC range 20–100% in the frequency interval 20 kHz–20 mHz. Each of the plotted values represent the impedance at one frequency where the values to the left represent high frequency and consequently, values to the right represents low frequencies. The almost vertical line at the highest measured frequencies is due to the inductive behaviour and is modelled by the inductance, L. The y-axis (negative imaginary impedance) crossing defines the series resistance, R_0, and the parallel RC elements, R_i and C_i, are defined by the curve fit over the complete measured frequency interval. Measurements confirm the same trend as observed in [86, 87] with an increase in the impedance span with a decrease in battery SOC level, i.e. moving the charge-transfer processes (semi-circular curve shapes) to the lower frequencies, which is also confirmed in [88]. From here it is also evident that the internal resistance given by the data sheet, see Table 3.2, only match for one single frequency, at around 80 Hz. For times of ca. 1 ms the resistance typically reach its minimum value, but for ca. 3 minutes and above, the resistance of a battery reach a "steady-state" value, determined according to Section 4.1.2.1.

So, a very important point here is that the data sheet value alone (see Table 3.2) is insufficient to be used if the losses and efficiency of the battery are important for an accurate system investigation. Instead, the here proposed measurement procedure is needed for an adequate determination of the battery's performance.

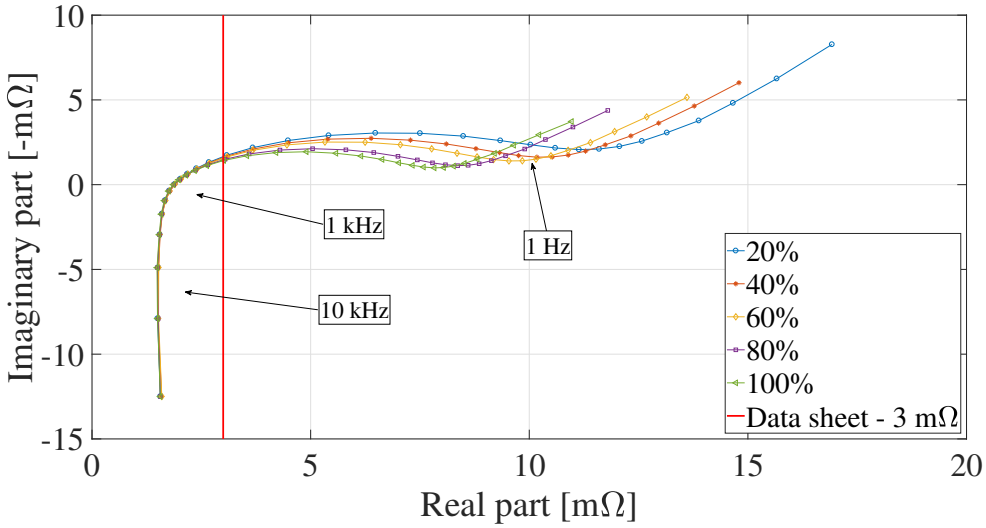

Figure 4.3: Nyquist plot of battery measurements at SOC levels 20–100% for the frequency interval 20 kHz–20 mHz together with data sheet value of battery resistance from Table 3.2.

4.1.4 Impact of Efficiency Representation

Figure 4.4 shows the battery power throughput from the two daily profiles in Figure 3.3, representing a summer (Figure 4.4a) and winter day (Figure 4.4b) respectively, together with the resulting losses for the three different battery efficiency representations; dynamic (measured current dependent resistance), ohmic (fixed R_0 from data sheet) and fixed round-trip efficiency of 90%[3]. The losses for the different representations and the two days are summarised in Table 4.2. From here, it is evident that the chosen fixed round-trip efficiency overestimates the battery losses and that the losses from the ohmic resistance, using (2.11), underestimates the losses compared with the dynamic model representation for these studied days.

Table 4.2: Comparison of battery losses for different battery efficiency representations (presented as % of total battery throughput) using measured data from June 13^{th} and January 20^{th}, see Figure 4.4a and 4.4b, with battery throughputs of 22.7 and 35.5 kWh respectively.

Efficiency Model	**Battery Losses – June**		**Battery Losses – January**	
	[kWh]	[%]	[kWh]	[%]
Fixed (η_{90})	1.17	94.9	1.82	94.9
Ohmic, data sheet	0.05	99.8	0.12	99.7
Dynamic, measured	0.44	98.1	0.80	97.8

[3] $\eta_{batt} = 90\%$ is used in the further study here for the constant efficiency if nothing else is stated

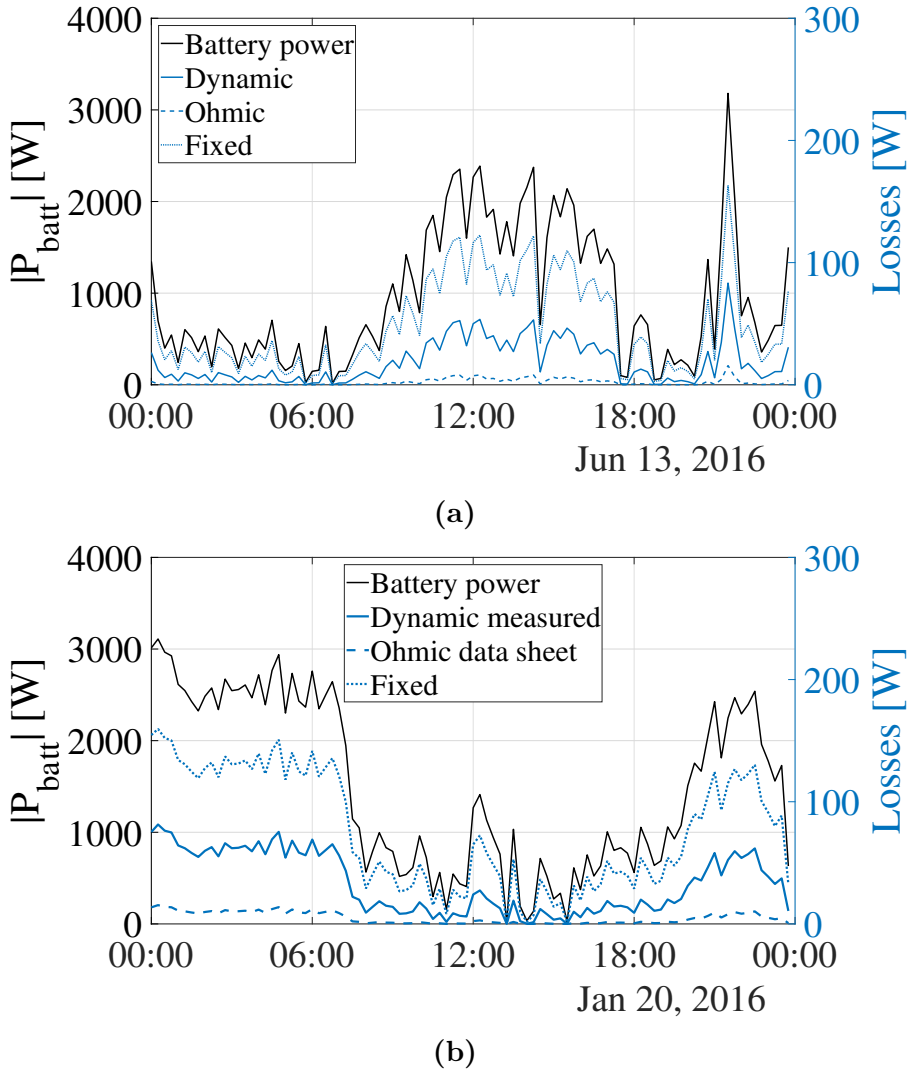

Figure 4.4: Battery losses for **(a)** June 13^{th} and **(b)** January 20^{th} using different battery efficiency representations; (i) dynamic (measured current dependent resistance), (ii) ohmic data sheet and (iii) fixed round-trip efficiency.

4.2 Power Electronic Measurements

In this chapter, the results of the measurements on the individual electrical components using the two methods described in Chapter 3.6 are presented. The analysed components are presented in Table 4.3 together with the method(s) used for loss determination.

Table 4.3: Power electronic components measured, and the method(s) used for each component.

Component	Input/Output	Method(s)
Rectifier (150 W)	230 VAC/27 VDC	Electrical
Rectifier (120 W)	230 VAC/24 VDC	Electrical & Calorimetric
Rectifier (75 W)	230 VAC/24 VDC	Electrical
DC/DC Converter (6 kW)	635±10/760 VDC	Electrical

4.2.1 Electrical Loss Measurements

Using (2.28)–(2.31) and the methodology for the electrical performance measurements described in Section 3.6.1 gives the resulting peak efficiencies presented in Table 4.4 for the respective converters, where the intermediate efficiencies are also presented. Here, η_{tot} is the conversion efficiency from the 230 VAC input to the final DC output voltage. The converter efficiency and losses for the 120 W converter as a function of its loading are shown in Figures 4.5b and 4.5a respectively.

Table 4.4: Conversion efficiencies from electrical measurements of the three AC/DC converters at 60% loading.

Converter	η_{tot}	$\eta_{AC/DC}$	$\eta_{DC/DC}$
150 W (230 VAC/27 VDC)	83.0%	94.1%	88.2%
120 W (230 VAC/24 VDC)	84.2%	97.6%	87.0%
75 W (230 VAC/24 VDC)	84.1%	94.0%	89.8%

The efficiency and characteristics of the DC/DC converter installed in the studied case between the battery and main DC link, can be seen in Figure 4.6 where measurements are done up until 67% loading and then extrapolated to cover the entire loading interval. Measurements were done for both charging and discharging of the battery to establish the efficiency in both directions. These measured values are fitted using a rational polynomial as

$$\eta_{DC/DC}(t_k) = \frac{k_1 p(t_k)^2 + k_2 p(t_k) + k_3}{p(t_k)^2 + q_1 p(t_k) + q_2} \tag{4.2}$$

where k_i and q_i are curve fitted values and $p(t_k)$ the converter loading in each time step t_k.

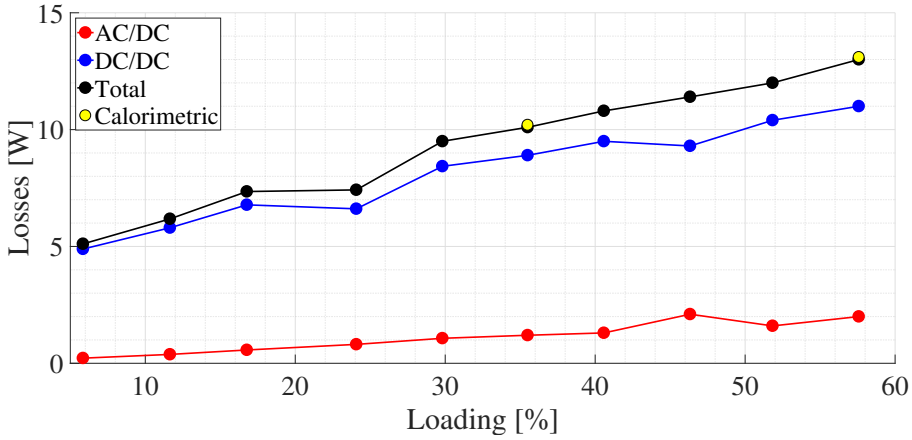

(a)

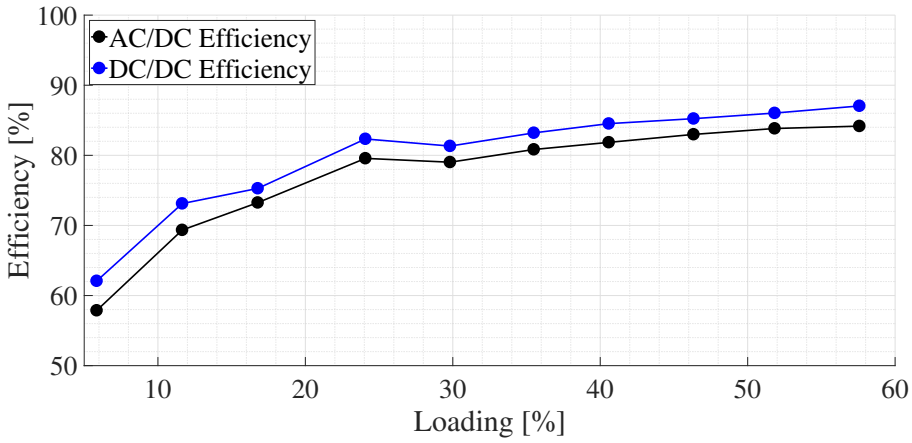

(b)

Figure 4.5: Measured converter losses (AC/DC) for the 120 W converter determined through electrical and calorimetric measurements **(a)** and corresponding efficiencies **(b)** as a function of loading.

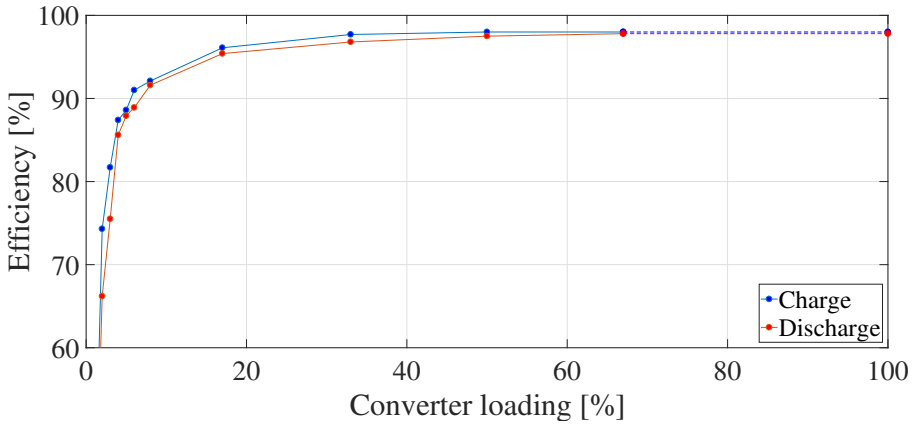

Figure 4.6: Measurement efficiency for the DC/DC converter as a function of loading for charge and discharge, together with extrapolated values (dashed lines).

In Figure 4.7, converter efficiencies found in literature and used in related studies on DC topology savings potentials [36,43–47] are shown together with the results from the experimental measurements[4]. The largest discrepancy is found for the lower power DC/DC converter, e.g. "DC/DC - Low". Since this conversion is present, and treated equally, for both topologies, see dashed perimeters in Figures 2.4 and 2.5, this does not influence the relative difference in the system's results.

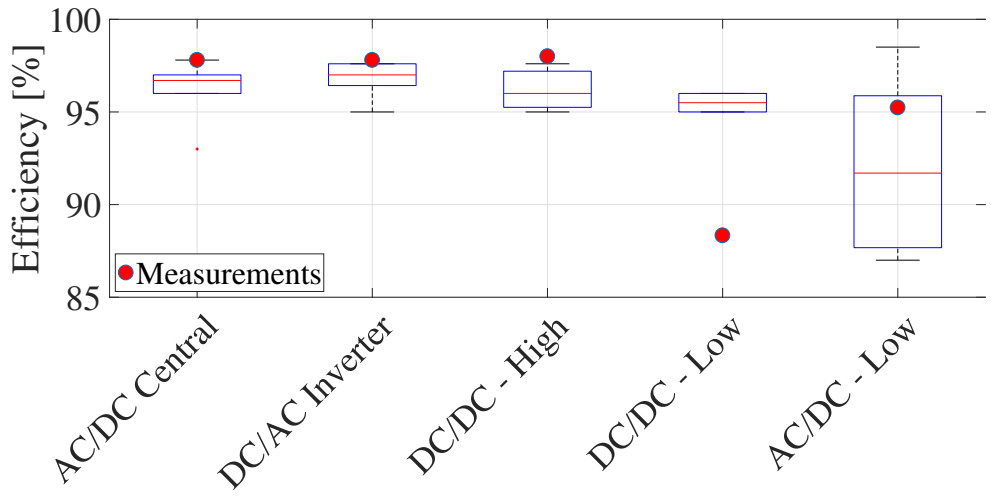

Figure 4.7: Converter efficiencies used in studies found in literature together with the measured peak converter efficiencies from this study.

4.2.2 Calorimetric Loss Measurements

The resulting calorimetric losses for the 120 W converter are shown in Figure 4.5a. Here, the resulting measured electrical losses, from Section 4.2.1, for the same converter are also presented and shows good coherence.

[4]Terminology: "**AC/DC Central**" = grid-tied AC/DC converter, "**DC/AC Inverter**" = grid-tied DC/AC inverter, "**DC/DC - High**" = DC/DC conversion for high power appliances, "**DC/DC - Low**" = DC/DC conversion for low power appliances and "**AC/DC - Low**" = AC/DC conversion for low power appliances.

5

Results – System Analysis

This chapter uses known and presented theory together with the methodologies outlined in Chapter 3 and the results from the component measurements and characteristics from Chapter 4 and applies this to the case study of a single-family residential building using the measurements presented in Sections 3.1 and 3.2.

Results include the modelling of different battery sizes and dispatch algorithms and their impact on the system performance (Section 5.1), the impact on system performance using three different battery loss representations (Section 5.2) and system performance's using AC and DC topologies (Section 5.3).

5.1 Battery Sizing for RISE Research Villa

Given the currently installed PV system at the Research Villa (3.7 kWp) and the load demand described in Table 3.1, different battery sizes and battery dispatch algorithms have been studied to see their respective impacts on the system's performance as explained in Section 3.3. Two performance figures have been studied that impacts the overall economic feasibility of the system: self-consumption and peak power demands.

5.1.1 Impact on System Self-consumption

As seen in Figure 5.1, increasing the battery size from 7.2 kWh to 27.0 kWh using TZ dispatch algorithm only results in a minor increase in SC and SS due to the limited PV capacity, and is therefore not a favourable option considering cost. These findings of saturated increase of SC with increased battery size have also been confirmed in previous studies [18, 89–91]. At a certain size the battery is not fully discharged during night time coverage which means that during the following day the excess PV energy will most likely be sufficient to fully-charge the battery during the early hours and after that the excess will be fed to the grid. The battery's frequency of state-of-charge (SOC) for the simulations using the TZ dispatch algorithm is shown in Figure 5.2. Here it is evident that the two most occurring states are at the battery's minimum and maximum state of charge; SOC_{min} and SOC_{max} respectively, which typically occurs during winter and summer time operation. Ideally the battery shall operate between these extreme points for best utilisation of its capacity. Batteries with high SOC levels in the morning will likely miss-out on PV surplus generated during the day and this energy is then instead fed to the grid.

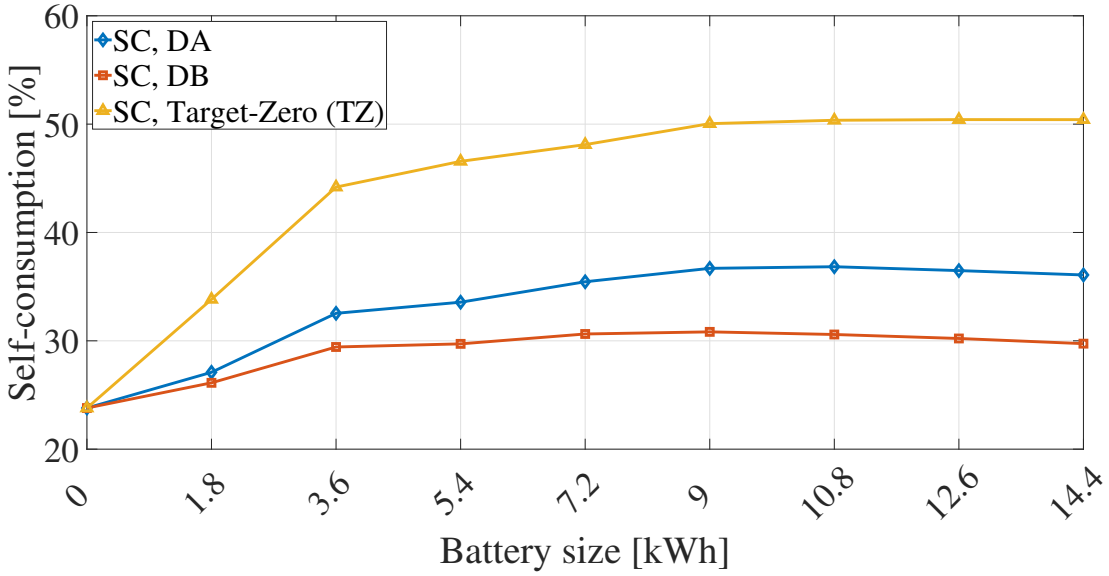

Figure 5.1: Results for self-consumption using dispatch algorithms; day-ahead (DA), day-behind (DB) and Target Zero with varying battery sizes

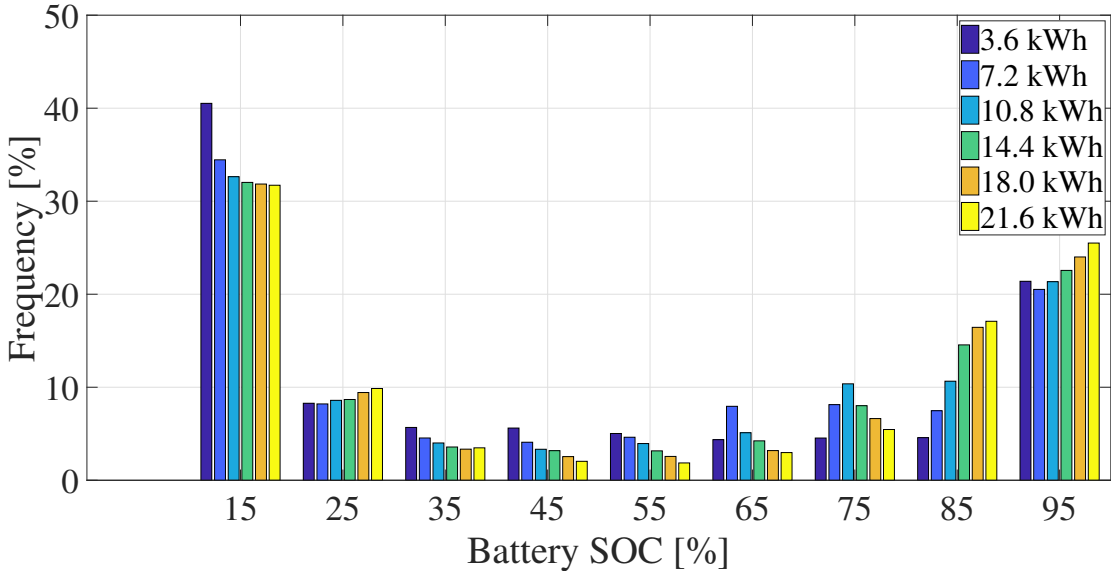

Figure 5.2: Frequency of battery SOC (state-of-charge) occurrences for Target Zero dispatch algorithm and different battery sizes.

It can be seen in Figure 5.1, for the day-ahead and day-behind dispatch algorithms that at a battery size of 10.8 kWh the self-consumption decreases slowly with increasing battery capacity. This is due to that the algorithms in SAM does not allow discharging of the batteries to the grid. This leads to that at a certain size the battery withdraws more energy from the grid and gives less to loads and thus operates at a high level of state-of-charge (SOC). This algorithm constraint makes it impossible for certain battery sizes to achieve a significant increase in SC compared to a case without battery as the battery start to require more charging from the grid and do less discharging to the load compared to a smaller battery.

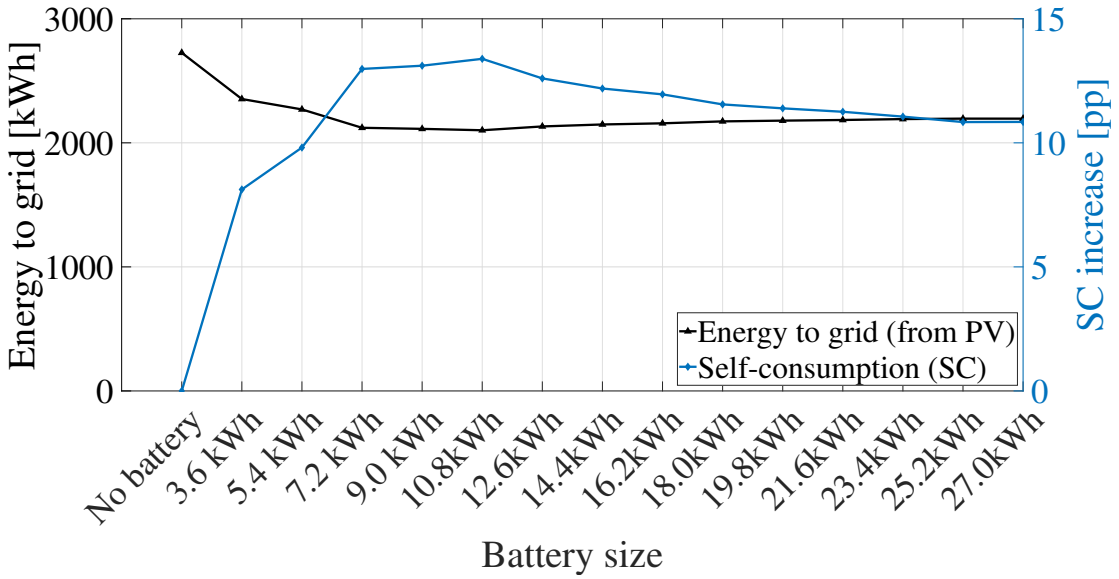

Figure 5.3: Energy exported from solar PV to the grid and percentage point increase in self-consumption (SC) for different battery sizes using day-ahead (DA) dispatch algorithm and the battery size interval 0–27 kWh.

This is supported when looking at energy imported and exported to the grid, Figure 5.3, in the battery interval 0–27 kWh where the minimum export of energy from solar PV to the grid occurs at a battery size around 7.2–10.8 kWh.

5.1.2 Impact on System Peak Powers

In future energy scenarios, where power supply will most likely become more crucial than energy due to the change in the electricity system, with more power peaks occurring, it is essential to study how a battery could be used for peak power shaving, both in terms of import from the grid and export of excess PV generation.

As for peak shaving using the TZ algorithm–maximum peaks from grid import were not decreased as the dispatch algorithm does not allow direct grid charging and thus no charging is allowed during periods with low solar generation and high peak demands (e.g. cold winter days with heat pump running at full power). This, since the objective function of the TZ algorithm is solely based on a power flow target, see Section 2.3.1.1, it works without any forecasting. As for maximum peak export from excess PV to the grid, some peak shaving would be possible for the larger battery sizes allowing the possibility to avoid any power curtailment limitations. An example of the grid interaction is shown in Figure 5.4, using load data from the NZEB replica building presented in Section 3.2, for battery sizes 0–20 kWh[1]. Here, the larger battery sizes limit the peak power export (to the grid) from 2.95 kW (without a battery) to 2.43 kW (battery size >10 kWh) and also the number of occasions for power export, see Figure 5.4a. As for grid import, the peaks are not limited for the larger battery sizes due to the dispatch algorithms objective function,

[1] Load data from the replica building is used here since it has a larger demand and thus gives a better visualisation of grid interaction.

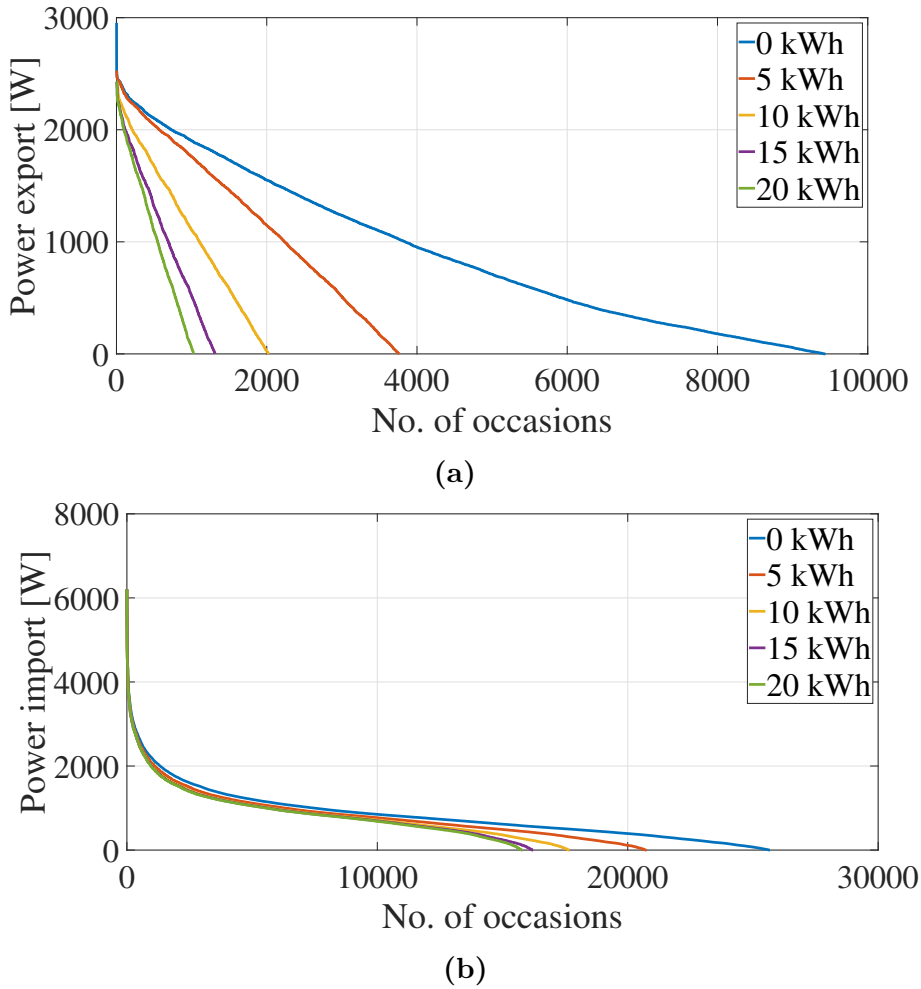

Figure 5.4: Grid export **(a)** and import **(b)** for NZEB replica house with a PV array of 3.7 kWp with battery power charge/discharge rate at 80% of its storage capacity.

but the number of occurring grid imports at the higher power level are limited, see Figure 5.4b.

5.2 Impact of Battery Loss Representations

A result comparison has been made using the three different efficiency representations and is summarised in Table 5.1 for a selection of key performance factors using the load and PV generation data for case "NZEB – Replica" in Table 3.1. For the quasi-dynamic (i.e. "Ohmic, data sheet") representation, the internal battery resistance, R_0, is taken from Table 3.2 and scaled to represent the entire battery pack through multiplication of the number of cells, i.e. 192[2]. The battery losses for the ohmic and dynamic (measured current dependent resistance) representations, are calculated using (2.11) and (2.14), with the difference that the latter considers

[2] Assuming all cells are series connected

the variation in internal resistance as a function of current, see Table 4.1. On an annual basis, the fixed efficiency representation overestimates the battery losses by more than 3.5 times and the ohmic model underestimates the same with almost one order of magnitude. Noteworthy is that despite this large difference in losses, the system self-consumption only differs by 2.4 percentage for the ohmic representations. Figure 5.5 shows the duration of the modelled battery current and resistance for an entire year's data[3]. Here, it can be noted that the modelled battery cell resistance far exceeds the value from the data sheet throughout the modelled time period.

Table 5.1: Comparison of system performance using different battery efficiency representations and measured data, see Figure 3.3a. "Ohmic, data sheet" represents the internal resistance value from the data sheet at 3 mΩ, see Table 3.2.

Battery	**Fixed (η_{90})**	**Ohmic, data sheet**	**Dynamic, measured**
Charging [kWh]	1329	1268	1229
Discharge [kWh]	1196	1263	1194
Losses [kWh]	129.6	4.6	35.4

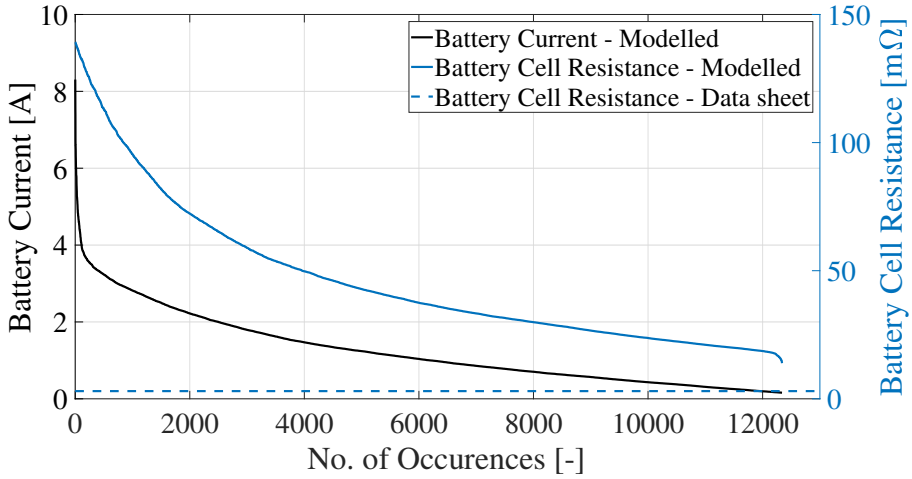

Figure 5.5: Modelled battery current and cell resistance using the dynamic loss representation (current dependent resistance) and the measured data, together with the data sheet cell resistance value at 3mΩ.

In Figure 5.6 the modelled battery efficiencies (Figure 5.6a) are shown for the three representations together with their respective losses (Figure 5.6b). Each point represents the loss and efficiency for each modelled time step, where the points (>6 kW) is an extrapolation to show the impact from higher battery power throughputs by up scaling the magnitude of the PV and load data. Noteworthy, is that for power levels below approximately 11 kW, the constant efficiency representation overestimates the battery's losses, compared to the dynamic case, while for power's above that, it underestimates the losses. This means that the fixed efficiency representation is only valid in a limited operating range of the battery. Furthermore, results

[3] Only data points when battery current exceeds 0 A are displayed for a better visualisation.

show that the internal resistance value from the data sheet does not represent the performance of the battery at any point of its operation. In fact, the discrepancy of the losses using the given internal resistance increases for higher power throughputs, as seen from the extrapolated points. Since the battery losses in the ohmic and dynamic scenarios are both a function of the battery current squared (and to some extent also the voltage), see (2.11) and (2.14), higher battery power (and current) throughputs will result in an exponential growth of the losses.

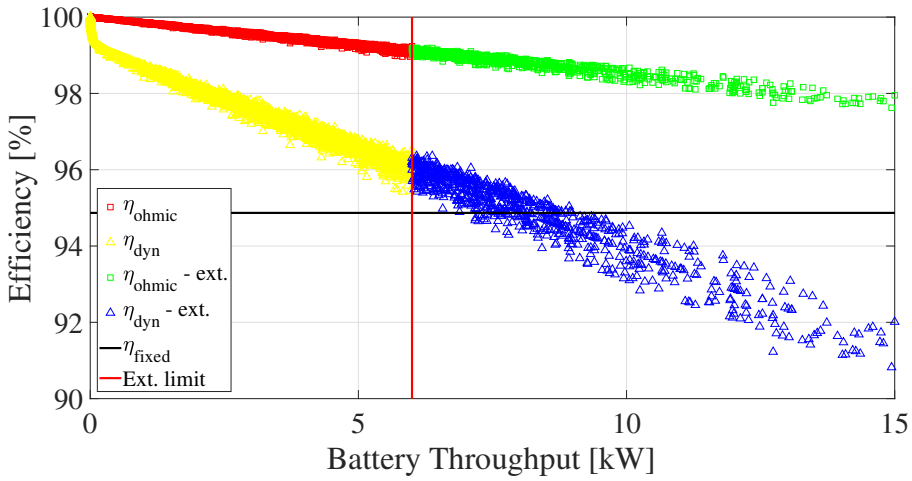

(a)

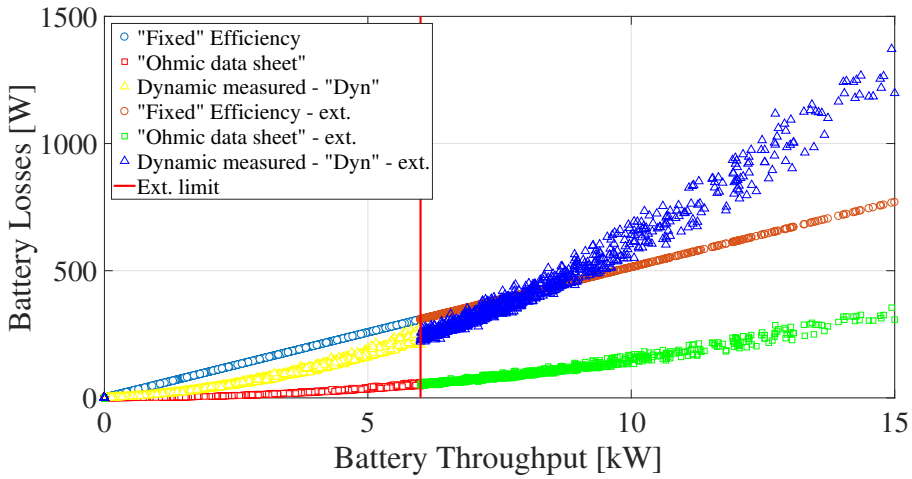

(b)

Figure 5.6: Battery losses (**a**) for the three modelled representations; ”Dyn”, ”Ohmic data sheet” and ”Fixed”, using measured data and the corresponding efficiencies (**b**). Each point represents the losses and efficiencies for each modelled time step. Where the points above 6kW represent an extrapolation to higher throughputs.

In Figure 5.7 a sensitivity analysis has been made by varying the battery size[4] to see the impact from different efficiency representations. Figure 5.7a shows the self-consumption (SC) of the generated PV energy with a saturating trend as the battery capacity increases, which was also confirmed in previous studies [18, 85, 89–92]. Figure 5.7b shows the total annual battery losses for the different efficiency representations with the same variation in battery sizes. In the region 0–2 kWh/kWp the standard deviation for the modelled SC for all efficiency representations is just above 1 percentage despite a standard deviation in losses of 80 kWh (see Figure 5.7b). Expanding the battery size to 2–5.4 kWh/kWp the standard deviation of the losses remains just above 80 kWh while it increases above 1.5 percentage for the self-consumption.

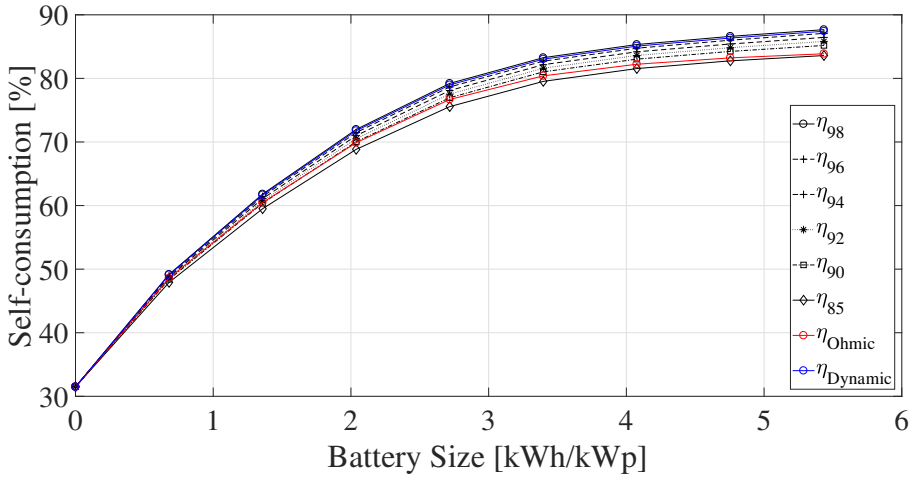

(a)

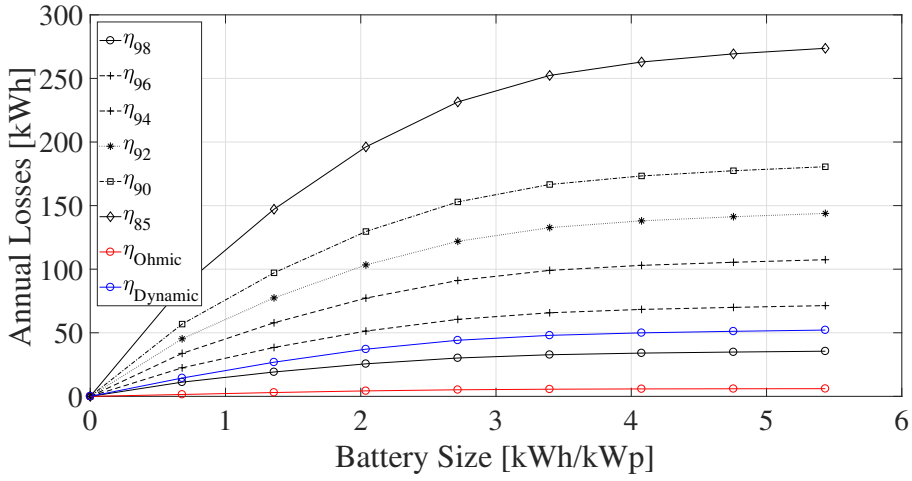

(b)

Figure 5.7: Sensitivity analysis on; **(a)** self-consumption (SC), and **(b)**; battery losses, using different battery efficiency representations ($\eta_{fixed} = \sqrt{0.98}$–$\sqrt{0.85}$, η_{Ω} and η_{dyn}), and by varying the battery size (PV size fixed at 3.7 kWp). The x-axis represents battery capacity (in kWh) over PV peak power (kWp).

[4] Battery power limit is set to 80% of the capacity, e.g. 10 kWh = 8 kW

5.3 Quasi-Dynamic Modelling of AC & DC Topologies

Results from the component losses, presented in Table 4.4, Figures 4.6 and 4.7 are used together with the topologies presented in Section 3.4 to determine the different system's performance.

The result comparison presented in Table 5.2 is for the five cases presented in Section 3.4, and all of them have identical system configurations in terms of PV and battery design. The modelling is done using the modified load profiles presented in Section 3.4.2 and power electronic efficiencies from Section 4.2. "Energy demand" is the total energy required—including system losses—from (3.3) and $\eta_{PV,\ system}$ the PV utilisation factor from (3.4). Noteworthy is that the PV energy produced is higher for the DC cases since it is fed directly to the main DC link without the need for any rectification, see (3.1) for correction factor. System efficiency, η_{system}, is calculated using (3.2). In Table 5.3, the energy demand and system efficiency, η_{system}, are presented for the five modelled cases but without the inclusion of PV or battery.

Table 5.2: Comparison of system performance of AC and DC distribution networks with PV and a battery storage at 3.7 kWp and 7.5 kWh respectively (DC_i refers to case 1–3 and 'a' and 'b' to the modelling of the "in-house" and "sub-station" conversions respectively).

	AC	**DC$_{1a}$**	**DC$_{1b}$**	**DC$_2$**	**DC$_3$**
Energy demand [kWh]	6844	6705	6611	6710	6 739
PV Energy [kWh]	3113		3178		
$\eta_{PV,\ system}$ [%]	88.6	89.8	92.2	89.7	89.3
η_{system} [%]	90.2	92.4	93.9	92.3	91.9

Table 5.3: Comparison of system performance of AC and DC distribution networks without PV and a battery storage.

	AC	**DC$_{1a}$**	**DC$_{1b}$**	**DC$_2$**	**DC$_3$**
Energy demand [kWh]	6533	6627	6486	6632	6661
η_{system} [%]	95.2	93.7	95.9	93.6	93.1

Savings in energy demand for case DC_{1a}, using a load dependent efficiency, is not present in the scenario without PV and battery, see Table 5.3, while it amounts to around 2% for the case with 3.7 kWp PV and 7.5 kWh battery storage, see Table 5.2. These results are also confirmed in [10,36,37,43,49], where the inclusion of a PV and battery system increases the energy savings for the DC cases, compared to an equivalent AC typology. The PV utilisation is also increased by close to 5 percentage points for the DC cases, compared to the AC topology, due to the reduced losses from the battery and PV inverter.

Figure 5.8 and Tables B.4–B.6, shows a loss breakdown for the modelled scenarios for three PV & battery systems. In Tables B.2 and B.3, the conduction and conversion losses for each appliances and modelled cases are shown for the PV and battery system of 3.7 kWp and 7.5 kWh respectively. For the DC scenarios, the grid-tied inverter s a major loss contributor when modelling a load dependent efficiency (DC_{1a}, DC_2 and DC_3). In DC_{1b}, where a constant efficiency is assumed for the sub-station conversion–with reference to the efficiency value used in other electrical studies [81–84]–the total losses are significantly reduced and already indicate a favourable option without the inclusion of PV and battery storage, see Figure 5.8a and Table 5.3. Comparing the results for DC_{1a} and DC_{1b}, having the same topology, also shows the difference in results when using a constant efficiency, which is commonly done in other studies [39, 45, 93–95].

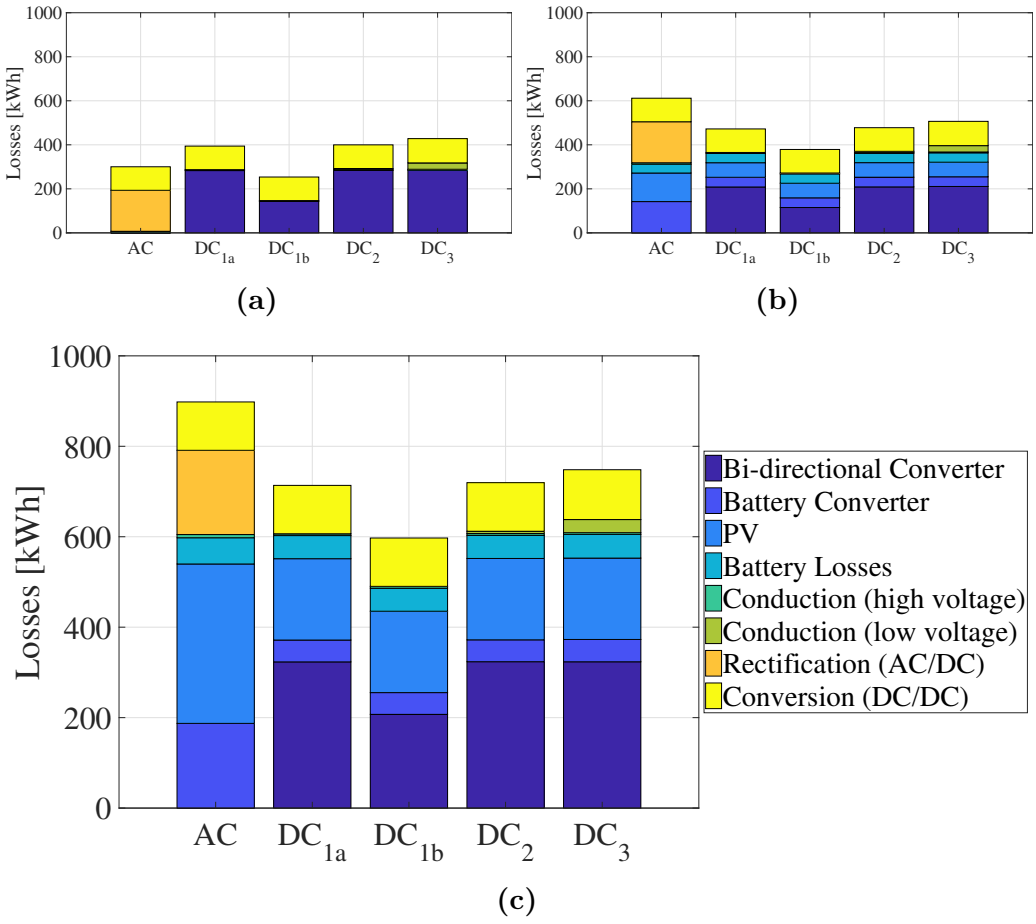

Figure 5.8: Loss contribution for the modelled scenarios and three different PV and battery configurations; **(a)** without PV and battery, **(b)** PV = 3.7 kWp and battery = 7.5 kWh, and **(c)** PV = 10 kWp and battery = 10 kWh.

When a PV and battery system is included, see Figures 5.8b and 5.8c, the losses for the AC case from the PV and battery are substantially higher than for the DC cases, meaning that the generated PV energy is better utilised in the DC systems, which is also shown in Tables 5.2 and B.5 for the 3.7 kWp/7.5 kWh case. When the energy is generated locally, the amount of grid import is also reduced–lowering the

losses from the grid-tied inverter in the DC cases. Comparing the grid-tied losses in Figures 5.8b and 5.8c shows that for the latter case, the grid-tied losses are increased due to an increase in the energy exported to the grid. For the two cases with a DC sub-voltage level (DC_2 and DC_3) an additional loss contribution is added from low-voltage conduction losses at 48 and 20 VDC respectively, which causes the annual losses to increase slightly.

The system efficiencies–calculated according to (3.2)–are presented in Figure 5.9 for the modelled cases and three different PV and battery configurations. Here, it can be noted that the system's efficiencies decrease when PV and battery are included, and decrease with their size, and is due to the additional component losses added. Furthermore, without any PV and battery system, only case DC_{1b}, using a constant efficiency, presents a favourable option in terms of energy efficiency, compared to the AC topology. The impact of the PV and battery system is also confirmed by Dastgeer et al. (2017) where no energy savings for a DC topology are found compared to an equivalent AC topology without the inclusion of PV and battery storage [61]. If DC generation and storage are included–via PV and an electrical battery–all four DC topologies show higher system efficiencies compared to the AC equivalent. For a system with 3.7 kWp/7.5 kWh, the four DC cases have efficiency gains of 2.5, 4.1, 2.4 and 1.9% respectively, and for the larger PV and battery system the equivalent numbers are 3.5, 5.6, 3.3 and 2.8%. The increase in absolute numbers of the PV utilisation are 4.9 and 9.8% respectively for the two systems: 3.7 kWp/7.5 kWh and 10 kWp/10 kWh.

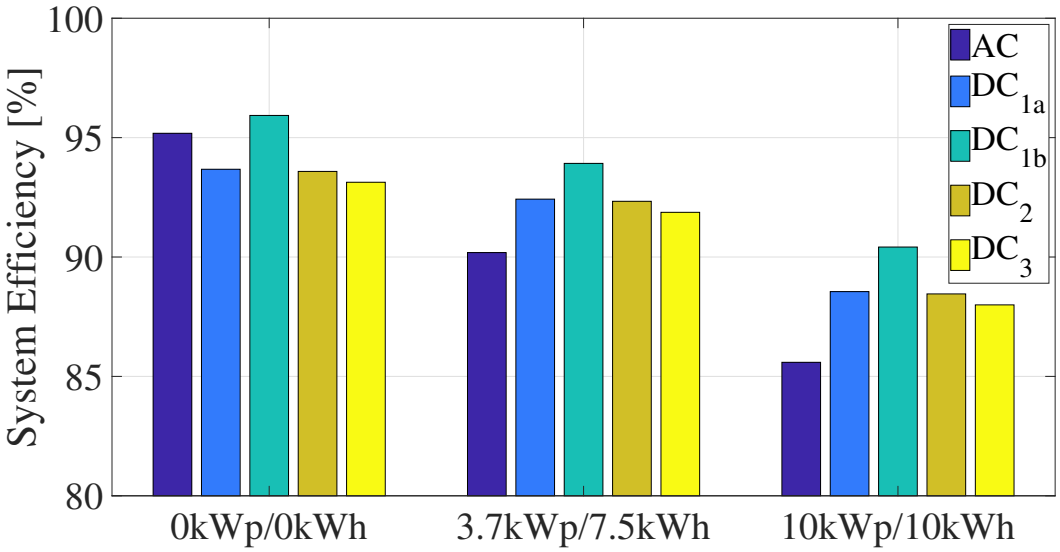

Figure 5.9: System efficiencies for the modelled cases and three different PV and battery configurations.

As seen in Figure 5.8 and, Tables B.5 and B.6, the major loss contributor for the DC cases is the grid-tied inverter, which is also confirm in [39], amounting to 40–50% for the DC cases with a load dependent inverter efficiency (DC_{1a}, DC_2 and DC_3). One way of reducing the grid-tied losses is thus to apply a modular operation where two (or more) converters are operated in parallel, where a smaller one is operated for the lower power throughputs, e.g. 0–10%, and another one for the larger power levels

(>10%). By doing so, the load dependent efficiency characteristics is improved. This is identified in [38] as a further improvement for DC distribution networks. Figure 5.10 shows a histogram of grid interaction with import (Figure 5.10a) and export (Figure 5.10b) of energy–as a function of loading–for case DC_{1a} with a PV and battery system of 3.7 kWp and 7.5 kWh respectively. Here, it is evident that much of the grid interaction is done at a low converter loading (>10% of the rated power of the inverter) and thus with high relative losses. An alternative–since these losses are dominated by grid import–would be to include demand response management and allow controllable loads to only withdraw energy under suitable conditions, i.e. during high demand occasions, when converter loading is higher, or match load demands in time. This is not included in this study but the performance gains from this should be quantified further in future studies, which will boost the energy performance further for DC topologies.

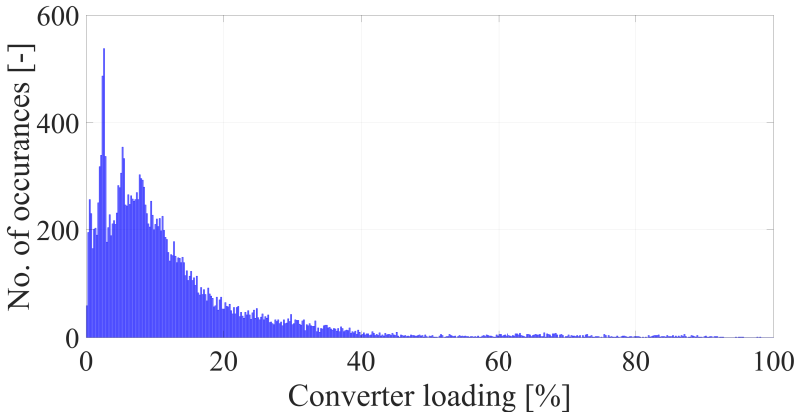

(a)

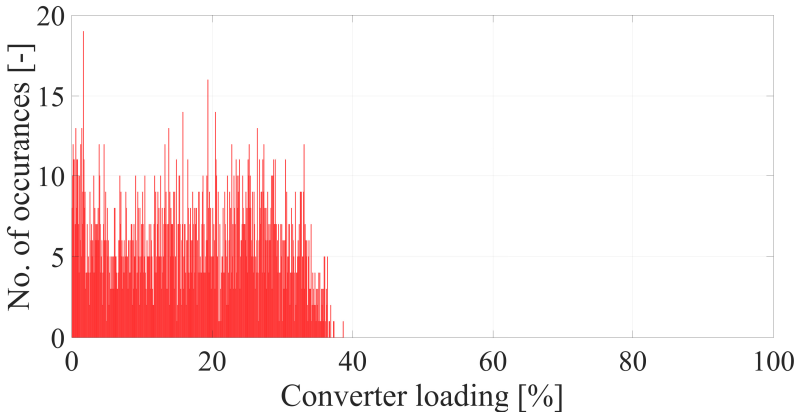

(b)

Figure 5.10: Histogram of grid interaction for case "DC_1a" with (**a**) import and export (**b**) for a system configuration of 3.7 kWp and 7.5 kWh, as a function of loading.

5.3.1 Energy Performance Comparison

A summary of literature findings on DC distribution savings potential are given in Figure 5.11 where either simulations or real demonstrations have been performed for DC distribution systems and compared to AC systems [36–40, 43–46, 96–99]. The variance in the results from literature are due to multiple factors including assumptions of power electronic efficiency's, system topology, the presence and sizing of PV and batteries, modelled or demonstrated results, etc. These are also compared with the findings from this study, with "NZEB – 1" for the system configuration of 3.7 kWp/7.5 kWh and "NZEB – 2" for the 10 kWp/10 kWh system configuration. Noteworthy is that all simulated cases from this study are lower than the ones found in literature. A possible explanation to this is the, by nature, low coincidence between load demand and PV generation, causing an increased interaction with the grid, mainly for grid import but also for export during PV peaks at noon. Thus, a suggestion for future studies would be to apply this model and compare the performance for a different scenario, e.g. climate and/or building type.

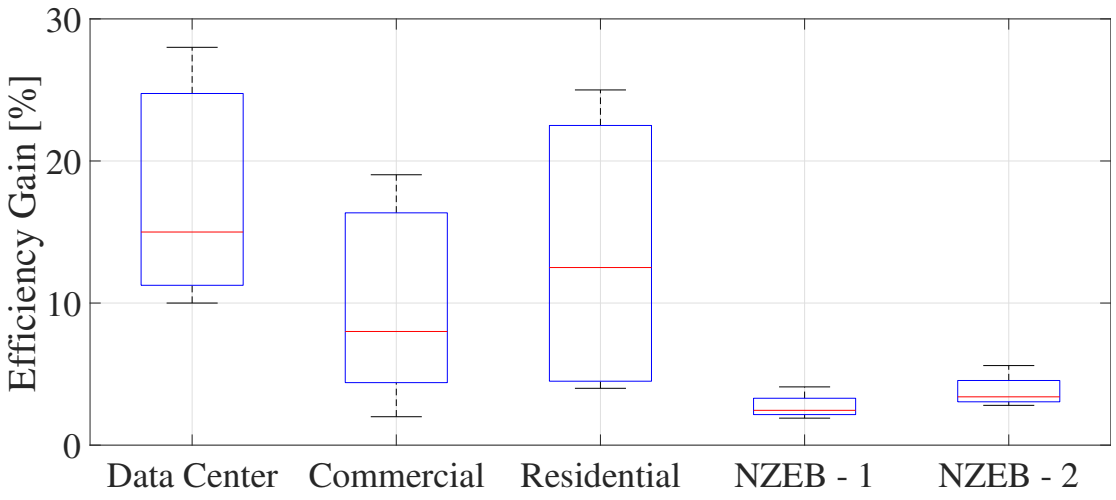

Figure 5.11: DC distribution savings potential for different building types found in literature together with the findings from this study on the residential building, where "NZEB – 1" is for the system configuration of 3.7 kWp/7.5 kWh and "NZEB – 2" for 10 kWp/10 kWh.

6

DC Distribution Networks in a Broader Context – Market Barriers

Despite all the identified advantages with DC distribution networks, full market penetration of DC distributed systems is still far away and there are still barriers to overcome before it replaces the existing AC system who has got market momentum. The lack of standardisation (voltage levels, safety, metering, etc.), demonstrations and proof-of-concepts, etc., which are partly due to the lack of demand has caught the DC concept in somewhat of a catch-22 situation and are some of the main challenges that needs to be overcome [8,10,37]. Some products are readily available on the market today for direct DC supply and some demonstrations are in place, but more efforts are needed in this area, both as a proof-of-concept but also as demonstrators to show the potential gains by switching to direct DC supply. Real demonstrations are also crucial to identify other, not foreseen, barriers that could be encountered, e.g. lack of practical DC experience of the electricians, legal barriers, safety consideration, etc. [37,60].

Following is an overview of some of the identified market barriers for further market penetration.

6.1 Barriers for DC Network Implementation

As of today, market penetration of local DC distributing networks in buildings are still scares. A few of the identified barriers for further implementation are mentioned below. It is no longer the case that AC has a technical advantageous over DC with lasts years developments in power electronics, instead there are now other market barriers that need to be handled.

Elsayed et al. (2015) studied the situation for DC Microgrids and concluded that one of the barriers identified was the lack of available standards for DC implementation [8]. In relation to AC equivalent, some aspects need different consideration regarding DC installation,

- power voltages
- plugs and sockets
- effects on human bodies

In addition, over voltage and current protection, earthing, fault detection and corrosion also need reconsideration compare to today's conventional AC installations

[100, 101].

Currently, work on a standardisation for DC distribution networks in residential buildings is done by different organisations, including International Electrotechnical Commission (IEC), Institution of Engineering and Technology (IET), EMerge Alliance, etc. in an attempt for a global harmonisation. A summary of the current standards and initiatives for residential DC distribution networks can be found in [100, 102, 103].

Previous studies have identified the lack of demonstrations of local DC networks in buildings [8]. As the installation of a DC network differs from an equivalent AC network, questions arise for these early adopters on practical issues with DC installations. These questions are for example,

- voltage level(s),
- cabling sizes,
- safety components and switches [101].

As the concept of internal DC networks and direct DC supply is a rather new phenomena, another barrier that has been identified in literature, and experienced through actual implementation and demonstration, is the lack of available products for direct DC supply [9, 37, 96, 104, 105]. On the one hand, there has been no incentive for developing these types of DC products as there has not been any market demand, but, on the other hand, no market has been developed as there has not been any products commercially available. Lately however, with the developed demonstration sites there has been a revoked interest in the development of new products that run directly on DC, especially after seeing the identified savings potential and gains when coupled with on-site renewable generation and storage. The lack of available products was identified in a market survey, summarised in [37, 106], as the most important issues to solve for a further implementation of DC distribution in buildings.

6.2 Author's Final Take

To conclude, are we seeing the re-birth of local DC networks given the observed mega-trends of price reductions in both solar PV and battery markets and last year's advances in power electronics? The short (and easy) answer to this is that "we will find out". The more extensive answer is that last year's trends and research within this subject have brought this discussion to the table again and with more demonstrations being built and savings potentials being realised, the chances of a re-birth might not be too far away. However, as mentioned above–there are still some non-technical barriers to overcome–before it takes the leap from a niche market to competing with conventional AC systems.

Despite the energy savings found in this, and other studies, the other market dimension of economy has not been considered in this study. As identified, there are still barriers to overcome before we will see any major market penetration of DC solutions, outside any niche markets. As with any other thing, time will tell, perhaps we are at the verge of round two of the battle of the currents?

7
Conclusion

Results from the modelling of different battery sizes and dispatch algorithms show that, for the studied case of RISE's Research Villa, additional gains in self-consumption when exceeding a battery size of 7.2 kWh are limited. Compared to the case without a battery, the self-consumption saturates at around 50% with a 7.5 kWh battery, adding an additional 24.3 percentage point to the self-consumption compared to a case without a battery, but does not show any significant increase thereafter. Furthermore, comparing the three modelled dispatch algorithms, the "Target Zero" (TZ) method shows a significant increase in self-consumption compared to the other methods who are designed primarily for peak-shaving. Potential peak-shaving using the TZ algorithm is also proven limited due to its objective function of maximising the self-consumption.

This work shows the importance of having a dynamic battery efficiency model, with a current dependent resistance, when studying the system performance for a PV/battery system in a residential building. A significant difference in battery losses is observed for the different battery efficiency representations, causing a discrepancy in the systems self-consumption when expanding the battery size. Results also show that neither the ohmic representation, nor the constant round-trip efficiency, show accurate coherence of the battery's efficiency under the studied dynamic conditions. The former underestimates the annual losses almost 10-folded when using the data from the manufacturer, while the latter gives a linear dependency which is only valid for a specific power interval, and almost three times higher annual battery losses.

Results from the modelling of the research villa, comparing DC distribution with traditional AC distribution, show that internal voltage distribution and load operation at 380 VDC reduces the losses with close to 40% for systems with PV and battery storage, and consequently reduces the total energy demand. It is also shown that the DC topologies better utilise the PV energy and battery storage by reducing the number of conversion steps in the system. Results show that the PV utilisation increases with 4.9% and 9.8% respectively for the two modelled PV and battery systems using a DC topology. Adding additional sub-voltage DC levels only reduces the energy savings from DC operation marginally due to increased conduction losses. However, this option is interesting from a personnel safety aspect since some of the high voltage sockets are avoided. A sub-voltage DC level can also be an alternative for USB-C type distribution, which also presents the possibility for load communication (IoT).

Results show that for systems without PV and battery, the conventional AC typology shows a higher system efficiency than (almost all) the suggested DC equivalents. This, since the grid-tied inverter, with a load dependent efficiency character-

istics, has high relative losses during low-load operation. When a constant grid-tied inverter efficiency is assumed, as typically done in several studies found in literature, the DC case is favourable even without the inclusion of PV and battery storage.

8

Future Work

Following are some suggestions where further work should be done based on the findings from this work,

- Investigate the impacts of interconnecting multiple houses, with local PV production and battery storage, connected through an internal DC system. How can these houses benefit from each other by sharing energy surplus and deficits–all distributed and operated using DC?
- What impact does an electrical vehicle (EV) have on the system performance if it would be possible to use the EV battery as a storage unit? To what extent would this lower the grid interaction and thereby increasing the systems performance?
- To get a deeper understanding of the potential for DC topologies, a sensitivity analysis should be done of the results with respect to the included power electronic converter performance and characteristics.
- Include alternative energy management–modular operation of the converter(s); how much could it improve the system performance? Results from this study show that the major loss contributor for the DC topology is the grid-tied converter and if grid interaction at low converter loading could be reduced, so could the system's losses.
- To accurately study the interaction between load and PV, more emphasise should be put on the temporal resolution. In this study, 15-minute average values are used for the analysis, which could be further improved with a high temporal resolution to catch the intermediate effects from the net load.
- If a higher temporal resolution is used for the PV and load profiles, a more accurate study of the battery's characteristics could be done using EIS (Electrochemical Impedance Spectroscopy) tests to catch the rapid changes occurring in the battery. This would further enhance the analysis of a PV & battery system characteristics and performance.
- As evident from the results and literature, the largest gains for a DC distribution network is when energy is supplied from the local source–either directly from the PV panels or via storage. Thus, the efficiency gain for such a system could be further improved if demand response is combined to allow for a better coincidence between demand and supply.
- This study is done for a residential building located in a Northern climate with less PV generation and poor coincidence between load demand and PV supply. Thus, studies in other climates would be preferable–using this model and methodology–to see the impact on system performance.
- Other building types should also be subject to further investigation as they

have demand load profiles that have a better coincidence with the available PV generation, e.g. office buildings. This effect could boost the efficiency gains from DC networks further as grid interaction could be minimised and PV energy better utilised.

Bibliography

[1] Z. Liu, *Global energy interconnection*. Academic Press, 2015.

[2] U. Nations, "United nations treaty collection chapter xxvii environment, 7. d paris agreement, paris, 12 december 2015 (cn 92.201)," 2016.

[3] (IEA), "Trends in photovoltaic applications 2019," 2019.

[4] J. Lindahl, "National survey report of pv power applications in sweden 2018," 2019.

[5] (IRENA), "Electricity storage and renewables: Costs and markets to 2030," 2017.

[6] Bloomberg, "New energy outlook 2019," 2019.

[7] F. Dastgeer, H. E. Gelani, H. M. Anees, Z. J. Paracha, and A. Kalam, "Analyses of efficiency/energy-savings of dc power distribution systems/microgrids: Past, present and future," *International Journal of Electrical Power & Energy Systems*, vol. 104, pp. 89–100, 2019.

[8] A. T. Elsayed, A. A. Mohamed, and O. A. Mohammed, "Dc microgrids and distribution systems: An overview," *Electric Power Systems Research*, vol. 119, pp. 407–417, 2015.

[9] E. Rodriguez-Diaz, M. Savaghebi, J. C. Vasquez, and J. M. Guerrero, "An overview of low voltage dc distribution systems for residential applications," in *Consumer Electronics-Berlin (ICCE-Berlin), 2015 IEEE 5th International Conference on*. IEEE, 2015, pp. 318–322.

[10] B. Glasgo, I. L. Azevedo, and C. Hendrickson, "Expert assessments on the future of direct current in buildings," *Environmental Research Letters*, vol. 13, no. 7, p. 074004, 2018.

[11] S. Schopfer, V. Tiefenbeck, and T. Staake, "Economic assessment of photovoltaic battery systems based on household load profiles," *Applied energy*, vol. 223, pp. 229–248, 2018. [Online]. Available: https://doi.org/10.1016/j.apenergy.2018.03.185

[12] J. Hoppmann, J. Volland, T. S. Schmidt, and V. H. Hoffmann, "The economic viability of battery storage for residential solar photovoltaic systems–a review and a simulation model," *Renewable and Sustainable Energy Reviews*, vol. 39, pp. 1101–1118, 2014. [Online]. Available: https://doi.org/10.1016/j.rser.2014.07.068

[13] M. Bortolini, M. Gamberi, and A. Graziani, "Technical and economic design of photovoltaic and battery energy storage system," *Energy Conversion and Management*, vol. 86, pp. 81–92, 2014. [Online]. Available: https://doi.org/10.1016/j.enconman.2014.04.089

[14] G. Mulder, D. Six, B. Claessens, T. Broes, N. Omar, and J. Van Mierlo, "The dimensioning of pv-battery systems depending on the incentive and selling price conditions," *Applied energy*, vol. 111, pp. 1126–1135, 2013. [Online]. Available: https://doi.org/10.1016/j.apenergy.2013.03.059

[15] M. Braun, K. Büdenbender, D. Magnor, and A. Jossen, "Photovoltaic self-consumption in germany: using lithium-ion storage to increase self-consumed photovoltaic energy," in *24th European Photovoltaic Solar Energy Conference (PVSEC), Hamburg, Germany*, 2009.

[16] J. Li and M. A. Danzer, "Optimal charge control strategies for stationary photovoltaic battery systems," *Journal of Power Sources*, vol. 258, pp. 365–373, 2014.

[17] R. Luthander, J. Widén, D. Nilsson, and J. Palm, "Photovoltaic self-consumption in buildings: A review," *Applied Energy*, vol. 142, pp. 80–94, 2015.

[18] E. Nyholm, J. Goop, M. Odenberger, and F. Johnsson, "Solar photovoltaic-battery systems in swedish households–self-consumption and self-sufficiency," *Applied energy*, vol. 183, pp. 148–159, 2016.

[19] A. Dietrich and C. Weber, "What drives profitability of grid-connected residential pv storage systems? a closer look with focus on germany," *Energy Economics*, vol. 74, pp. 399–416, 2018.

[20] S. Ried, P. Jochem, and W. Fichtner, "Profitability of photovoltaic battery systems considering temporal resolution," in *2015 12th International Conference on the European Energy Market (EEM)*. IEEE, 2015, pp. 1–5. [Online]. Available: https://doi.org/10.1109/eem.2015.7216632

[21] T. Beck, H. Kondziella, G. Huard, and T. Bruckner, "Assessing the influence of the temporal resolution of electrical load and pv generation profiles on self-consumption and sizing of pv-battery systems," *Applied energy*, vol. 173, pp. 331–342, 2016.

[22] V. Bertsch, J. Geldermann, and T. Lühn, "What drives the profitability of household pv investments, self-consumption and self-sufficiency?" *Applied Energy*, vol. 204, pp. 1–15, 2017. [Online]. Available: https://doi.org/10.1016/j.apenergy.2017.06.055

[23] G. Litjens, E. Worrell, and W. Van Sark, "Economic benefits of combining self-consumption enhancement with frequency restoration reserves provision by photovoltaic-battery systems," *Applied energy*, vol. 223, pp. 172–187, 2018. [Online]. Available: https://doi.org/10.1016/j.apenergy.2018.04.018

[24] J. B. Nørgaard, T. Kerekes, and D. Séra, "Case study of residential pv power and battery storage with the danish flexible pricing scheme," *Energies*, vol. 12, no. 5, p. 799, 2019. [Online]. Available: https://doi.org/10.3390/en12050799

[25] C. Truong, M. Naumann, R. Karl, M. Müller, A. Jossen, and H. Hesse, "Economics of residential photovoltaic battery systems in germany: The case of tesla's powerwall," *Batteries*, vol. 2, no. 2, p. 14, 2016. [Online]. Available: https://doi.org/10.3390/batteries2020014

[26] Y. Ru, J. Kleissl, and S. Martinez, "Storage size determination for grid-connected photovoltaic systems," *IEEE Transactions on sustainable*

energy, vol. 4, no. 1, pp. 68–81, 2012. [Online]. Available: https://doi.org/10.1109/tste.2012.2199339

[27] K. Heine, A. Thatte, and P. C. Tabares-Velasco, "A simulation approach to sizing batteries for integration with net-zero energy residential buildings," *Renewable energy*, vol. 139, pp. 176–185, 2019. [Online]. Available: https://doi.org/10.1016/j.renene.2019.02.033

[28] S. M. Schoenung and W. V. Hassenzahl, "Long-vs. short-term energy storage technologies analysis: a life-cycle cost study: a study for the doe energy storage systems program." Sandia National Laboratories, Tech. Rep., 2003. [Online]. Available: https://doi.org/10.2172/918358

[29] D. Energieagentur, "dena-netzstudie ii integration erneuerbarer energien in die deutsche stromversorgung im zeitraum 2015 2020 mit ausblick 2025," 2010. [Online]. Available: https://doi.org/10.1007/s12398-011-0054-0

[30] P. Grünewald, T. Cockerill, M. Contestabile, and P. Pearson, "The role of large scale storage in a gb low carbon energy future: Issues and policy challenges," *Energy Policy*, vol. 39, no. 9, pp. 4807–4815, 2011. [Online]. Available: https://doi.org/10.1016/j.enpol.2011.06.040

[31] B. Battke, T. S. Schmidt, D. Grosspietsch, and V. H. Hoffmann, "A review and probabilistic model of lifecycle costs of stationary batteries in multiple applications," *Renewable and Sustainable Energy Reviews*, vol. 25, pp. 240–250, 2013. [Online]. Available: https://doi.org/10.1016/j.rser.2013.04.023

[32] E. A. Grunditz and T. Thiringer, "Characterizing bev powertrain energy consumption, efficiency, and range during official and drive cycles from gothenburg, sweden," *IEEE Transactions on Vehicular Technology*, vol. 65, no. 6, pp. 3964–3980, 2015. [Online]. Available: https://doi.org/10.1109/tvt.2015.2492239

[33] S. Skoog, "Parameterization of equivalent circuit models for high power lithium-ion batteries in hev applications," in *2016 18th European Conference on Power Electronics and Applications (EPE'16 ECCE Europe)*. IEEE, 2016, pp. 1–10. [Online]. Available: https://doi.org/10.1109/epe.2016.7695340

[34] O. Theliander, A. Kersten, M. Kuder, E. Grunditz, and T. Thiringer, "Lifep0 4 battery modeling and drive cycle loss evaluation in cascaded h-bridge inverters for vehicles," in *2019 IEEE Transportation Electrification Conference and Expo (ITEC)*. IEEE, 2019, pp. 1–7. [Online]. Available: https://doi.org/10.1109/itec.2019.8790460

[35] A. Chaudhry, "Investigation of lithium-ion battery parameters using pulses and eis," *BSc. Thesis, Chalmers University of Technology*, 2018.

[36] V. Vossos, K. Garbesi, and H. Shen, "Energy savings from direct-dc in us residential buildings," *Energy and Buildings*, vol. 68, pp. 223–231, 2014.

[37] B. Glasgo, I. L. Azevedo, and C. Hendrickson, "How much electricity can we save by using direct current circuits in homes? understanding the potential for electricity savings and assessing feasibility of a transition towards dc powered buildings," *Applied Energy*, vol. 180, pp. 66–75, 2016.

[38] G.-S. Seo, J. Baek, K. Choi, H. Bae, and B. Cho, "Modeling and analysis of dc distribution systems," in *Power Electronics and ECCE Asia (ICPE & ECCE), 2011 IEEE 8th International Conference on*. IEEE, 2011, pp. 223–227.

[39] D. Denkenberger, D. Driscoll, E. Lighthiser, P. May-Ostendorp, B. Trimboli, and P. Walters, "Dc distribution market, benefits, and opportunities in residential and commercial buildings," 2012.

[40] J. Hofer, B. Svetozarevic, and A. Schlueter, "Hybrid ac/dc building microgrid for solar pv and battery storage integration," in *DC Microgrids (ICDCM), 2017 IEEE Second International Conference on*. IEEE, 2017, pp. 188–191.

[41] M.-H. Ryu, H.-S. Kim, J.-W. Baek, H.-G. Kim, and J.-H. Jung, "Effective test bed of 380-v dc distribution system using isolated power converters," *IEEE transactions on industrial electronics*, vol. 62, no. 7, pp. 4525–4536, 2015.

[42] Ó. Lucía, I. Cvetkovic, H. Sarnago, D. Boroyevich, P. Mattavelli, and F. C. Lee, "Design of home appliances for a dc-based nanogrid system: An induction range study case," *IEEE Journal of Emerging and Selected Topics in Power Electronics*, vol. 1, no. 4, pp. 315–326, 2013.

[43] R. Weiss, L. Ott, and U. Boeke, "Energy efficient low-voltage dc-grids for commercial buildings," in *DC Microgrids (ICDCM), 2015 IEEE First International Conference on*. IEEE, 2015, pp. 154–158.

[44] D. Fregosi, S. Ravula, D. Brhlik, J. Saussele, S. Frank, E. Bonnema, J. Scheib, and E. Wilson, "A comparative study of dc and ac microgrids in commercial buildings across different climates and operating profiles," in *DC Microgrids (ICDCM), 2015 IEEE First International Conference on*. IEEE, 2015, pp. 159–164.

[45] S. Backhaus, G. W. Swift, S. Chatzivasileiadis, W. Tschudi, S. Glover, M. Starke, J. Wang, M. Yue, and D. Hammerstrom, "Dc microgrids scoping study—estimate of technical and economic benefits," *Los Alamos National Laboratory, LA-UR-15-22097*, 2015.

[46] M. Noritake, K. Yuasa, T. Takeda, H. Hoshi, and K. Hirose, "Demonstrative research on dc microgrids for office buildings," in *Telecommunications Energy Conference (INTELEC), 2014 IEEE 36th International*. IEEE, 2014, pp. 1–5.

[47] E. Planas, J. Andreu, J. I. Gárate, I. M. De Alegría, and E. Ibarra, "Ac and dc technology in microgrids: A review," *Renewable and Sustainable Energy Reviews*, vol. 43, pp. 726–749, 2015.

[48] D. L. Gerber, R. Liou, and R. Brown, "Energy-saving opportunities of direct-dc loads in buildings," *Applied Energy*, vol. 248, pp. 274–287, 2019.

[49] D. L. Gerber, V. Vossos, W. Feng, C. Marnay, B. Nordman, and R. Brown, "A simulation-based efficiency comparison of ac and dc power distribution networks in commercial buildings," *Applied Energy*, vol. 210, pp. 1167–1187, 2018.

[50] P. Denholm, R. Margolis, and J. Milford, "Production cost modeling for high levels of photovoltaics penetration," National Renewable Energy Lab.(NREL), Golden, CO (United States), Tech. Rep., 2008.

[51] P. Denholm, M. O'Connell, G. Brinkman, and J. Jorgenson, "Overgeneration from solar energy in california. a field guide to the duck chart," National Renewable Energy Lab.(NREL), Golden, CO (United States), Tech. Rep., 2015.

[52] Swedish Energy Agency, "Summary of energy statistics for dwellings and non-residential premises for 2016," 2017.

[53] N. Sommerfeldt, H. Muyingo, and T. af Klintberg, "Photovoltaic systems for swedish prosumers: A technical and economic analysis focused on cooperative multi-family housing," 2016.

[54] C. Sandels, D. Brodén, J. Widén, L. Nordström, and E. Andersson, "Modeling office building consumer load with a combined physical and behavioral approach: Simulation and validation," *Applied energy*, vol. 162, pp. 472–485, 2016.

[55] Sweden's Government Office, "Förordning (2016:899) om bidrag till lagring av egenproducerad elenergi," 2016.

[56] W. J. Cole, C. Marcy, V. K. Krishnan, and R. Margolis, "Utility-scale lithium-ion storage cost projections for use in capacity expansion models," in *North American Power Symposium (NAPS), 2016*. IEEE, 2016, pp. 1–6.

[57] R. L. Fares and M. E. Webber, "The impacts of storing solar energy in the home to reduce reliance on the utility," *Nature Energy*, vol. 2, no. 2, p. 17001, 2017. [Online]. Available: https://doi.org/10.1038/nenergy.2017.1

[58] M. Schreiber and P. Hochloff, "Capacity-dependent tariffs and residential energy management for photovoltaic storage systems," in *Power and Energy Society General Meeting (PES), 2013 IEEE*. IEEE, 2013, pp. 1–5.

[59] A.-L. Klingler and L. Teichtmann, "Impacts of a forecast-based operation strategy for grid-connected pv storage systems on profitability and the energy system," *Solar Energy*, vol. 158, pp. 861–868, 2017.

[60] E. Vossos, S. Pantano, R. Heard, and R. Brown, "Dc appliances and dc power distribution: A bridge to the future net zero energy homes," 2017.

[61] F. Dastgeer and H. E. Gelani, "A comparative analysis of system efficiency for ac and dc residential power distribution paradigms," *Energy and Buildings*, vol. 138, pp. 648–654, 2017.

[62] Y. Liu, L. Zhang, J. Jiang, S. Wei, S. Liu, and W. Zhang, "A data-driven learning-based continuous-time estimation and simulation method for energy efficiency and coulombic efficiency of lithium ion batteries," *Energies*, vol. 10, no. 5, p. 597, 2017.

[63] J. Kang, F. Yan, P. Zhang, and C. Du, "A novel way to calculate energy efficiency for rechargeable batteries," *Journal of Power Sources*, vol. 206, pp. 310–314, 2012. [Online]. Available: https://doi.org/10.1016/j.jpowsour.2012.01.105

[64] A. Narula, "Modeling of ageing of lithium ion battery at low temperatures," *Department of Electric Power Engineering Chalmers, Gothenburg*, 2014.

[65] Z. Geng, T. Thiringer, Y. Olofsson, J. Groot, and M. West, "On-board impedance diagnostics method of li-ion traction batteries using pseudo-random binary sequences," in *2018 20th European Conference on Power Electronics and Applications (EPE'18 ECCE Europe)*. IEEE, 2018, pp. P–1.

[66] "Conductors of insulated cables," International Electrotechnical Commission, Standard, Nov. 2004.

[67] N. Mohan, T. M. Undeland, and W. P. Robbins, *Power electronics: converters, applications, and design*. John wiley & sons, 2003.

[68] G. Notton, V. Lazarov, and L. Stoyanov, "Optimal sizing of a grid-connected pv system for various pv module technologies and inclinations, inverter efficiency characteristics and locations," *Renewable Energy*, vol. 35, no. 2, pp. 541–554, 2010.

[69] D. Christen, U. Badstuebner, J. Biela, and J. W. Kolar, "Calorimetric power loss measurement for highly efficient converters," in *Power Electronics Conference (IPEC), 2010 International*, 2010, pp. 1438–1445.

[70] M. Sverko and S. Krishnamurthy, "Calorimetric loss measurement system for air and water cooled power converters," in *2013 15th European Conference on Power Electronics and Applications (EPE)*. IEEE, 2013, pp. 1–10.

[71] C. Duran, "Bifacial solar cells: high efficiency design, characterization, modules and applications," Ph.D. dissertation, 2012.

[72] J. F. Weaver, "If bifacial panels can compete on price the (backsheet) choice is clear," 2019.

[73] S. Dubey, J. N. Sarvaiya, and B. Seshadri, "Temperature dependent photovoltaic (pv) efficiency and its effect on pv production in the world–a review," *Energy Procedia*, vol. 33, pp. 311–321, 2013.

[74] L. Nohrstedt, "Guide: Solcellernas tre generationer," 2017.

[75] K. Mertens, *Photovoltaics: fundamentals, technology and practice*. John Wiley & Sons, 2013.

[76] Energiföretagen, "Energiåret 2017," Available at https://www.energiforetagen.se/statistik/energiaret/ [Accessed: 2019/02/13].

[77] U. Alfadel, "Analysing the peak shaving effect and the increase in self consumption and self sufficiency of battery storage when coupled to a single family house," 2017, unpublished Master Thesis.

[78] E. Alliance, "380 vdc architectures for the modern data center," *EMerge Alliance, San Ramon, CA, USA*, 2013.

[79] D. E. Geary, D. P. Mohr, D. Owen, M. Salato, and B. Sonnenberg, "380v dc eco-system development: present status and future challenges," in *Intelec 2013; 35th International Telecommunications Energy Conference, SMART POWER AND EFFICIENCY*. VDE, 2013, pp. 1–6.

[80] D. J. Becker and B. Sonnenberg, "Dc microgrids in buildings and data centers," in *2011 IEEE 33rd International Telecommunications Energy Conference (INTELEC)*. IEEE, 2011, pp. 1–7.

[81] M. A. Bahmani, T. Thiringer, A. Rabiei, and T. Abdulahovic, "Comparative study of a multi-mw high-power density dc transformer with an optimized high-frequency magnetics in all-dc offshore wind farm," *IEEE Transactions on power delivery*, vol. 31, no. 2, pp. 857–866, 2015.

[82] T. Jimichi, M. Kaymak, and R. W. De Doncker, "Comparison of single-phase and three-phase dual-active bridge dc-dc converters with various semiconductor devices for offshore wind turbines," in *2017 IEEE 3rd International Future Energy Electronics Conference and ECCE Asia (IFEEC 2017-ECCE Asia)*. IEEE, 2017, pp. 591–596.

[83] S. Cui, N. Soltau, and R. W. De Doncker, "A high step-up ratio soft-switching dc–dc converter for interconnection of mvdc and hvdc grids," *IEEE Transactions on Power Electronics*, vol. 33, no. 4, pp. 2986–3001, 2017.

[84] T. Thiringer, M. Bahmani, A. Mannikoff, J. Söoderbom, M. Kharezy, H. Hagmar, and A. Lindskog, "Besparingspotential för likströmsdistribution - en förstudie," Chalmers University of Technoology, Tech. Rep., 2017.

[85] P. Ollas, J. Persson, C. Markusson, and U. Alfadel, "Impact of battery sizing on self-consumption, self-sufficiency and peak power demand for a low energy single-family house with pv production in sweden," in *2018 IEEE 7th World Conference on Photovoltaic Energy Conversion (WCPEC)(A Joint Conference of 45th IEEE PVSC, 28th PVSEC & 34th EU PVSEC)*. IEEE, 2018, pp. 0618–0623.

[86] D. A. Howey, P. D. Mitcheson, V. Yufit, G. J. Offer, and N. P. Brandon, "Online measurement of battery impedance using motor controller excitation," *IEEE transactions on vehicular technology*, vol. 63, no. 6, pp. 2557–2566, 2014.

[87] U. Westerhoff, K. Kurbach, F. Lienesch, and M. Kurrat, "Analysis of lithium-ion battery models based on electrochemical impedance spectroscopy," *Energy Technology*, vol. 4, no. 12, pp. 1620–1630, 2016.

[88] S. Rodrigues, N. Munichandraiah, and A. Shukla, "Ac impedance and state-of-charge analysis of a sealed lithium-ion rechargeable battery," *Journal of Solid State Electrochemistry*, vol. 3, no. 7-8, pp. 397–405, 1999.

[89] R. Thygesen and B. Karlsson, "Simulation and analysis of a solar assisted heat pump system with two different storage types for high levels of pv electricity self-consumption," *Solar Energy*, vol. 103, pp. 19–27, 2014.

[90] S. Quoilin, K. Kavvadias, A. Mercier, I. Pappone, and A. Zucker, "Quantifying self-consumption linked to solar home battery systems: Statistical analysis and economic assessment," *Applied Energy*, vol. 182, pp. 58–67, 2016.

[91] J. Widén and J. Munkhammar, "Evaluating the benefits of a solar home energy management system: impacts on photovoltaic power production value and grid interaction," in *eceee 2013 Summer Study, Presqu'île de Giens, France, June 3-8, 2013*, 2013.

[92] E. Nyholm, *The role of Swedish single-family dwellings in the electricity system*. Doctoral Thesis. Chalmers Univerist of Technology. Sweden, 2016.

[93] L. Parker, R. Maxwell, B. Gentry, M. Wilder, R. Saines, and J. Camerson, "From silos to systems: Issues in clean energy and climate change," 2010.

[94] A. Sannino, G. Postiglione, and M. H. Bollen, "Feasibility of a dc network for commercial facilities," in *Conference Record of the 2002 IEEE Industry Applications Conference. 37th IAS Annual Meeting (Cat. No. 02CH37344)*, vol. 3. IEEE, 2002, pp. 1710–1717.

[95] B. A. Thomas, I. L. Azevedo, and G. Morgan, "Edison revisited: Should we use dc circuits for lighting in commercial buildings?" *Energy Policy*, vol. 45, pp. 399–411, 2012.

[96] B. T. Patterson, "Dc, come home: Dc microgrids and the birth of the" enernet"," *IEEE Power and Energy Magazine*, vol. 10, no. 6, pp. 60–69, 2012.

[97] G. AlLee and W. Tschudi, "Edison redux: 380 vdc brings reliability and efficiency to sustainable data centers," *IEEE Power and Energy Magazine*, vol. 10, no. 6, pp. 50–59, 2012.

[98] D. L. Gerber, V. Vossos, W. Feng, C. Marnay, B. Nordman, and R. Brown, "A simulation-based efficiency comparison of ac and dc power distribution networks in commercial buildings," *Applied Energy*, 2017.

[99] P. Savage, R. Nordhaus, and S. Jamieson, "Dc microgrids: Benefits and barriers, from silos to systems: Issues in clean energy and climate change," 2010.

[100] International Electrotechnical Commission, "Lvdc: electricity for the 21st century," 2018.

[101] M. Monadi, M. A. Zamani, J. I. Candela, A. Luna, and P. Rodriguez, "Protection of ac and dc distribution systems embedding distributed energy resources: A comparative review and analysis," *Renewable and sustainable energy reviews*, vol. 51, pp. 1578–1593, 2015.

[102] International Electrotechnical Commission, "Lvdc: another way," 2018.

[103] ——, "Electricity access more than a promise: Lvdc," 2018.

[104] S. F. Porter, D. Denkenberger, C. Mercier, E. P. May-Ostendorp, and P. Turnbull, "Reviving the war of currents: Opportunities to save energy with dc distribution in commercial buildings," 2014.

[105] S. Pantano, P. May-Ostendorp, and K. Dayem, "Demand dc. accelerating the introduction of dc power in the home," *CLASP, May*, 2016.

[106] V. Vossos, K. Johnson, M. Kloss, M. Khattar, D. Gerber, and R. Brown, "Review of dc power distribution in buildings: A technology and market assessment," *LBNL Report, Berkeley*, 2017.

A

Residential Building Blueprints

Figures A.1 and A.2 shows the lighting layout and cabling on floors 1 and 2 of the studied user-case, being a single-family residential building. Figures A.3 and A.4 shows the layout and cabling for the sockets and stationary loads on floors 1 and 2, together with the physical location of some of the main loads.

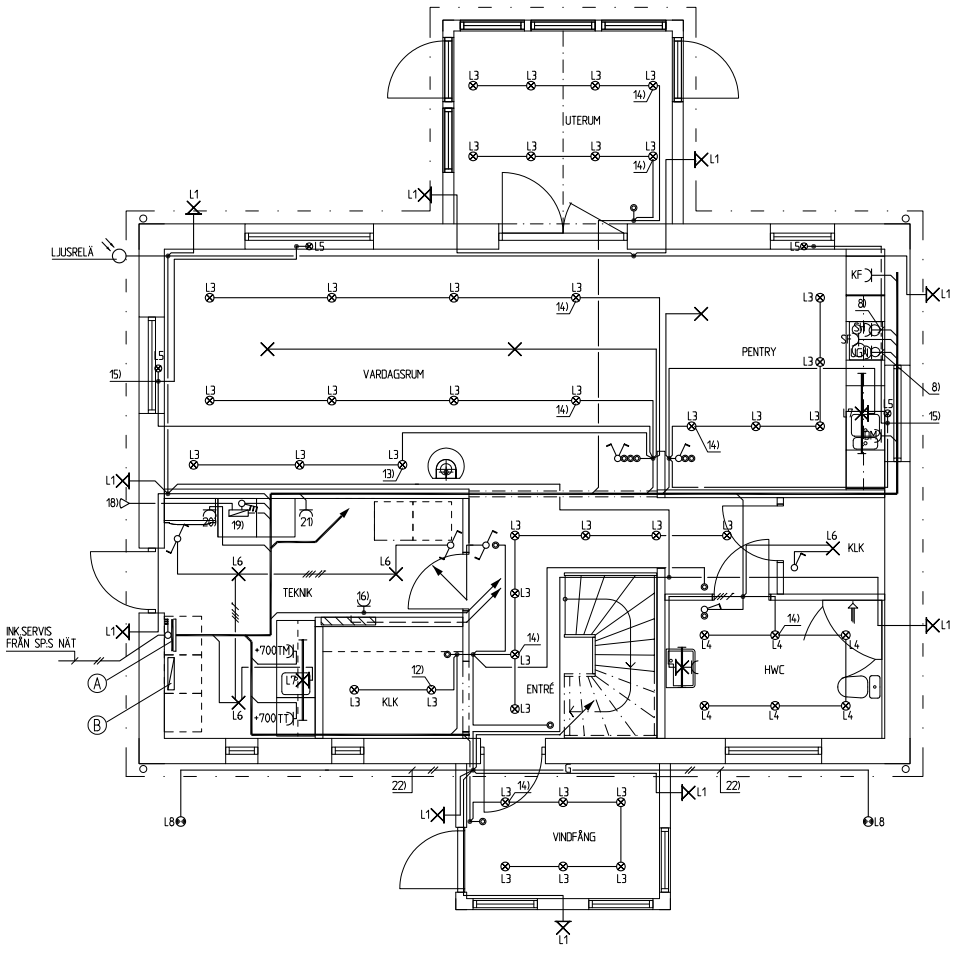

Figure A.1: Lighting layout on floor 1, where "L3" is an LED light of 7 W. **Translations**: "Teknik" = technical room, "Vindfång" = entrance hall, "Vardagsrum" = living room, "Uterum" = conservatory and "KLK" = closet. Printed A4 scale = 1:120

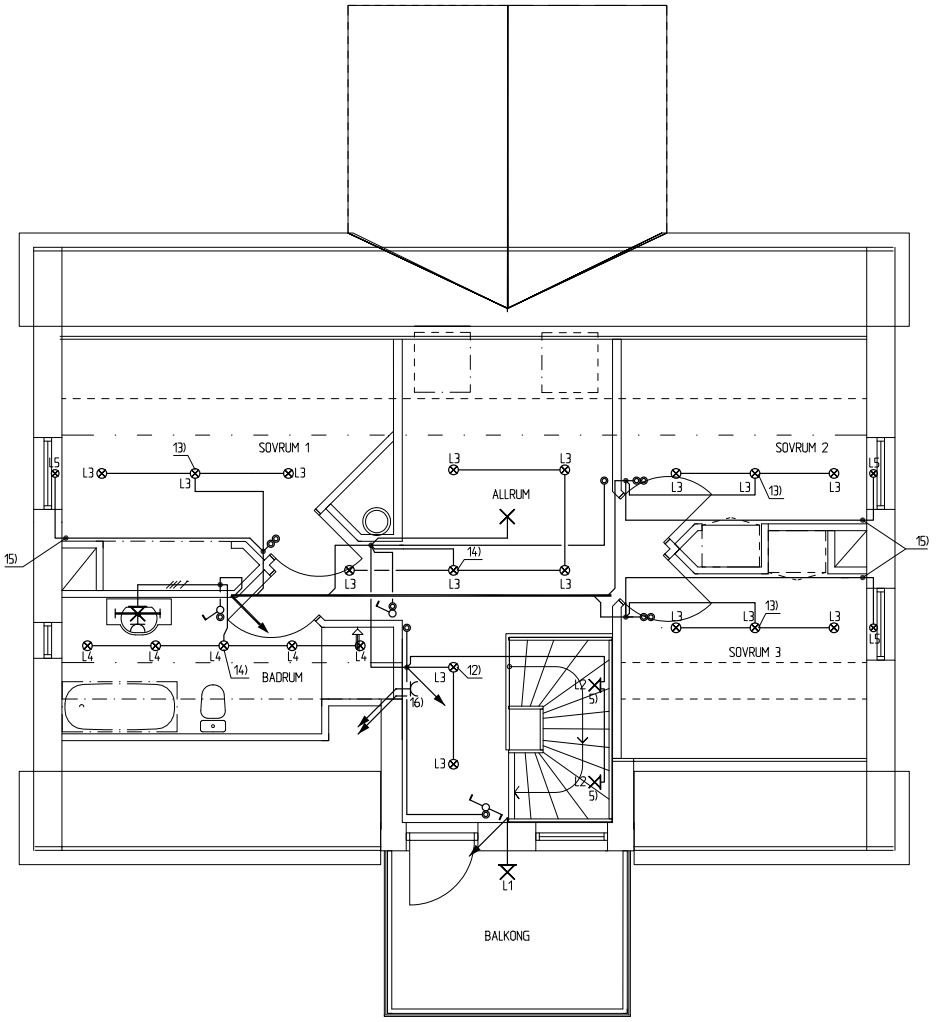

Figure A.2: Lighting layout on floor 2, where "L3" is an LED light of 7 W. **Translation**: "Balkong" = balcony, "Badrum" = bathroom, "Sovrum" = bedroom and "Allrum" = living room. Printed A4 scale = 1:120

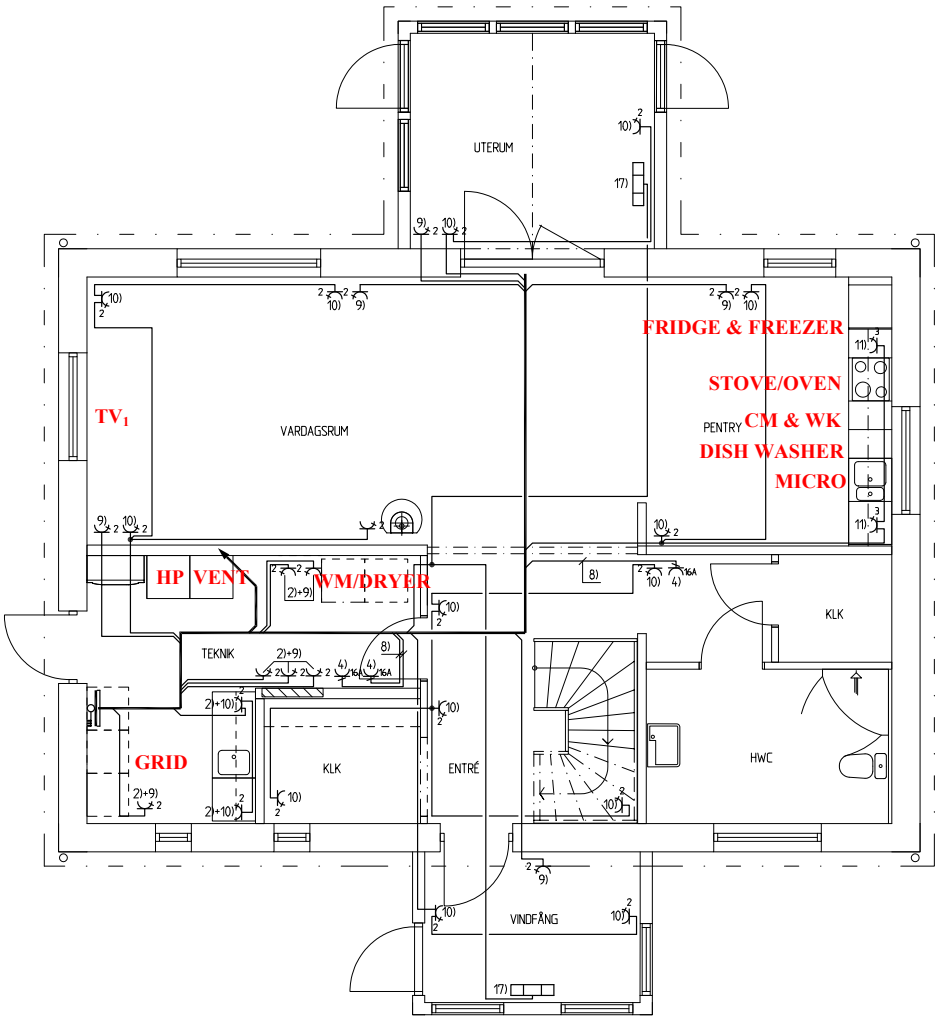

Figure A.3: Blueprints of floor 1 cabling and sockets layout for the modelled single-family residential building together with the physical placement of the main loads. **Translations**: "Teknik" = technical room, "Vindfång" = entrance hall, "Vardagsrum" = living room, "Uterum" = conservatory and "KLK" = closet. **Abbreviations**: "HP" = heat pump, "Vent" = ventilation, "WM" = washing machine, "Dryer" = clothes dryer, "CM" = coffee machine, "WK" = water kettle, "Micro" = microwave oven and "Grid" = grid connection. Printed A4 scale = 1:120

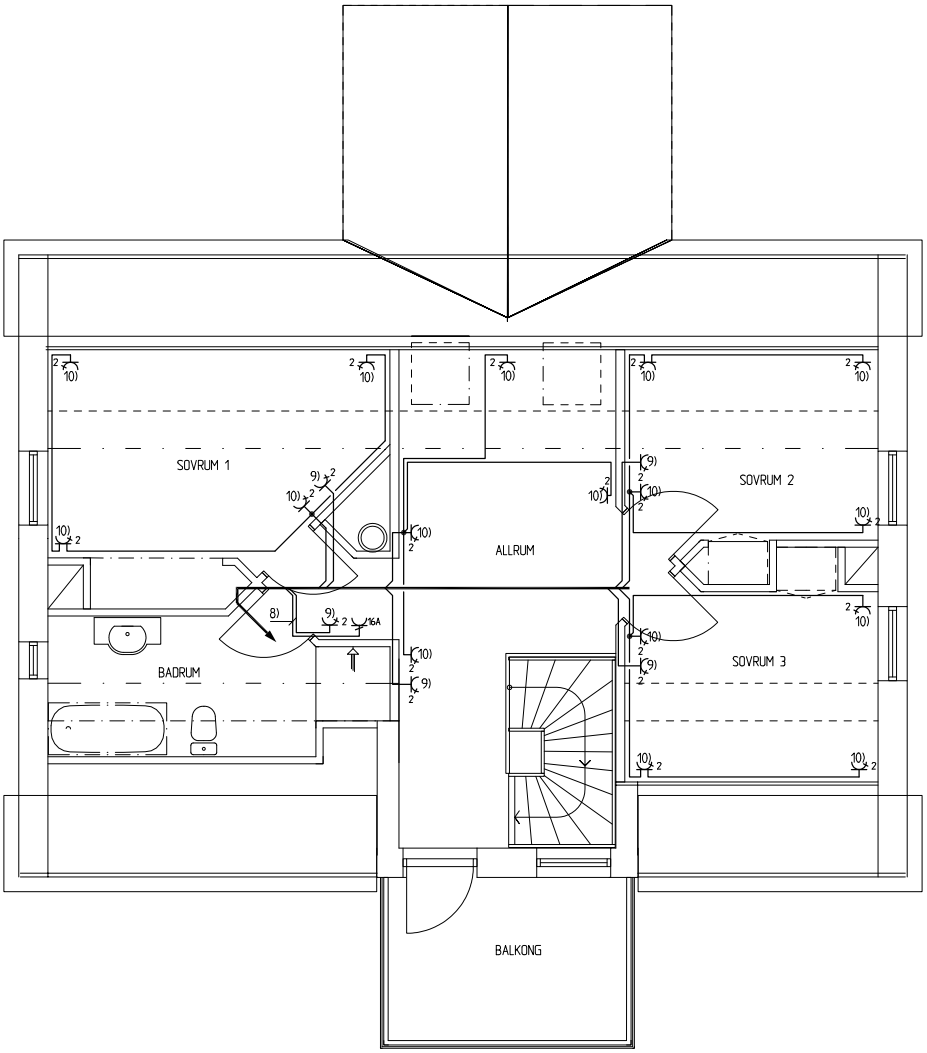

Figure A.4: Blueprints of floor 2 cabling and sockets layout for the modelled single-family residential building. **Translation**: "Balkong" = balcony, "Badrum" = bathroom, "Sovrum" = bedroom and "Allrum" = living room. Printed A4 scale = 1:120

B

Load Data & Loss Separation

B.1 Load Data

Table B.1 shows the cable feeder lengths and distribution voltages used in the modelling of the conduction losses, together with the annual load consumption and maximum power. Here, "Others" consists of the power sockets throughout the house and the feeder length and maximum power is thus dependent on the active socket and plugged-in appliance. The table also shows the physical location of the appliance assumed during the modelling, see also Figures A.1–A.4.

B.2 Loss Separation – Appliances & Power Electronic Converters

Tables B.2 and B.3 shows a separate of the losses for each appliance and the five modelled cases when using 3.7 kWp PV array and 7.5 kWh battery storage. Noticeable is the relatively large conduction losses for the TV's, with the maximum power from Table B.1, when supplied with 20 VDC.

Tables B.4–B.6 shows the power electronic converter losses and total conduction losses for all five cases and the three PV and battery systems modelled. These results can also be seen in Figures 5.8a–5.8c.

Table B.1: Load data used for the modelling. The distribution voltage, U_{dist}, and cable feeder length's for lighting and some other appliances vary depending on the chosen system topology and active lamp/socket. "Room" also shows the physical location of the appliance, see Figures A.1–A.4.

Appliance	**Feeder Length [m]**	**Annual Energy [kWh]**	**Max. Power [kW]**	$U_{dist,\ DC}$ **[V]**	**Room**
Heat pump	3.1	2 213	5.18	380	"Teknik"
Ventilation	3.2	801	0.18	380	"Teknik"
Lighting	1.2–12.5	343	0.29	24/48/380	"All"
Water pumps	1.5	272	0.40	380	"Teknik"
Dish Washer	6.3	261	2.0	380	"Pentry"
Washing Machine	3	251	2.2	380	"Teknik"
Stove/Oven	6.4	379	5.0	380	"Pentry"
Clothes Dryer	3	248	3.0	380	"Teknik"
Microwave oven	6.3	61	0.7	380	"Pentry"
Cooking hood	6.4	28.8	0.2	380	"Pentry"
Fridge & Freezer	6.8	399	0.18	380	"Pentry"
TV_1 & TV_2	5–10	192	0.09	24/48	"Vardagsrum", floor 1 and 2
Laptop	10	21	0.019	24/48	"Sovrum 2"
Internet	7	70	0.008	24/48	"Sovrum 3"
Vacuum cleaner	5	145	1.0	380	"Entré"
Coffee machine	6.4	126	1.0	380	"Pentry"
Water kettle	6.4	84	1.2	380	"Pentry"
Others	5–15	313	0.003–0.2	24/48	"All"

Table B.2: Calculated conduction and conversion losses per appliance for the five modelled cases and with a PV and battery system of 3.7 kWp and 7.5 kWh respectively. Rectification in the DC cases are done by the grid-tied inverter, thus the "0":s. The larger loads are also not subject to any additional DC/DC conversion. **NB!** Sums may differ due to rounding.

Appliance	**Conduction [Wh]**					**Rectification [kWh]**					
	AC	DC_{1a}	DC_{1b}	DC_2	DC_3	**AC**	DC_{1a}	DC_{1b}	DC_2	DC_3	
Heat pump	606	444	444	444	444	66.4	0	0	0	0	...
Ventilation	271	99	99	99	99	24.0	0	0	0	0	...
Lighting	57	21	21	1331	2083	10.3	0	0	0	0	...
Water pumps	94	35	35	35	35	8.2	0	0	0	0	...
Dish washer	809	592	592	592	592	7.8	0	0	0	0	...
Washing machine	467	342	342	342	342	7.5	0	0	0	0	...
Stove/oven	830	730	730	730	730	11.4	0	0	0	0	...
Clothes dryer	838	512	512	512	512	7.4	0	0	0	0	...
Microwave oven	234	86	86	86	86	1.8	0	0	0	0	...
Cooking hood	32	12	12	12	12	0.9	0	0	0	0	...
Fridge & Freezer	431	158	158	158	158	12.0	0	0	0	0	...
TV_1 & TV_2	150	54	54	3436	19794	5.8	0	0	0	0	...
Laptop	4	1	1	80	462	0.6	0	0	0	0	...
Internet	2	1	1	56	322	2.1	0	0	0	0	...
Vacuum cleaner	400	147	147	147	147	4.3	0	0	0	0	...
Coffee machine	700	256	256	256	256	3.8	0	0	0	0	...
Water kettle	564	207	207	207	207	2.5	0	0	0	0	...
Others	613	365	365	369	6636	9.4	0	0	0	0	...
Total [kWh]	**7.1**	**4.1**	**4.1**	**8.9**	**32.9**	**186.2**	**0**	**0**	**0**	**0**	...

Table B.3: *Continuation of Table B.2.* Calculated conduction and conversion losses per appliance for the five modelled cases and with a PV and battery system of 3.7 kWp and 7.5 kWh respectively. Rectification in the DC cases are done by the grid-tied inverter, thus the ”0”:s. The larger loads are also not subject to any additional DC/DC conversion. **NB!** Sums may differ due to rounding.

Appliance		**Conversion (DC/DC) [kWh]**					**Total [kWh]**				
		AC	DC_{1a}	DC_{1b}	DC_2	DC_3	**AC**	DC_{1a}	DC_{1b}	DC_2	DC_3
Heat pump	...	0	0	0	0	0	67.0	0.4	0.4	0.4	0.4
Ventilation	...	0	0	0	0	0	24.3	0.1	0.1	0.1	0.1
Lighting	...	44.6	44.6	44.6	44.6	44.6	55.0	44.6	44.6	45.9	46.7
Water pumps	...	0	0	0	0	0	8.3	0.04	0.04	0.04	0.04
Dish washer	...	0	0	0	0	0	8.6	0.6	0.6	0.6	0.6
Washing machine	...	0	0	0	0	0	8.0	0.3	0.3	0.3	0.3
Stove/oven	...	0	0	0	0	0	12.2	0.7	0.7	0.7	0.7
Clothes dryer	...	0	0	0	0	0	8.2	0.5	0.5	0.5	0.5
Microwave oven	...	0	0	0	0	0	2.0	0.09	0.09	0.09	0.09
Cooking hood	...	0	0	0	0	0	0.9	0.01	0.01	0.01	0.01
Fridge & Freezer	...	0	0	0	0	0	12.4	0.2	0.2	0.2	0.2
TV_1 & TV_2	...	27.0	27.0	27.0	27.0	27.0	33.0	27.1	27.1	30.4	46.8
Laptop	...	2.5	2.5	2.5	2.5	2.5	3.1	2.5	2.5	2.6	3.0
Internet	...	8.7	8.7	8.7	8.7	8.7	10.8	8.7	8.7	8.8	9.0
Vacuum cleaner	...	0	0	0	0	0	4.7	0.1	0.1	0.1	0.1
Coffee machine	...	0	0	0	0	0	4.5	0.7	0.7	0.7	0.7
Water kettle	...	0	0	0	0	0	3.1	0.3	0.3	0.3	0.3
Others	...	24.2	24.2	24.2	24.2	24.2	34.2	24.6	24.6	24.6	30.8
Total [kWh]	...	**107.0**	**107.0**	**107.0**	**107.0**	**107.0**	**300.3**	**111.5**	**111.5**	**116.3**	**140.3**

Table B.4: Power electronic losses [kWh] for all five modelled cases and without the inclusion of PV and battery, see also Figure 5.8a

	Case				
Component	AC	DC_{1a}	DC_{1b}	DC_2	DC_3
Grid-tied inverter	0	283	143	283	285
Conduction (high voltage)	7	4	4	4	4
Conduction (low voltage)	0	0	0	5	29
Rectification (AC/DC)	186	0	0	0	0
Conversion (DC/DC)	107	107	107	107	110
Total [kWh]	**300**	**394**	**254**	**399**	**428**

Table B.5: Power electronic losses [kWh] for all five modelled cases and with a PV array and battery size of 3.7 kWp and 7.5 kWh respectively, see also Figure 5.8b.

	Case				
Component	AC	DC_{1a}	DC_{1b}	DC_2	DC_3
Grid-tied inverter	0	208	115	209	211
Battery converter	142	44	44	44	44
PV inverter	130	66	66	66	66
Battery losses	40	43	42	42	43
Conduction (high voltage)	7	4	4	4	4
Conduction (low voltage)	0	0	0	5	29
Rectification (AC/DC)	186	0	0	0	0
Conversion (DC/DC)	107	107	107	107	110
Total [kWh]	**612**	**472**	**378**	**477**	**507**

Table B.6: Power electronic losses [kWh] for all five modelled cases and with a PV array and battery size of 10 kWp and 10 kWh respectively, see also Figure 5.8c

	Case				
Component	AC	DC_{1a}	DC_{1b}	DC_2	DC_3
Grid-tied inverter	0	323	207	324	324
Battery converter	187	48	48	48	49
PV inverter	352	180	180	180	180
Battery losses	58	51	51	51	52
Conduction (high voltage)	7	4	4	4	4
Conduction (low voltage)	0	0	0	5	29
Rectification (AC/DC)	186	0	0	0	0
Conversion (DC/DC)	107	107	107	107	110
Total [kWh]	**897**	**713**	**597**	**719**	**748**